ELIAS FEITOSA ARAUJO

THE ROLE OF NAD$^+$ COMPARTMENTATION AND DYNAMICS IN *Arabidopsis thaliana*

Thesis presented to the Universidade Federal de Viçosa as part of the requirement of the Plant Physiology Graduate Program for the obtention of the degree of *Doctor Scientiae.*

Advisor: Adriano Nunes Nesi

VIÇOSA - MINAS GERAIS

2020

Ficha catalográfica preparada pela Biblioteca Central da Universidade Federal de Viçosa - Câmpus Viçosa

T
A663r
2020

Araujo, Elias Feitosa, 1988-
The role of NAD+ compartmentation and dynamics in *Arabidopsis thaliana* / Elias Feitosa Araujo. – Viçosa, MG, 2020.
134 f. : il. (algumas color.) ; 29 cm.

Texto em inglês.
Orientador: Adriano Nunes Nesi.
Tese (doutorado) - Universidade Federal de Viçosa.
Inclui bibliografia.

1. *Arabidopsis thaliana* - Metabolismo. 2. *Arabidopsis thaliana* - Desenvolvimento. 3. NAD (Coenzima).
I. Universidade Federal de Viçosa. Departamento de Biologia Vegetal. Programa de Pós-Graduação em Fisiologia Vegetal.
II. Título.

CDD 22. ed. 583.64

ELIAS FEITOSA ARAUJO

THE ROLE OF NAD⁺ COMPARTMENTATION AND DYNAMICS IN *Arabidopsis thaliana*

Thesis presented to the Universidade Federal de Viçosa as part of the requirement of the Plant Physiology Graduate Program for the obtention of the degree of *Doctor Scientiae*.

APPROVED: 19th February 2020.

Assent:

Elias Feitosa Araujo
Author

Adriano Nunes Nesi
Advisor

ACKNOWLEDGEMENTS

I thank my advisor Professor Adriano Nunes Nesi for his advice during my doctorate. I am grateful to him to always believe in my work, to encourage me to go to Germany and to always support me in my experiments and discussions. I thank also Professor Wagner L. Araújo for his kind support whenever I needed his advice to execute my experiments and also for all the recommendation letters he prepared to me to apply for scholarships. I thank Professor Markus Schwarzländer for his support during my period in Germany and for his precious contributions to my thesis.

I thank my dear mon and my father for their love and affection during my whole life. Despite the difficulties, they were always there to support me and to always remind me that I could be better every day. I love you so much.

I thank my sister Micaele for being my best friend and my person. There is no one in the world that I can trust more than her. She is the first person to know every single detail of my life and I am sure that she is as proud as I am to be able to finish my PhD. Thank you for being such a nice person in my life. I love you more than I can explain Binha!

I thank my dear sister Lidiane for always being kind with me and to share so much love. You bring joy to my life. Thank you to your support and love during this time, I love you.

I thank my grandfather and my grandmother for their love. I will always remember the best days of my life close to you. I love you forever.

I thank my sweet niece Anna Clara for being the reason of my happiness since she was born. There are no words to explain how much I love you. I am also grateful to my little boys Lucca and Davi. You are so smart guys and I love you so much.

I thank my lovely friend Carlota for her love, affection and support in my life. You have such a big space in my heart and I will always be grateful to have you like a sister that I could choose. Je t'adore beaucoup.

I thank my dear friend Ana for her support, affection and love. I love you so much, no words to explain. Thank you for everything you have done until now.

I thank my dear friends Márcio, Leandro, Fabrício, Gelso and Juninho for their love and affection. You are always in my mind and in my heart, I love you all.

I thank my friends made during my period at UCP, Rininha, Paulete and Regina. You are sweet girls with a great power. Love you all.

I thank my dear friends from Viçosa, Talita, Claudinha, Rodrigo, Camila, Rafael, Gabriel, Alex, Inácio, Mateus, Mateusinho, Michele, Xistim, Alice, Franklin and Jô. I love you all and I will never forget our moments together. Miss you all.

I thank my friend Cordula for being such a nice person since I arrived in Münster. Thank for your support and affection.

I thank my colleagues from UCP and Plant energy group for the nice moments spent together.

I thank the Universidade federal de Viçosa, in special to the Plant Physiology Program, for support and for providing all conditions required to develop my work. I thank all the staff of the Plant Physiology Department and also the group of Professor Markus for hosting me in a such kind way.

Many thanks for all other people who in some way had ever helped or supported me along my journey and whose names are mentioned here.

I am also grateful to the financial support of CNPq (National Council for Scientific and Technological Development) and CAPES (Coordination for Scientific Support for Post Graduate Level Training; CAPES PrInt program by scholarships granted.

ABSTRACT

ARAUJO, Elias Feitosa, D.Sc., Universidade Federal de Viçosa, February, 2020. **The role of NAD$^+$ compartmentation and dynamics in *Arabidopsis thaliana*.** Advisor: Adriano Nunes Nesi.

Nicotinamide adenine dinucleotide (NAD$^+$) is a fundamental coenzyme required to regulate plant central metabolism and redox status homeostasis. Plants produce NAD$^+$ via *de novo* and salvage pathways. Despite early steps of the two pathways occur in different subcellular compartments, *de novo* in chloroplasts and salvage in cytosol, both pathways produce the final product NAD$^+$ exclusively in the cytosol. Thus, NAD$^+$ must be imported into organelles to drive biological processes inside them. In *Arabidopsis thaliana*, three genes have been identified as NAD$^+$ carriers, namely *NDT1* (*At*2g47490) and *NDT2* (*At*1g25380), both targeted to the inner mitochondrial membrane, and the peroxisomal transporter *PXN* (*At*2g39970). The previous functional characterization of *NDT1*, *NDT2* and *PXN* have revealed their importance for seed production and quality, seedling establishment, photosynthesis, metabolism, stomatal density and stomatal conductance. To extend our knowledge on the importance of NAD$^+$ dynamics, we used mutants for NAD$^+$ transport and focused in comprehend: (1) how altered NAD$^+$ distribution affects stomatal development in cotyledons, (2) the crosstalk between NAD$^+$ transport and elevated atmospheric CO_2 concentration and (3) NAD$^+$ dynamics *in vivo* under different environmental cues. The results indicate that NAD negatively regulates stomatal development in cotyledons of Arabidopsis. Seedlings with reduced expression of mitochondrial (*NDT1* and *NDT2*) and peroxisomal (*PXN*) NAD$^+$ transporter genes displayed reduced numbers of stomata lineage cells and reduced stomatal density. Furthermore, cotyledons of wild-type seedlings treated with exogenous NAD$^+$ and cotyledons of mutant plants with reduced NAD$^+$ breakdown capacity also exhibited reduced stomatal number. Impaired NAD$^+$ transport and the exogenous NAD$^+$ feeding were further associated with the induction of abscisic acid (ABA)-responsive genes. Additionally, NAD$^+$ feeding of *aba-2* and *ost1* seedlings, impaired in ABA synthesis and ABA signaling, respectively, did not impact on stomatal number, whereas the inhibition of ABA synthesis rescued the stomatal phenotype in NAD$^+$ carrier mutants. Moreover, *in vivo* measurement of ABA dynamics in seedlings of an ABA-specific optogenetic reporter - ABAleon2.1 treated with NAD$^+$ showed increases in ABA content, suggesting that NAD$^+$ impacts on stomatal development through ABA synthesis and signaling. The results demonstrate

that intracellular NAD^+ homeostasis is essential for normal stomatal development, and provide a link between central metabolism and developmental plasticity. Posteriorly, NAD^+ carrier mutants were grown under elevated CO_2 concentrations and overall results showed that, under high CO_2, the mutants displayed reductions in total biomass and leaf number compared to the control under ambient CO_2. Furthermore, higher levels of photorespiratory intermediates such as glutamate and glycine were found in the mutant lines under elevated CO_2. Moreover, mutant lines produced much less seeds than wild-type plants regardless of CO_2 concentration, demonstrating that NAD^+ compartmentalization is fundamental during reproductive phase in both ambient and high CO_2 concentration. With the aim to deeper study NAD^+ dynamics, we transformed wild-type and a *ndt1* mutant line with the Peredox-mCherry sensor that permits the measuring of cytosolic NADH dynamics *in vivo*. The cytosol of *ndt1* mutant lines presented higher levels of NADH/NAD^+ compared to the control line. Additionally, increased cytosolic levels of NADH/NAD^+ in leaves of *ndt1* mutants was observed upon the exogenous feeding of sugars and tricarboxylic acid (TCA) cycle intermediates. Surprisingly, light, mitochondrial electron transport chain (mETC) inhibitors and oxygen deprivation treatment did not show significant differences in cytosolic NADH/NAD^+ content in *ndt1* mutants compared to wild-type. The results provide evidence of disruption of NAD^+ balance among organelles in *ndt1* mutants and show the power of this technique to follow NADH dynamics *in vivo*. Collectively, the data presented provide different inputs to show that, not only NAD^+ metabolism, but also NAD^+ distribution across organelles, are fundamental to drive essential biological processes in plants. Furthermore, this study proposes a direct link between central metabolism and early developmental process such as stomatal development.

Keywords: Nicotinamide adenine dinucleotide. NAD^+ transport. Metabolism. Development.

RESUMO

ARAUJO, Elias Feitosa, D.Sc., Universidade Federal de Viçosa, fevereiro de 2020. **O papel da compartimentalização e das dinâmicas de NAD$^+$ em *Arabidopsis thaliana***. Orientador: Adriano Nunes Nesi.

Nicotinamide adenina dinucletídeo (NAD$^+$) é uma coenzima fundamental para a regulação do metabolismo central e do estado redox celular. Plantas produzem NAD$^+$ através das vias *de novo* e salvamento. Apesar de começarem em diferentes compartimentos, *de novo* nos cloroplastos e salvamento no citosol ambas as vias sintetizam NAD$^+$ como produto final no citosol. Desta forma, o NAD$^+$ precisa ser importado pelas organelas para exercer suas funções no interior das mesmas. Em Arabidopsis três genes foram identificados como transportadores de NAD$^+$ sendo dois localizados na membrana interna da mitocôndria *NDT1* (*At*2g4790) e *NDT2* (*At*1g25380) e um na membrana do peroxissomo *PXN* (*At*2g39970). A caracterização funcional dos genes NDT1, NDT2 e PXN revelou a importância a importância desses genes para a produção e qualidade de sementes, estabelecimento de plântulas, fotossíntese, metabolismo e regulação do número de estômatos e condutância estomática. Para aumentar nosso conhecimento sobre a importância das dinâmicas de NAD$^+$, utilizamos mutantes para o transporte de NAD$^+$ e nos focamos em compreender: (1) como a distribuição de NAD$^+$ afeta o desenvolvimento estomático em cotilédones, (2) a interação entre transporte de NAD$^+$ e altas concentrações de gás carbônico e (3) dinâmicas de NAD$^+$ in vivo em diferentes situações ambientais. Os resultados indicam que o NAD$^+$ regula negativamente o desenvolvimento estomático em cotilédones de Arabidopsis. Plântulas com reduzida expressão dos transportadores de NAD$^+$ mitocondriais (*NDT1* e *NDT2*) e do peroxissomo (*PXN*) apresentaram reduzidos números de células formadoras de estômatos e densidade estomática. Além disso, cotilédones tratados com NAD$^+$ de forma exógena e cotilédones de plantas com reduzida capacidade de mobilização de NAD$^+$ também exibiram menor densidade estomática. O impedimento de transporte de NAD$^+$ e o tratamento exógeno com NAD$^+$ foram associados com a indução de genes responsivos ao hormônio ABA. Adicionalmente, o tratamento de NAD$^+$ em mutantes para a síntese (*aba-2*) e sinalização (*ost1*) de ABA não impactou o número de estômatos enquanto o uso de um inibidor da biossíntese de ABA recuperou o fenótipo de estômatos dos mutantes para o transporte de NAD$^+$. Ademais, a mensuração in vivo das dinâmicas de ABA em plântulas do sensor de ABA (ABA-specific optogenetic

repórter – ABAleon2.1) tratadas com NAD^+ mostraram aumentos nos níveis de ABA, sugerindo que o NAD^+ impacta o número estomático através da síntese e sinalização de ABA. Os resultados demonstraram que a homeostase intracelular de NAD^+ é essencial para o correto desenvolvimento estomático e fornece uma ligação entre o metabolismo central e a plasticidade do desenvolvimento. Posteriormente crescemos os mutantes para o transporte de NAD^+ em elevadas concentrações de CO_2 e em geral os resultados mostraram que as plantas mutantes apresentaram menor biomassa e número de folhas que o controle em altas concentrações de CO_2. Adicionalmente, plantas mutantes acumularam intermediários da fotorrespiração, tais como glutamato e glicina em alto CO_2. Além disso, plantas mutantes produziram muito menos sementes que plantas WT em resposta ao CO_2, demonstrando que a compartimentalização do NAD^+ é fundamental durante a fase reprodutiva em condição ambiente e de alto CO_2. Com o objetivo de estudar as dinâmicas de NAD^+ transformamos plantas controle e plantas com reduzida expressão do gene *NDT1* com o sensor de NAD^+ chamado Peredox-mCherry que permite a mensuração da dinâmica de NADH/NAD^+ no citosol *in vivo*. O citosol das plantas mutantes *ndt1* apresentaram maiores níveis de NADH/NAD^+ comparado com o citosol de plantas controle. Adicionalmente, aumentos nos níveis de NADH/NAD^+ em folhas de *ndt1* foram observados após o tratamento destas com açúcares e intermediários do ciclo dos ácidos tricarboxílicos. Surpreendentemente, os tratamentos com luz, inibidores da cadeia de transporte mitocondrial e indução de estresse por oxigênio não apresentaram diferenças significativas nos teores de NADH/NAD^+ entre mutantes e plantas controle. Os resultados apresentam evidência do desbalanço de NAD^+ entre as organelas em plantas mutantes e mostra ainda como essa técnica é valiosa para estudar as dinâmicas de NADH *in vivo*. Coletivamente, os dados apresentados mostram que não apenas o metabolismo do NAD^+ é fundamental para regular processos biológicos essenciais, mas também sua distribuição entre organelas. Além disso, este estudo propõem uma ligação direta entre o metabolismo central e processos iniciais de desenvolvimento como o desenvolvimento estomático.

Palavras-chave: Nicotinamida adenina dinucleotídeo. Transporte de NAD^+. Metabolismo. Desenvolvimento.

TABLE OF CONTENT

GENERAL INTRODUCTION

Different from prokaryotic cells the eukaryotic organisms present a compartmentation of metabolism and several other functions in different parts of the cell (Lunn, 2007). Despite having specific biochemical and physical features each compartment depends on each other for supplies of metabolites and molecules (Lunn, 2007; Krueger et al., 2011). To functionally operate the traffic of metabolites, molecules and ions across the organelles must be tightly regulated to allow proper metabolism in subcellular compartments (Weber and Fischer, 2007). Biological membranes present a barrier for the free passage of some metabolites and molecules, therefore carrier proteins are required to taken up and to export metabolites from organelles (Linka and Weber, 2010; Haferkamp and Schmitz-Esser, 2012; Toleco et al., 2020).

Arabidopsis genome possess three genes responsible to encode NAD^+ carriers, *At*2g47490 (*NDT1*), *At*1g25380 (*NDT2*) and *At*2g39970 (*PXN*) (Palmieri et al., 2009; Bernhardt et al., 2012). All of them belong to the Mitochondrial Carrier Family (MCF) of proteins and, therefore, display highly similar secondary structures (Palmieri et al., 2011). The biochemical characterization of NDT1 and NDT2 proteins revealed that they have 61% of amino acids similarity being NDT2 forty-five per cent bigger in length in its C-termini region (Palmieri et al., 2009). Furthermore, the exchange properties of NDT1 and NDT2 are similar; both preferably accepting NAD^+ in counter exchange with AMP and ADP. For quite some time, NDT1 and NDT2 proteins have been firstly shown to be targeted to the inner membranes of plastids and mitochondria, respectively (Palmieri et al., 2009). Nevertheless, recent subcellular localization demonstrated that NDT1 protein locates to the inner mitochondrial membrane (de Souza Chaves et al., 2019). This finding raises the question for the reasons why mitochondria posse two different genes encoding proteins with the same function. Despite the need for further studies, a plausible reason could be the essentiality of NAD^+ to drive pivotal processes inside mitochondria, but also the requirement of NAD^+ in this organelle to face stress conditions. Additionally, the biochemical characterization of PXN protein revealed that this carrier transports NAD^+ in counter exchange mainly with AMP and is target to the peroxisomal membrane (Bernhardt et al., 2012; Van Roermund et al., 2016).

Given that the final steps of *de novo* and salvage pathways of NAD^+ biosynthesis occur in the cytosol (Noctor et al., 2006; Gakière et al., 2018), it is necessary that NAD^+ transporters uptake NAD^+ from cytosol into organelles. Attempts

to study the roles of NAD^+ distribution across subcompartments have revealed the importance of NAD^+ compartmentation for several biological processes (Bernhardt et al., 2012; de Souza Chaves et al., 2019; Feitosa-Araujo et al., 2020). Reduced expression of *NDT1* gene negatively impacted stomatal density, stomatal conductance, seed production and quality along with deregulation of NAD(P)(H) pool (de Souza Chaves et al., 2019). Similarly, mutants for *NDT2* gene displayed reduced seed yield and quality and decreased stomatal number and stomatal conductance (de Souza Chaves et al., 2019; Feitosa-Araujo et al., 2020). Furthermore, the functional characterization of *PXN* mutants demonstrated that these plants were unable to efficiently mobilize fatty acids during beta oxidation process (Bernhardt et al., 2012). These findings are in agreement with previous studies that described the fundamental importance of NAD^+ in various biological process, included pollen grain viability and pollen tube growth (Hashida et al., 2007), seed germination (Hunt et al., 2007), stomatal movements (Hashida et al., 2010), flowering (Liu et al., 2009), senescence (Schippers et al., 2008), nitrogen assimilation (Takahashi et al., 2009), abscisic acid and proline accumulation (Wei et al., 2019) and pathogen defense (Pétriacq et al., 2016).

To extend our knowledge on how NAD^+ dynamics affects fundamental process regarding plant development and metabolism, this thesis is largely focused on understand the role of NAD^+ in stomatal development, the possible interaction between elevated CO_2 concentrations and redox metabolism along with *in vivo* measurement of cytosolic NADH/NAD^+ dynamics. To this aim this thesis was divided in three chapters, as briefly explained below.

CHAPTER 1: Nicotinamide adenine dinucleotide dynamics modulate stomatal development in an abscisic acid-dependent manner

Stomata are epidermal pores formed by a pair of guard cells and are of pivotal importance to regulate the control of gas exchange in land plants. Given the importance of NAD^+ as a signal molecule and a redox coenzyme in plant central metabolism, we decided to study how NAD^+ dynamics could relate to early developmental processes such as stomatal development. We used three different approaches in this study: mutants impacted in NAD^+ uptake into mitochondria (*ndt1* and *ndt2*) and peroxisomes (*pxn-1*), mutants inefficient in NAD^+ breakdown (*parp-1*,

parp-2 and *parp-3*) and chemical feeding of NAD^+. Collectively, our data suggest that NAD^+ directly impact abscisic acid metabolism leading to an inhibition of stomata biogenesis-related genes. Consequently, NAD^+ is proposed here as a negative regulator of stomatal development in Arabidopsis cotyledons.

CHAPTER 2: The importance of NAD^+ transporters in responses to elevated CO_2

Over the last, years the number of studies describing the effects of elevated CO_2 concentration on plant growth and productivity has increased. Rising in CO_2 concentration has been linked to reductions in both stomatal number and conductance. Given that NAD^+ carrier mutants were shown to have a lower number of stomata and that studies showing the interactions of high CO_2 and redox balance are scarce, we decided to investigate the physiological consequences of NAD^+ carrier mutants grown under high CO_2. Collectively, the results obtained show that NAD^+ carrier mutants accumulate photorespiratory intermediates and present lower stomatal conductance which lead to a reduced biomass gain under high CO_2. Furthermore, during the reproductive phase the positive effects of CO_2 are not pronounced in NAD^+ carried mutants as in control plants.

CHAPTER 3: NAD^+ mitochondrial transporter NDT1 is important for cytosolic NADH/NAD^+ dynamics upon environmental cues

The distribution of NAD^+ among organelles is required to maintain the redox homeostasis and biological processes in subcellular compartments. Traditionally, NAD(P)(H) measurement are based on enzymatic quantification that do not allow discrimination in each compartment where this molecule is being quantified. To circumvent this issue and study NAD(H) dynamics, we transformed plants with reduced *NDT1* expression with the Peredox-mCherry sensor that allows *in vivo* measurements of cytosolic NADH/NAD^+ dynamics. The results demonstrate that the cytosol of *NDT1* mutants compared to the control is more reduced in normal condition and under sugar treatment. The findings provide evidence on the importance of NDT1 carrier protein to maintain NAD^+ levels in subcellular compartments and the power of the *in vivo* measurement technique here applied.

REFERENCES

Bernhardt, K., Wilkinson, S., Weber, A.P.M., and Linka, N. (2012). A peroxisomal carrier delivers NAD^+ and contributes to optimal fatty acid degradation during storage oil mobilization. Plant J. **69**: 1–13.

Feitosa-Araujo, E., de Souza Chaves, I., Florian, A., Fonseca-Pereira, P., Apfata, JAC., Heyneke, E., Medeiros, D. B., Pires, M.V., Mettler-Altmann, T., Neuhaus, H.E., Palmieri, F., Araújo, W.L., Obata, T., Weber, A.P.M., Linka, N., Fernie, A.R., Nunes-Nesi, A. (2020). Down-regulation of a mitochondrial NAD^+ transporter (NDT2) alters seed production and germination in Arabidopsis. Plant Cell Physiol.

Gakière, B. et al. (2018). NAD biosynthesis and signaling in plants. CRC. Crit. Rev. Plant Sci. **37**: 259–307.

Haferkamp, I. and Schmitz-Esser, S. (2012). The plant mitochondrial carrier family: Functional and evolutionary aspects. Front. Plant Sci. **3**: 2.

Hashida, S., Takahashi, H., Kawai-yamada, M., and Uchimiya, H. (2007). Arabidopsis thaliana nicotinate/nicotinamide mononucleotide adenyltransferase (AtNMNAT) is required for pollen tube growth.: 694–703.

Hashida, S.N., Itami, T., Takahashi, H., Takahara, K., Nagano, M., Kawai-Yamada, M., Shoji, K., Goto, F., Yoshihara, T., and Uchimiya, H. (2010). Nicotinate/nicotinamide mononucleotide adenyltransferase-mediated regulation of NAD biosynthesis protects guard cells from reactive oxygen species in ABA-mediated stomatal movement in Arabidopsis. J. Exp. Bot. **61**: 3813–3825.

Hunt, L., Holdsworth, M.J., and Gray, J.E. (2007). Nicotinamidase activity is important for germination. Plant J. **51**: 341–351.

Krueger, S., Giavalisco, P., Krall, L., Steinhauser, M.C., Büssis, D., Usadel, B., Flügge, U.I., Fernie, A.R., Willmitzer, L., and Steinhauser, D. (2011). A topological map of the compartmentalized *Arabidopsis thaliana* leaf metabolome. PLoS One **6**.

Linka, N. and Weber, A.P.M. (2010). Intracellular metabolite transporters in plants. Mol. Plant **3**: 21–53.

Liu, Y.-J., Nunes-Nesi, A., Wallström, S. V, Lager, I., Michalecka, A.M., Norberg, F.E.B., Widell, S., Fredlund, K.M., Fernie, A.R., and Rasmusson, A.G. (2009). A redox-mediated modulation of stem bolting in transgenic Nicotiana sylvestris

differentially expressing the external mitochondrial NADPH dehydrogenase. Plant Physiol. **150**: 1248–1259.

Lunn, J.E. (2007). Compartmentation in plant metabolism. J. Exp. Bot. **58**: 35–47.

Noctor, G., Queval, G., and Gakière, B. (2006). NAD(P) synthesis and pyridine nucleotide cycling in plants and their potential importance in stress conditions. J. Exp. Bot. **57**: 1603–1620.

Palmieri, F. et al. (2009). Molecular identification and functional characterization of *Arabidopsis thaliana* mitochondrial and chloroplastic NAD^+ carrier proteins. J. Biol. Chem. **284**: 31249–31259.

Palmieri, F., Pierri, C.L., Grassi, A. De, Nunes-Nesi, A., Fernie, A.R., Group, M.P., Vic, U.F. De, Mu, A., De Grassi, A., Nunes-Nesi, A., and Fernie, A.R. (2011). Evolution, structure and function of mitochondrial carriers: A review with new insights. Plant J. **66**: 161–181.

Pétriacq, P., Ton, J., Patrit, O., Tcherkez, G., and Gakière, B. (2016). NAD acts as an integral regulator of multiple defense layers. Plant Physiol. **172**: 1465–1479.

Van Roermund, C.W.T., Schroers, M.G., Wiese, J., Facchinelli, F., Kurz, S., Wilkinson, S., Charton, L., Wanders, R.J.A., Waterham, H.R., Weber, A.P.M., and Linka, N. (2016). The peroxisomal NAD carrier from Arabidopsis imports NAD in exchange with AMP. Plant Physiol. **171**: 2127–2139.

Schippers, J.H.M., Nunes-Nesi, A., Apetrei, R., Hille, J., Fernie, A.R., and Dijkwel, P.P. (2008). The Arabidopsis onset of leaf death5 mutation of quinolinate synthase affects nicotinamide adenine dinucleotide biosynthesis and causes early ageing. Plant Cell **20**: 2909–2925.

de Souza Chaves, I. et al. (2019). The mitochondrial NAD^+ transporter (NDT1) plays important roles in cellular NAD^+ homeostasis in *Arabidopsis thaliana*. Plant J. **100**: 487–504.

Takahashi, H., Takahara, K., Hashida, S.N., Hirabayashi, T., Fujimori, T., Kawai-Yamada, M., Yamaya, T., Yanagisawa, S., and Uchimiya, H. (2009). Pleiotropic modulation of carbon and nitrogen metabolism in Arabidopsis plants overexpressing the NAD kinase2 gene. Plant Physiol. **151**: 100–113.

Toleco, M.R., Naake, T., Zhang, Y., Heazlewood, J.L., and Fernie, A.R. (2020). Plant mitochondrial carriers: Molecular gatekeepers that help to regulate plant central carbon metabolism. Plants **9**: 117.

Weber, A.P.M. and Fischer, K. (2007). Making the connections - The crucial role of metabolite transporters at the interface between chloroplast and cytosol. FEBS Lett. **581**: 2215–2222.

Wei, M., Zhuang, Y., Li, H., Li, P., Huo, H., Shu, D., Huang, W., and Wang, S. (2019). The cloning and characterization of hypersensitive to salt stress mutant, affected in quinolinate synthase, highlights the involvement of NAD in stress-induced accumulation of ABA and proline. Plant J.: 0–2.

Chapter 1: Nicotinamide adenine dinucleotide dynamics modulate stomatal development in an abscisic acid-dependent manner

Elias Feitosa-Araujo[1], Paula da Fonseca Pereira[1], Mateus Miranda Pena[1], David Barbosa Medeiros[2], Leonardo Perez de Souza[2], Andreas P.M. Weber[3], Wagner L. Araújo[1], Alisdair R. Fernie[2], Markus Schwarzländer[4], Adriano Nunes-Nesi[1]

[1] Departamento de Biologia Vegetal, Universidade Federal de Viçosa, 36570-900 Viçosa, Minas Gerais, Brazil
[2] Max-Planck-Institute of Molecular Plant Physiology Am Mühlenberg 1, 14476 Potsdam-Golm, Germany
[3] Department of Plant Biochemistry, Heinrich Heine University Düsseldorf, 40225, Düsseldorf, Germany.
[4] Institute for Plant Biology and Biotechnology, University of Münster, Schlossplatz 8, D-48143 Münster, Germany

*Correspondence:

Adriano Nunes-Nesi
Departamento de Biologia Vegetal,
Universidade Federal de Viçosa,
36570-900 Viçosa, Minas Gerais, Brazil
Phone: +55-31-3612-5357
Email: nunesnesi@ufv.br

ABSTRACT

Nicotinamide adenine dinucleotide (NAD^+) plays a central role in redox metabolism across the kingdoms of life. Additional roles in posttranslational protein modification and cell signaling have become apparent more recently, implicating NAD^+ as a potential integrator between central metabolism and programs regulating stress responses and development. Here we found that NAD^+ negatively regulates stomatal development in cotyledons of *Arabidopsis thaliana*. Plants with reduced capacity for NAD^+ transport from the cytosol into the mitochondria or the peroxisomes exhibited reduced numbers of stomata lineage cells and reduced stomatal density. Cotyledons of plants with reduced NAD^+ breakdown capacity and NAD^+-treated cotyledons also presented reduced stomatal number. Expression of stomatal lineage-related genes was repressed in plants with reduced expression of NAD^+ transporters as well as in plants treated with NAD^+. Impaired NAD^+ transport was further associated with an induction of abscisic acid (ABA)-responsive genes. Inhibition of ABA synthesis rescued the stomatal phenotype in mutants deficient in intracellular NAD^+ transport, whereas exogenous NAD^+ feeding of *aba-2* and *ost1* seedlings, impaired in ABA synthesis and ABA signaling respectively, did not impact stomatal number. Additionally, *in vivo* measurement of ABA dynamics in seedlings of an ABA-specific optogenetic reporter - ABAleon2.1 treated with NAD^+ showed increases in ABA content suggesting that NAD^+ impacts on stomatal development through ABA synthesis and signaling. Our results demonstrate that intracellular NAD^+ homeostasis as set by synthesis, breakdown and transport is essential for normal stomatal development, and provide a link between central metabolism and developmental plasticity.

Key words: Arabidopsis; Stomatal development; NAD^+ metabolism; NAD^+ transport; ABA

INTRODUCTION

Nicotinamide adenine dinucleotide (NAD^+) and its phosphorylated derivative nicotinamide adenine dinucleotide phosphate ($NADP^+$) coenzymes are of pivotal importance for a wide range of reduction-oxidation (redox) reactions (Barron et al., 2000; Noctor et al., 2006; Takahashi et al., 2009; Gakière et al., 2018). Besides playing a key role as a redox carrier, NAD^+ also participates in a myriad of intracellular signaling processes by serving as substrate for several regulatory proteins (Kulkarni and Brookes, 2019; Strømland et al., 2019). This includes processes related to calcium homeostasis (Guse, 2015; Pétriacq et al., 2016a), defense regulatory hormones (Pétriacq et al., 2016b), DNA damage repair (Briggs and Bent, 2011), and cell cycle regulation (Demarest et al., 2019). Remarkably, recent studies have demonstrated that alterations in the levels of NAD^+ itself may act as a signal and affect the pools of metabolites and/or the expression of genes involved in cellular homeostasis and stress tolerance (Gakière et al., 2018). In view of the duality of NAD^+ as a redox carrier in central metabolic reactions and a signal molecule, the manipulation of NAD^+ metabolism can, therefore, exert a prominent role in diverse biological processes.

Given the importance of NAD^+, the precise intracellular partitioning of the cellular NAD(P) pool is critical (Strømland et al., 2019; Kulkarni and Brookes, 2019). In fact, the ratio of NAD^+ to its counterpart $NADP^+$ is highly compartmentally dependent, and thus compartmentation simplifies the cellular roles of NAD^+ (Kulkarni and Brookes, 2019). In plants, specialized transport proteins are responsible for the provision of NAD^+ to the cellular organelles (Palmieri et al., 2009; Bernhardt et al., 2012; Gakière et al., 2018; de Souza Chaves et al., 2019). Two carrier proteins located in the inner mitochondrial membrane, namely NDT1 (*At*2g47490) and NDT2 (*At*1g25380), and one targeted to the peroxisomal membrane, PXN (*At*2g39970), have been previously identified and biochemically characterized as NAD^+ transporters in Arabidopsis (Palmieri et al., 2009; Agrimi et al., 2012; Bernhardt et al., 2012; Van Roermund et al., 2016; de Souza Chaves et al., 2019). Analyses of the corresponding single mutants showing reduced expression of *NDT1* (de Souza Chaves et al., 2019), *NDT2* (Feitosa-Araujo et al., 2020) and *PXN* (Bernhardt et al., 2012) demonstrated that changes in the NAD^+ transport can, by altering NAD^+ homeostasis, influence several different cellular processes.

Indeed, NAD^+ homeostasis has been found to affect both plant growth and development (Noctor et al., 2006; Hashida et al., 2009; Noctor and Foyer, 2016). Functional characterization of genes of the *de novo* biosynthesis and salvage pathways of NAD^+ has pinpointed the importance of this metabolite in underpinning a range of developmental processes. These processes comprise, among others, pollen grain viability and pollen tube growth (Hashida et al., 2007), germination (Hunt et al., 2007), stomatal movement (Hashida et al., 2010), leaf senescence (Schippers et al., 2008) and flowering (Liu et al., 2009). Despite the large number of studies indicating an important role of NAD^+ metabolism and transport in biochemical processes and metabolism, the links between NAD^+ and the regulation of developmental processes remain poorly defined. This is partly due to the central position of NAD^+ in metabolism and signaling, meaning that any major disruption can be expected to result in the impairment of several downstream processes, leading to pleiotropy, which makes it difficult to assign specific roles directly to changes in NAD^+ levels.

Recently, the functional characterization of two Arabidopsis lines exhibiting reduced expression of the genes encoding mitochondrial NAD^+ carriers indicated that, among the cellular processes affected by impaired NAD^+ transport, are aspects related to the stomata function (de Souza Chaves et al., 2019). Accordingly, plants exhibiting reduced expression of either *NDT1* or *NDT2* displayed reductions in both stomatal conductance (g_s) and density (de Souza Chaves et al., 2019). These data demonstrated that NAD^+ transport mediated by NDT1 and NDT2 appears to play an important role in cellular events related to the control of stomatal development. Therefore, further investigation should be performed to understand how plant NAD^+ dynamics coordinates changes in endogenous signals to mediate stomatal formation in Arabidopsis.

The development of stomata, epidermal pores facilitating gas exchange, shows considerable plasticity (Lee and Bergmann, 2019) and can be modulated by both endogenous signals and environmental factors. As such, the number and distribution of stomata is regulated by multiple environmental stimuli, including light (Kang et al., 2009; Lee et al., 2017), water availability (Yoo et al., 2019), temperature (Lau et al., 2018) and CO_2 (Engineer et al., 2014). Moreover, plant hormones also appear to underpin this developmental plasticity. In this respect, the involvement of a considerable number of plant hormones has been suggested including abscisic acid

(ABA), gibberellins, auxins, brassinosteroids, ethylene and jasmonate (Tanaka et al., 2013; Saibo et al., 2003; Balcerowicz et al., 2014; Gudesblat et al., 2012; Kim et al., 2012; Han et al., 2018; González et al., 2017).

Each stage of stomatal development from the protodermal cell differentiation to a mature stoma is precisely controlled. The major steps of stomatal development are well characterized in *A. thaliana*, starting with the asymmetric division of a meristemoid mother cell (MMC) to give rise to a meristemoid. The meristemoid in turn undergoes several asymmetric divisions prior to differentiation into a guard mother cell (GMC). Subsequently, the GMC performs a symmetrical division, forming the pair of juxtaposed guard cells of the stomata (Bergmann and Sack, 2007; Pillitteri and Torii, 2007, 2012; Simmons and Bergmann, 2016; Lee and Bergmann, 2019).

The coordinated action of a set of transcriptional regulators is also essential for stomatal initiation and progression. The basic helix–loop–helix (bHLH) transcription factors SPEECHLESS (SPCH), MUTE and FAMA are the major regulators of stomatal biogenesis (Ohashi-Ito and Bergmann, 2006; MacAlister et al., 2007; Pillitteri and Torii, 2007). SPCH promotes the entry into the stomatal lineage leading to a differentiation of protodermal cells into MMC and the subsequently meristemoid production (Lampard et al., 2008; Lau et al., 2014). Posteriorly, MUTE is required to regulate the transition from meristemoid to GMC (Pillitteri et al., 2007). The final cell division, the symmetric division of a GMC into the guard cells, is regulated by the action of FAMA (Ohashi-Ito and Bergmann, 2006; Lee et al., 2014; Matos et al., 2014). To efficiently play their function and regulate target genes, the bHLH transcription factors SPCH, MUTE and FAMA heterodimerize with two other bHLH transcription factors, called INDUCER OF CBP EXPRESSION 1/SCREAM (ICE1/SCRM) and SCREAM2 (SCRM2) (Kanaoka et al., 2008). All five transcription factors are critical for regular stomatal biogenesis, which is severely affected in the respective mutants. Furthermore, several studies have shown the participation of additional factors regulating stomatal development, including EPIDERMAL PATTERNING FACTORS 1 and 2 (EPF1, EPF2) (Hara et al., 2007; Hunt and Gray, 2009b), STOMAGEN (STOM) (Sugano et al., 2010; Hunt et al., 2010), STOMATAL DENSITY AND DISTRIBUTION1 (SDD1) (Von Groll et al., 2002), CO_2 RESPONSE SECRETED PROTEASE (CRSP) (Berger and Altmann, 2000), MITOGEN-ACTIVATED PROTEIN KINASE (MAPK) (Bergmann et al., 2004; Wang et al., 2007; Lampard et al., 2008), TOO MANY MOUTHS (TMM) (Yang Ming and Sack,

1995; Nadeau and Sack, 2002) and ERECTA (ER), ERECTA-LIKE1 (ERL1), ERECTA-LIKE2 (ERL2) (Shpak et al., 2003, 2005; Masle et al., 2005).

The information above collectively confirms that the formation and distribution of stomata are tightly regulated processes. Research over the last decades has considerably advanced our understanding of the cellular and molecular mechanisms for stomatal development (Lee and Bergmann, 2019). From these studies, new components regulating stomatal fate and pattern have gradually been identified. Here, we used Arabidopsis cotyledons as a model to dissect the roles of cellular NAD^+ homeostasis as a potential new component of stomatal development. For this purpose, we evaluated stomatal development in plants showing reduced NAD^+ transport capacity into either mitochondrion (*NDT1* and *NDT2* mutants) or peroxisome (*PXN* mutants). Moreover, we also evaluated NAD^+-treated WT seedlings alongside corresponding mutants of the three isoforms of the NAD^+-consuming enzymes poly(ADP-ribose)polymerase (PARP) of Arabidopsis. The idea behind this approach was manipulate cellular NAD^+ dynamics to disturb intracellular NAD^+/NADH homeostasis. Our observations consistently point to the induction of ABA synthesis as a dominating effect of compromised NAD^+ dynamics as a link between subcellular NAD^+ compartmentation and stomatal development in Arabidopsis.

RESULTS

NAD^+ carriers and NAD^+ biosynthesis genes are highly expressed in guard cells

Given our current interest in unravelling the cellular roles of NAD^+ homeostasis in stomatal development, we first performed a meta-analysis of publicly available transcriptome data. Notably, we observed a differential expression of NAD^+ biosynthesis genes and NAD^+ carrier genes between leaves and guard cells (http://bar.utoronto.ca) (Supplemental Figure 1). To further test this observation, we analyzed patterns of NAD^+-related transcripts from whole leaf extracts and isolated epidermis fragments (which are strongly enriched in guard cells) by quantitative real-time PCR (qRT-PCR). In agreement with the microarray data, the expression of all genes belonging to *de novo* and salvage pathways of NAD^+ biosynthesis alongside the NAD^+ carrier genes were more abundant in the epidermal fragments as compared to that in whole leaves (Supplemental Figure 1). This observation indicates a prominent role of NAD^+ in guard cells.

NAD^+ transport into mitochondria and peroxisomes impacts stomatal development

To shed light on the role that intracellular NAD^+ carriers play in stomatal development, we used the homozygous T-DNA lines for *NDT1* and *NDT2* as well as the peroxisomal carrier *PXN-1*. We used cotyledons as a model analyzing their epidermal composition by bright-field microscopy at 4 and 8 days after sowing. Interestingly, decreased expression of NAD^+ carrier genes correlated with decreased stomatal numbers as compared to control plants, indicating perturbed stomatal development (Figure 1A). A detailed analysis revealed that both number and index of meristemoids (Figure 1B and 1C) were reduced in the mutant lines at day 4. Additionally, number and index of GMCs were increased in all evaluated mutant lines (Figure 1D and 1E). The mutants also displayed a decreased number and index of mature stomata (Figure 1F and 1G). Consequently, the sum of meristemoids, GMCs and stomata per area and the index of the sum were both reduced in mutant lines (Supplemental Figure 2A and 2B), which led to a diminished potential to form stomata (Supplemental Figure 2C). By contrast, the number of pavement cells per area was significantly lower only for *pxn-1* line at day 4 and 8 (Supplemental Figure 2D). Yet, when the number of pavement cells were divided by the total cell number, the mutants showed an increased pavement cell index (Supplemental Figure 2E), mirroring the reduced stomatal density. Even though the NAD^+ carrier mutants displayed disturbance in stomatal development, the one-cell-spacing rule (at least one pavement cell between two adjacent stomata) (Wang et al., 2007) was not affected in these lines. Altogether, these data corroborate our proposal of a link between intracellular NAD^+ transport and/ or partitioning and stomatal number.

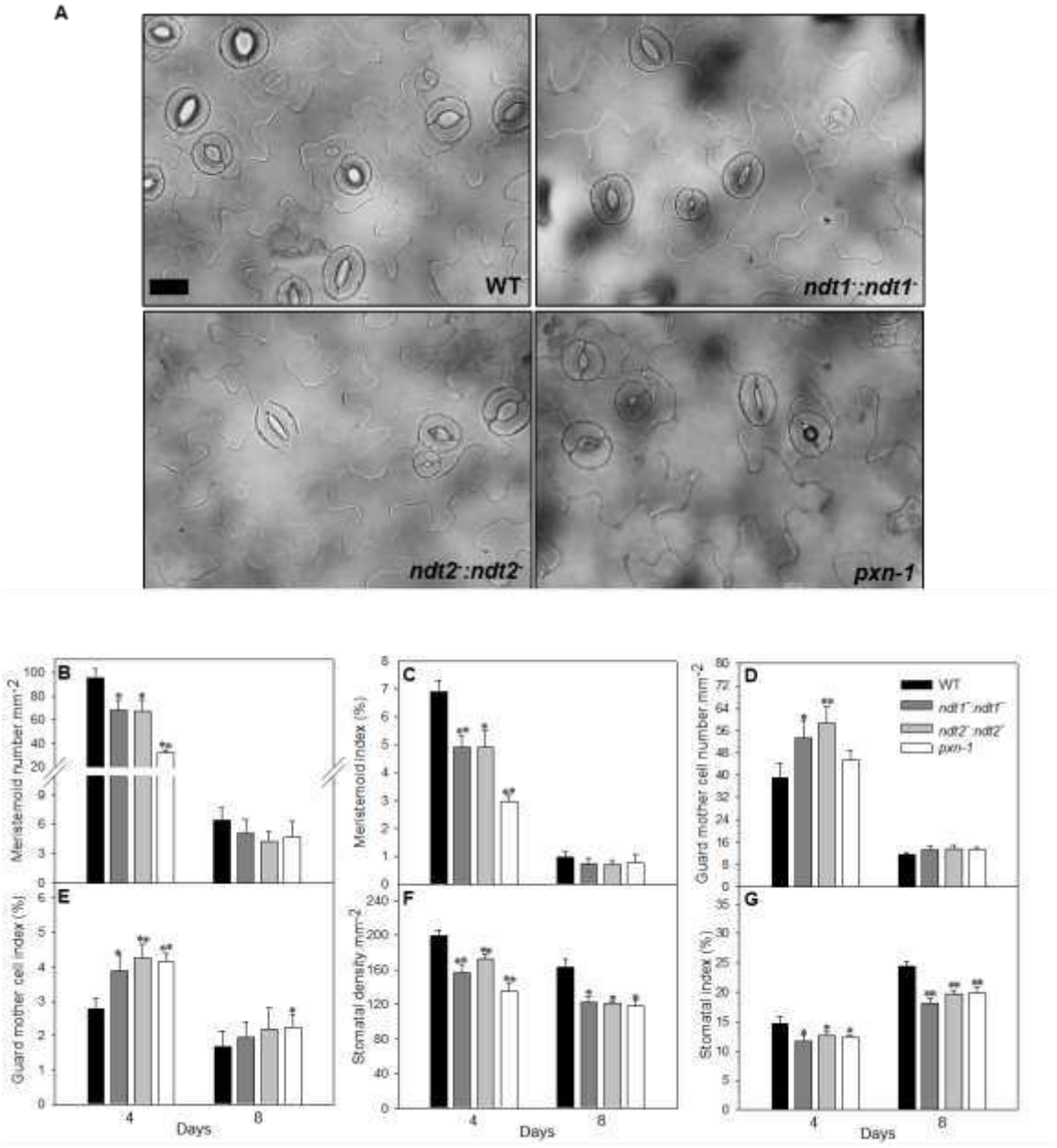

Figure 1: NAD⁺ transport into mitochondria and peroxisomes impacts stomatal development in *Arabidopsis thaliana* cotyledons.

Abaxial epidermal layer of cotyledons were photographed at 4 and 8 days after sowing on soil and analyzed by optical microscopy. **A)** Epidermal composition in cotyledons of Arabidopsis lines with decreased expression of organellar NAD⁺ transporter (*NDT1, NDT2* and *PXN*). Scale bar = 20 µm **B)** Meristemoid number.mm^{-2}, **C)** Meristemoid index, **D)** Guard mother cell number.mm^{-2}, **E)** Guard mother cell index, **F)** Stomatal density, **G)** Stomatal index. Values are presented as means ± SE (n=12). Asterisks represents values that were judged to be significantly different from the WT (*$p < 0.05$, **$p < 0.01$). WT: black bars, *ndt1^{-}:ndt1^{-}* : dark gray bars, *ndt2^{-}:ndt2^{-}*: gray bars and *pxn-1*: white bars.

Reduced expression of NAD+ transporter genes affects stomata and pavement cell sizes

To further understand the influence of impaired organellar NAD+ dynamics on epidermal and guard cell development, we investigated the biometrical parameters of stomata and pavement cells at further depth. Stomatal areas and stomatal length of *ndt1-:ndt1-* and *pxn-1* were increased compared to WT at day 4 while at day 8 only *ndt1-:ndt1-* and *ndt2-:ndt2-* displayed higher increases in these parameters (Table 1). Further, *ndt1-:ndt1-* and *ndt2-:ndt2-* showed increases in pavement-cell area, length and width, while *pxn-1* line demonstrated a reduction of these parameters compared with their WT counterparts at day 8 (Table 1).

	4 days			
	WT	*ndt1-:ndt1-*	*ndt2-:ndt2-*	*pxn-1*
Stomatal area (mm2)	265.46 ± 10.42	**300.15 ± 9.72**	277.48 ± 2.01	**304.51 ± 13.36**
Stomatal length (µm)	20.00 ± 0.46	**21.21 ± 0.12**	19.73 ± 0.34	**21.27 ± 0.33**
Pavement cell area (µm²)	1257.4 ± 53.3	**1112.9 ± 15.8**	**1408.3 ± 31.6**	**1506.4 ± 43.6**
Pavement cell length (µm)	56.9 ± 1.9	**47.4 ± 0.7**	58.8 ± 1.4	**64.5 ± 1.4**
Pavement cell width (µm)	19.6 ± 0.8	18.0 ± 0.7	21.0 ± 0.5	20.9 ± 0.4

	8 days			
	WT	*ndt1-:ndt1-*	*ndt2-:ndt2-*	*pxn-1*
Stomatal area (mm2)	346.54 ± 8.92	**390.73 ± 14.85**	**398.45 ± 12.20**	325.43 ± 5.06
Stomatal length (µm)	23.02 ± 0.16	**24.66 ± 0.25**	**24.94 ± 0.53**	23.07 ± 0.46
Pavement cell area (µm²)	2840.7 ± 124.0	**3725.4 ± 114.4**	**4192.2 ± 279.3**	**2290.9 ± 81.1**
Pavement cell length (µm)	91.2 ± 2.7	**104.6 ± 2.2**	**113.7 ± 5.8**	**75.5 ± 2.2**
Pavement cell width (µm)	31.6 ± 0.8	**40.9 ± 0.7**	**42.7 ± 1.8**	**24.5 ± 0.5**

Table I: Reduced expression of NAD+ transporter genes affects stomata and pavement cell sizes.
Cotyledons of WT and NAD+ carrier mutants were photographed at 4 and 8 days after sowing and had their abaxial surfaces analyzed by optical microscopy. Measurements were performed in 500 stomata and 500 pavement cells per genotype. Values are means ± SE (n = 12) and significant differences between WT and mutants, using Student's t-test, are indicated by bold numbers.

NAD+ distribution affects gene expression of stomatal biogenesis regulators

Since stage switches during stomatal development require precise transcriptional control (Simmons and Bergmann, 2016) and considering the reduced potential to form stomata exhibited by NAD+ carrier mutants, we next evaluated whether the expression of key genes related to stomatal biogenesis was affected for these mutations. For this purpose, quantitative real-time PCR (qRT-PCR) analysis was performed in seedlings harvested at 2, 4 and 8 days after sowing (Figure 2). Only transcriptional behavior of genes previously documented to be involved in stomatal biogenesis was evaluated, included that of *EPF1, EPF2, ERECTA, ERECTA LIKE 1, ERECTA LIKE 2, TMM, SCRM/1, SCRM2, SPCH, MUTE, FAMA* and *SDD1* (for further

details, see “Materials and Methods” and Supplemental Table 1). The results for mutant lines were compared with their respective WT at each time point. Down regulation in the expression of *SPCH* was observed for the three mutants at day 4 (Figure 2A) while only *ndt1⁻:ndt1⁻* and *pxn-1* lines displayed a reduced expression of the *MUTE* gene at this stage (Figure 2B). By contrast to the expression pattern of *SPCH*, the transcript abundance of *FAMA* were higher in *ndt1⁻:ndt1⁻* and *ndt2⁻:ndt2⁻* lines at day 4 (Figure 2C). In respect to the expression of *SCRM1/ICE1* gene at day 4, up-regulation was observed for *ndt1⁻:ndt1⁻* and *ndt2⁻:ndt2⁻* while decreased expression was found for *pxn-1* line (Figure 2D). Similarly, when the expression of *SCRM2* was assessed, it was demonstrated that higher gene expression took place at days 2 and 4 for *ndt1⁻:ndt1⁻* and *ndt2⁻:ndt2⁻* lines (Figure 2E). The relative transcript abundance of *EPF1* gene decreased for *ndt1⁻:ndt1⁻* line at day 2, while higher *TMM* expression was observed in *ndt2⁻:ndt2⁻* line at day 4 (Figure 2F and 2G). Concerning the expression of *EPF2*, major changes were observed at days 4 and 8, where a significant increase in the expression of this gene was observed (Figure 2H). The expression analysis of the *SDD1* gene demonstrated its up-regulation at day 4 for *ndt1⁻:ndt1⁻* and *ndt2⁻:ndt2⁻* lines (Figure 2I). Transcript abundance of genes belonging to the ERECTA family of receptor kinases was evaluated. The results showed that the *ER* gene had their relative transcript abundance augmented in *ndt1⁻:ndt1⁻* and *ndt2⁻:ndt2⁻* lines at day 4, while increases were only observed for *ndt1⁻:ndt1⁻* and *pxn-1* at day 8 (Figure 2J). Similarly, the *ERL1* gene displayed increments in its transcript abundance for *ndt1⁻:ndt1⁻*, *ndt2⁻:ndt2⁻* and *pxn-1* at day 4 and only for *ndt1⁻:ndt1⁻* and *pxn-1* at day 8 (Figure 2K). On the other hand, the *ERL2* gene demonstrated to have an early increment in its transcript abundance for *ndt2⁻:ndt2⁻* and *pxn-1* at day 2 and an increased expression for *ndt1⁻:ndt1⁻* and *ndt2⁻:ndt2⁻* lines at day 4 (Figure 2L). These results suggest that the efficient NAD^+ transport across organelle membranes are important to regulate the gene expression of stomatal developmental related genes.

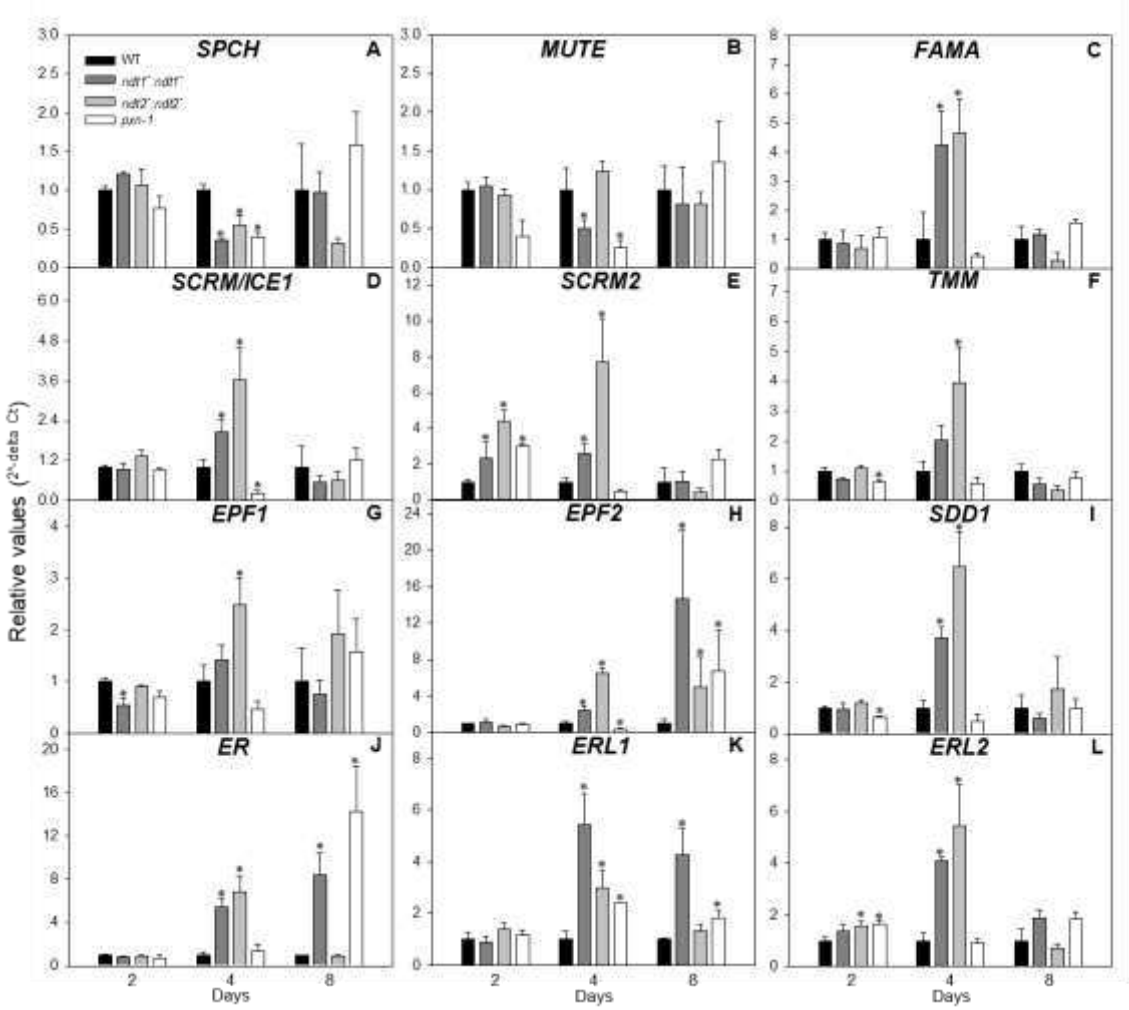

Figure 2: Gene expression analysis of stomata biogenesis-related genes in seedlings of *Arabidopsis thaliana* carrying mutations in NAD$^+$ transporters from mitochondria and peroxisomes.

Relative abundance of transcripts was determined for genes related to stomatal biogenesis: **A)** *SPCH*, **B)** *MUTE*, **C)** *FAMA*, **D)** *SCRM/ICE1*, **E)** *SCRM2/ICE2*, **F)** *TMM*, **G)** *EPF1*, **H)** *EPF2*, **I)** *SDD1*, **J)** *ER*, **K)** *ERL1* and **L)** *ERL2*. Total RNA was extracted from seedlings at 2, 4 and 8 days after sowing on soil. Actin was used as endogenous control. Values are compared with the WT of each time point and presented as means ± SE (n=4). Significant differences between WT and mutants, using Student's t-test, are indicated by asterisks * (*$p < 0.05$; ** $p < 0.01$). Abbreviations: EPF1 - epidermal patterning factor; EPF2 – epidermal factor 2; TMM: too many mouths; SPCH – SPEECHLESS; SDD1 – stomatal density and distribution 1; ER – ERECTA; ERL1 – ERECTA like 1; and ERL2 – ERECTA like 2. WT: black bars, *ndt1$^-$:ndt1$^-$* : dark gray bars, *ndt2$^-$:ndt2$^-$*: gray bars and *pxn-1*: white bars.

The reduced expression of NAD$^+$ transporter genes impacts NAD$^+$ homeostasis and stimulate up-regulation of superoxide responsive marker gene *ZAT12*

We next evaluated whether the reduced expression of genes encoding NAD$^+$ carriers would impact the expression of genes belonging to the *de novo* and salvage pathways for NAD$^+$ biosynthesis. To extend this molecular characterization, transcript abundance of *Aspartate oxidase (AO), Quinolinate synthase (QS), Quinolinate phosphoribosyltransferase (QPT), Nicotinamide mononucleotide adenylyltransferease (NMNAT), NAD synthetase (NADS), Poly(ADP-ribose)polymerase 1 (PARP1), Poly(ADP-ribose)polymerase 2 (PARP2), Nudix hydrolase 7 (NUDIX7), Nicotinamidase 1 (NIC1), Nicotinamidase 4 (NIC4), Nicotinate phosphoribosyltransferase 1 (NaPRT1), Nicotinate phosphoribosyltransferase 2 (NaPRT2), NAD kinase 1 (NADK1), NAD kinase 2 (NADK2)* and *NAD kinase 3 (NADK3)* was determined by quantitative real-time PCR (qRT-PCR) at 2, 4 and 8 days after sowing (Figure 3A). The transcript abundance of *Ao* was shown to be increased for *ndt2$^-$:ndt2$^-$* line at day 4 while *Qs* presented an up-regulation at day 4 for *ndt2$^-$:ndt2$^-$* and at day 8 for *ndt1$^-$:ndt1$^-$* and *ndt2$^-$:ndt2$^-$* lines. The transcript abundance of *QPT* was demonstrated to be augmented for *ndt1$^-$:ndt1$^-$* at day 2 and for *ndt2$^-$:ndt2$^-$* at day 4 and 8. The *NMNAT* expression was generally up-regulated in the mutants in comparison to WT levels in all evaluated time points. At day 8, transcript abundance of *NADS* was higher for all mutants, than their respective WTs. The transcript abundance of *PARP1* at day 4 was lower in all the mutants but higher at day 8 for all mutants than in the WT. Conversely, *PARP2* exhibited higher transcript abundance in mutant lines only at day 8, whereas *NUDIX7* displayed only minor changes in expression. *NIC1* and *NIC3* transcript abundance were consistently higher in mutant lines at day 8. The expression of *NaPRT1* and *NaPRT2* genes, was higher in the mutants at days 4 and 8 (Figure 3A). With the aim of investigating whether the compromised gene expression of NAD$^+$ transporters would also impact genes of NADP$^+$ biosynthesis, we also assessed the gene expression of NAD$^+$ kinases. Transcript abundance of both *NADK1* and *NADK2* were both increased in *ndt1$^-$:nd12$^-$* and *ndt2$^-$:ndt2$^-$* lines at days 2 and 4, whereas higher expression of *NADK3* was observed only at day 4. Looking at the transcript abundance of the transporters themselves revealed that *NDT1* expression showed minor changes, and was increased only at day 4 for *pxn-1* line. On the other hand, *NDT2* expression diminished in all mutant lines, except for *ndt1$^-$:ndt1$^-$* line at day 2.

Similarly, transcript abundance of *PXN* gene were consistently at a lower level in all mutant lines (Figure 3A, Supplemental Figure 4).

We next accessed the amount of pyridine nucleotides in the same samples (Figure 3B).

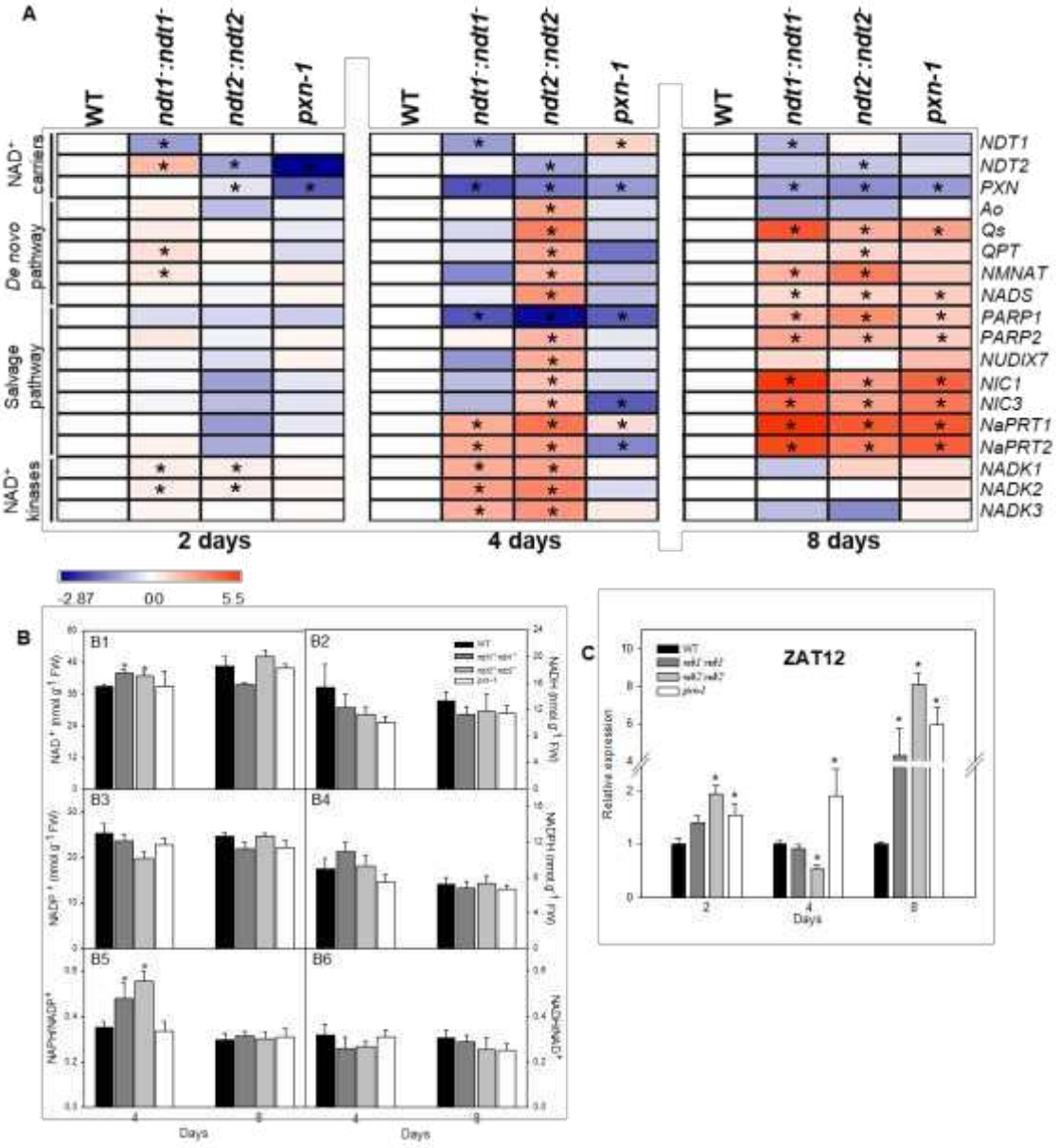

Figure 3: NAD⁺ transport affects the NAD⁺ homeostasis leading to oxidative stress

A) Transcript abundance of *Arabidopsis thaliana* NAD metabolism genes: *Nicotinamide adenine dinucleotide transporter 1 (NDT1), Nicotinamide adenine dinucleotide transporter 2 (NDT2), Peroxisomal nicotinamide adenine dinucleotide carrier (PXN), Aspartate oxidase (AO), Quinolinate synthase (QS), Quinolinate phosphoribosyltransferase (QPT), Nicotinamide mononucleotide adenylyltransferease (NMNAT), NAD synthetase (NADS)* and salvage pathway *Poly(ADP-ribose)polymerase 1 (PARP1), Poly(ADP-ribose)polymerase 2 (PARP2), Nudix hydrolase 7 (NUDIX7), Nicotinamidase 1 (NIC1), Nicotinamidase 3 (NIC3), nicotinate*

phosphoribosyltransferase 1 (NaPRT1), Nicotinate phosphoribosyltransferase 2 (NaPRT2), and *NAD kinases* (*NADK1, NADK2* and *NADK3*). RNA was isolated from seedlings at 2, 4 and 8 days after sowing on soil. Actin was used as endogenous control. **B)** Pyridine nucleotide content in seedlings. Samples of WT and NAD carrier mutant seedlings were collected at 4 and 8 days after sowing. Values are compared with the WT at each time point and presented as means SE (n=4, gene expression; n=5, pyridine nucleotide). **C)** Relative expression of *ZAT12* gene, a superoxide responsive gene. Asterisks indicate values that were determined by Student's t-test to be significantly different ($p < 0.05$) from wild type. WT: black bars, *ndt1⁻:ndt1⁻* : dark gray bars, *ndt2⁻:ndt2⁻*: gray bars and *pxn-1*: white bars.

Comparing to the WT of the same time point, the content of NAD^+ was higher in *ndt1⁻:ndt1⁻* and *ndt2⁻:ndt2⁻* lines at day 4, while no apparent changes in the other NAD^+ derivatives were observed (Figure 3B1). However, the deduced NADPH/$NADP^+$ ratio was increased in *ndt1⁻:ndt1⁻* and *ndt2⁻:ndt2⁻* suggesting that cellular redox balance has been disturbed in leaves of mutant plants showing reduced expression of mitochondrial NAD^+ transporters (Figure 3B5). Given that both the expression of genes belonging to NAD^+ salvage pathway and levels of NAD^+ itself increased in the mutant lines, and considering the important role of NAD^+ for the cellular redox state in plants (Noctor et al., 2006), we next evaluated the expression of the superoxide marker gene *Zinc-Finger Protein 12* (ZAT12) (Xu et al., 2017) as a mean to provide an indirect detection of reactive oxygen species (ROS) accumulation (Mehterov et al., 2012; Gadjev et al., 2006). Interestingly, the expression of *ZAT12* was higher in mutant lines (Figure 3C), suggesting that inefficient NAD^+ uptake into organelles may lead to the activation of stress signaling pathways that lead to ROS generation (Choudhury et al., 2017).

The reduced stomatal density in NAD^+ carrier mutants is linked to ABA metabolism

It is known that altered expression of genes involved with ABA metabolism impacts the number of stomatal cells (Tanaka et al., 2013). The role played by ABA during stomatal development is mainly due to its ability to inhibit the entry into stomatal-lineage cells. The functional characterization of *NDT1* and *NDT2* mutants showed that these plants exhibit a reduced seed germination, a phenotype related to ABA (de Souza Chaves et al., 2019). Furthermore, NAD(P)(H) has been associated with ABA biosynthesis and signaling processes (Arias et al., 2018; Wei et al., 2019; Hunt and Gray, 2009a). Taken together, these facts lead us to hypothesize that the altered subcellular NAD^+ compartmentation in the mutants under study could be leading to

changes in the metabolism of ABA, which could possibly help to explain the reduced stomatal density found in the NAD^+ transport mutants. In order to test this hypothesis, we first assessed the expression of two genes encoding enzymes for ABA biosynthesis (ABA1, ABA2), that are sensitive to processes involving NAD(P)(H). Both *ABA1* and *ABA2* genes presented higher expressions in NAD^+ carrier mutants (Figure 4A1 and 4A2, respectively). Next, the expression of the ABA-responsive genes *ABF3, RD29A, RD29B* and *ICK1*, was measured. All of them were up-regulated in the mutant lines after 2 days in the light (Figure 4A3, 4A4, 4A5 and 4A6), which suggests a higher internal ABA content or enhanced ABA signaling in the NAD^+ transport mutants than in WT seedlings. Furthermore, analysis comprising genes of ABA and NAD^+ metabolism along with genes belonging to stomatal development demonstrated that these genes are co-expressed (Figure 4B). To verify whether exogenous ABA would affect stomatal density in NAD^+ carrier mutants, we grew the seedlings in medium containing 1µM of ABA for 8 days. The stomatal density decreased in WT seedlings, but in all NAD^+ carrier mutants it remained unchanged compared to the control condition (Figure 4C). We subsequently analyzed stomatal density of WT and mutant lines on medium with norflurazon, an inhibitor that prevents ABA production. As shown in Figure 4C, no differences among them were observed after norflurazon treatment, demonstrating that NAD^+ carrier mutant lines were able to produce stomata as efficiently as the WT under this condition. Surprisingly, the ABA content was unaltered among the lines and WT plants (Figure 4D), suggesting that the mutant plants are more sensitive to the internal ABA content. It has been shown that ADP-ribosyl cyclases use NAD^+ as substrate to produce cyclic ADP ribose (cADPR) which can in turn lead to increases in the concentration of cytosolic free Ca^{2+} (Hetherington and Brownlee, 2004b; Zhang and Li, 2006). Since the levels of cytosolic Ca^{2+} may influence ABA signaling (Webb et al., 2001; Siegel et al., 2009), we assessed the expression of two Ca^{2+}-responsive genes described by Whalley et al. (2011) in order to verify whether NAD^+ transporter mutants would present a differential ABA response based on Ca^{2+} signaling.

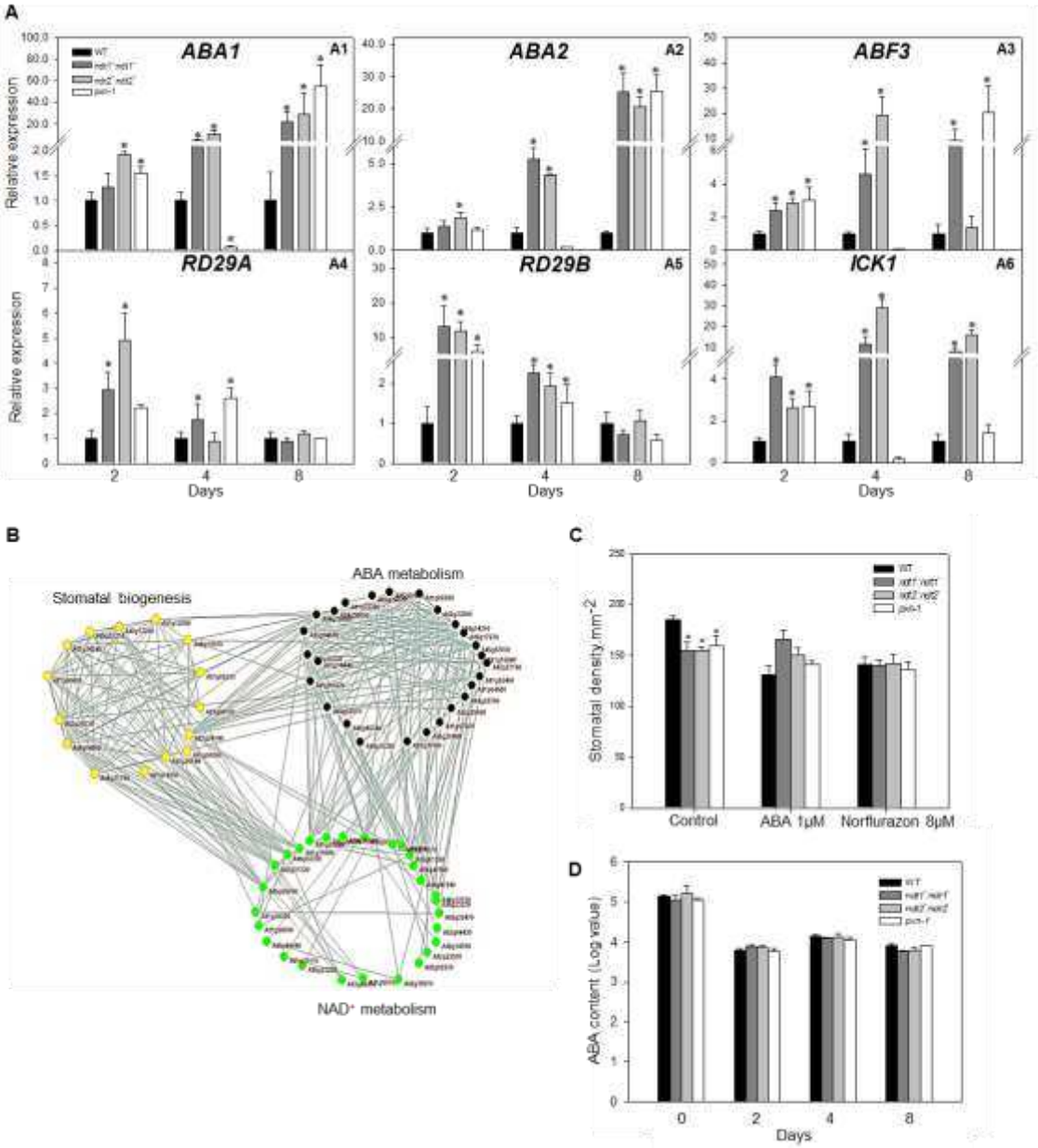

Figure 4: A crosstalk between NAD⁺ transport and ABA metabolism may have an influence on stomatal number in NAD⁺ carrier mutants.
A) Gene expression analysis of genes responsive to internal concentrations of ABA (*ABF3, RD29A, RD29B, ICK*) and two genes of ABA biosynthesis pathway (*ABA1* and *ABA2*). **B)** Co-expression analysis of genes belonging to NAD⁺ and ABA metabolism and genes related to stomatal biosynthesis using Pajek software. Transcriptional data was performed using coexpression PRIMe database using as trap genes listed in supplementary table. **C)** Stomatal density in 8 days-old seedlings treated with ABA and Norflurazon (ABA biosynthesis inhibitor). **D)** ABA measurement in dry seeds and seedlings at 2, 4 and 8 days after germination. Asterisks demarcate values that were judged to be significantly different from the WT ($p < 0.05$).

The expression of *At*1g02400 and *At*1g01470 was shown to be up-regulated at 2 and 8 days in *ndt2⁻:ndt2⁻* line, while significantly increased expression in the three mutants lines was observed only for the gene *At*1g01470 at day 8 (Supplemental

Figure 4). Furthermore, RD29A, RD29B and ABF3 have been described as possible candidates in Ca^{2+}-mediated signaling pathways and as shown in Figure 4A they displayed increased expression in all mutant lines (Galon et al., 2010). Together these results provide evidence that NAD^+ carrier mutant lines are more sensitive to internal levels of ABA must probably due to an enhanced sensitivity of ABA signaling.

Cotyledons of plants with reduced NAD^+ breakdown capacity and NAD^+-treated cotyledons present reduced stomatal density

Since NAD^+ carrier mutants presented reduced stomatal density, we decided to verify whether NAD^+ itself would be able to impact stomatal development. Firstly, WT seedlings were grown for 8 days in a medium containing 2.5 mM of NAD^+, period after which was verified that the levels of endogenous NAD^+ were significantly higher in NAD^+ treated seedlings in comparison with the untreated ones (Figure 5A). We next grew plants carrying the fluorescent sensor of the cytosolic NADH/NAD^+ redox state, Peredox-mCherry (Hung et al., 2011) on MS medium containing 1.5 mM of NAD^+. According to our results, the seedlings expressing the Peredox-mCherry sensor exhibited a more reduced state when grown in the medium with NAD^+ compared to the ones grown in the control medium without NAD^+, which implies that NAD^+ was able to enter their cells and influence the internal NAD(H) homeostasis (Figure 5B and Supplemental Figure 5A). To verify a possible influence of NAD^+ on stomatal density, we grew seedlings of WT and NAD^+ carrier mutants on MS media with three different NAD^+ concentrations (0.5, 1.5 and 2.5 mM). Notably, reduced stomatal density was observed in NAD^+-treated WT seedlings independently of the NAD^+ concentration applied, compared to untreated WT seedlings (Figure 5C). By contrast, seedlings carrying mutation in NAD^+ transporters were shown to be insensitive to NAD^+ application in terms of stomatal development (Supplemental Figure 6).

PARP genes encode enzymes responsible for recycling NAD^+ and belong to the salvage pathway of NAD^+ biosynthesis as well as playing an important role in DNA repair. We hypothesized that PARP mutants may have a dysfunctional NAD^+ homeostasis that could lead to a negative impact in stomatal number. Aiming to evaluate whether PARP silenced lines, which are unable to efficiently breakdown NAD^+, would exhibit altered stomatal development, we decided to quantify the stomatal number in previously described *PARP1, PARP2* and *PARP3* mutants (Pham et al.,

2015). Indeed, cotyledons of *PARP* mutants displayed a reduced stomatal density (Figure 5D). Thus, these results suggest that NAD^+ transport, metabolism and the total NAD pool are important in the regulation of stomatal number.

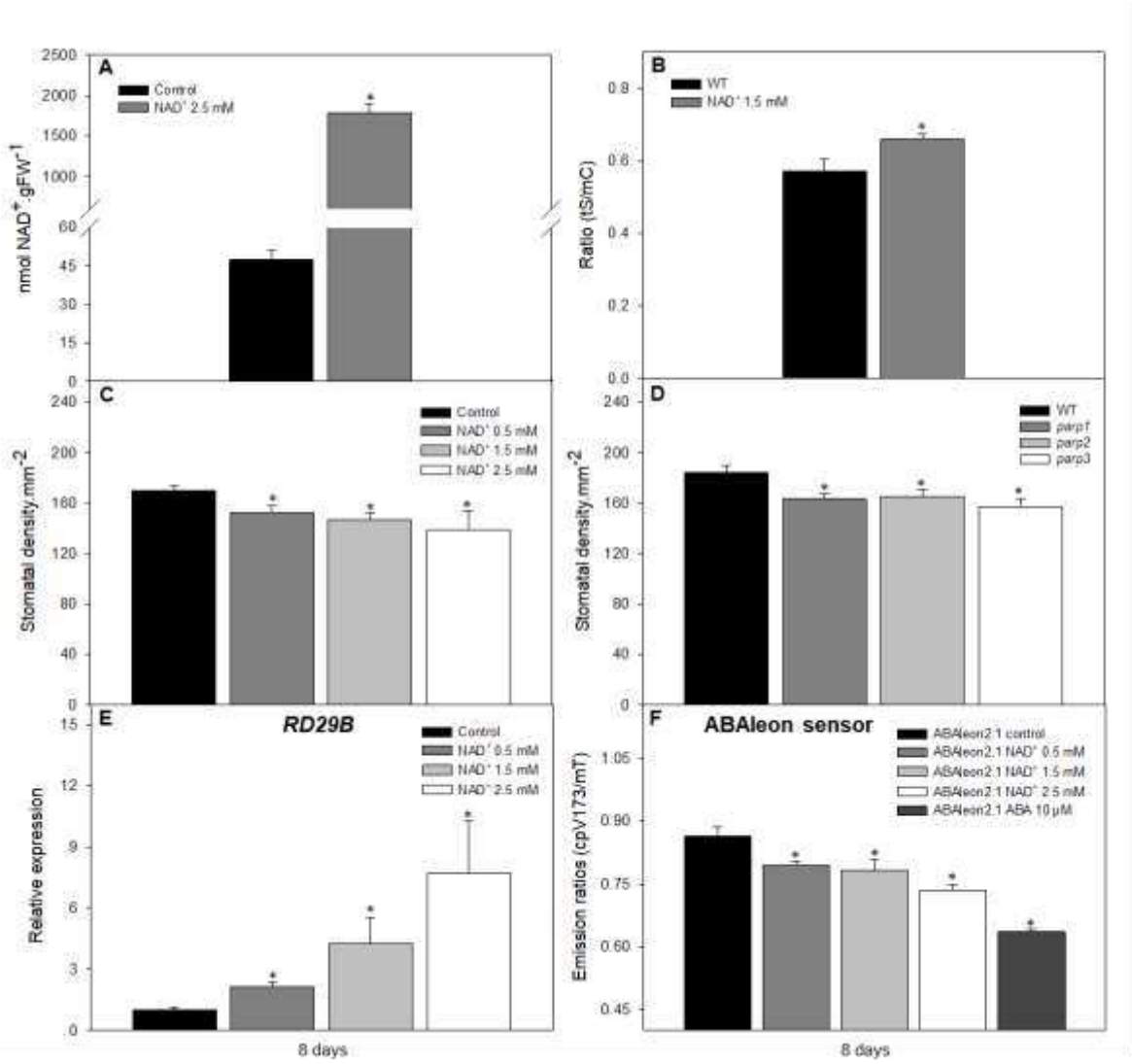

Figure 5: Exogenous NAD^+ feeding and inefficiently NAD^+ breakdown negatively impact stomatal number in *Arabidopsis* cotyledons.
A) NAD^+ measurement in Col-0 seedlings grown on medium containing 2.5 mM of NAD^+ after 8 days in light. **B)** Cytosolic NADH/NAD^+ dynamics reported by plants expressing Peredox-mCherry sensor grown on medium containing 1.5 mM NAD^+. Peredox-mCherry is composed by a T-Sapphire (tS) chromophore linked to a biding domain for NAD^+ or NADH. The mCherry (mC) fluorophore permits the normalization to sensor abundance and higher tS/mC ratio means more NADH is bound. **C)** Stomatal density of Col-0 seedlings treated with exogenous NAD^+. Seedlings were grown on medium containing 0, 0.5, 1.5 and 2.5 mM of NAD^+ for 8 days. Abaxial surfaces of 10 cotyledons per genotype were photographed and analyzed by optical microscopy. **D)** Stomatal density of PARP mutants (*parp1, parp2* and *parp3)*, plants inefficient in NAD breakdown. **E)** Transcript abundance of the ABA responsive gene (*RD29B*) in Col-0 seedlings grown in medium containing different contents of NAD^+. RNA was isolated from seedlings at 8 days and *Actin2* was used as endogenous control. **F)** *In vivo* ABA

dynamics reported by the sensor ABAleon. Seedlings of ABAleon2.1 treated with 0, 0.5, 1.5 and 2.5 mM of NAD^+ and ABA 10 µM for 8 days. In the presence of ABA, the distance or orientation between the fluorescent probes mTurquoise (mT) and cpVenus173 (cpV173) are increasing, thus leading to reduced cpV173/mT ratios.Asterisks represents values that were judged to be significantly different from the WT or among treatments (T test* $p < 0.05$, ** $p < 0.01$).

Subsequently, we assessed the gene expression of an ABA-responsive gene (*RD29B*) in WT seedlings treated with NAD^+ to evaluate whether exogenous NAD^+ treatment impacts the ABA response. The expression of *RD29B* gene was shown to be increased in response to the different NAD^+ concentrations applied (Figure 5E). To further test this hypothesis, and considering that ABAleon sensor is able to report the levels and the dynamic of ABA in living plants (Waadt et al., 2014) we treated ABAleon2.1 seedlings with either NAD^+ or ABA for 6 days. Interestingly, seedlings treated with NAD^+ displayed increases in ABA content in response to the different NAD^+ concentrations applied (Figure 5F and Supplemental Figure 5C). Together, these results suggest that NAD^+ impacts ABA metabolism leading to a reduced stomatal number.

The interaction between NAD^+ and ABA metabolism regulates stomatal number

As described above, mutants in NAD^+ metabolism and NAD^+-treated seedlings displayed a reduced stomatal number. Additionally, the expression of ABA-responsive genes was shown to be augmented in these mutants and exogenous NAD^+ feeding increased ABA production. Together, these results led us to suggest a direct link between NAD^+ and ABA regulating stomatal development in Arabidopsis. Therefore, we investigated whether the exogenous application of NAD^+ or ABA would impact the stomata-lineage cell number and the pavement cell length as presented in NAD^+ carrier mutants. To this end, Col-0 seedlings were grown for 8 days in medium containing 1.5 mM of NAD^+ or 1µM of ABA and had their abaxial surface photographed and analyzed. The exogenous administration of either NAD^+ or ABA reduced the meristemoid and stomatal density and increased the guard mother cell number and pavement cell length in a very similar way (Figure 6A). Subsequently, the expression of the three master genes (*SPCH, MUTE, FAMA*) responsible to regulate the cell transitions into stomatal cell was assessed. Both treatments with NAD^+ and ABA reduced the expression of *SPCH* and *FAMA* genes after 3 and 6 days of treatment

whereas the expression of *MUTE* gene was increased in treated plants only 8 days after the treatments (Figure 6B).

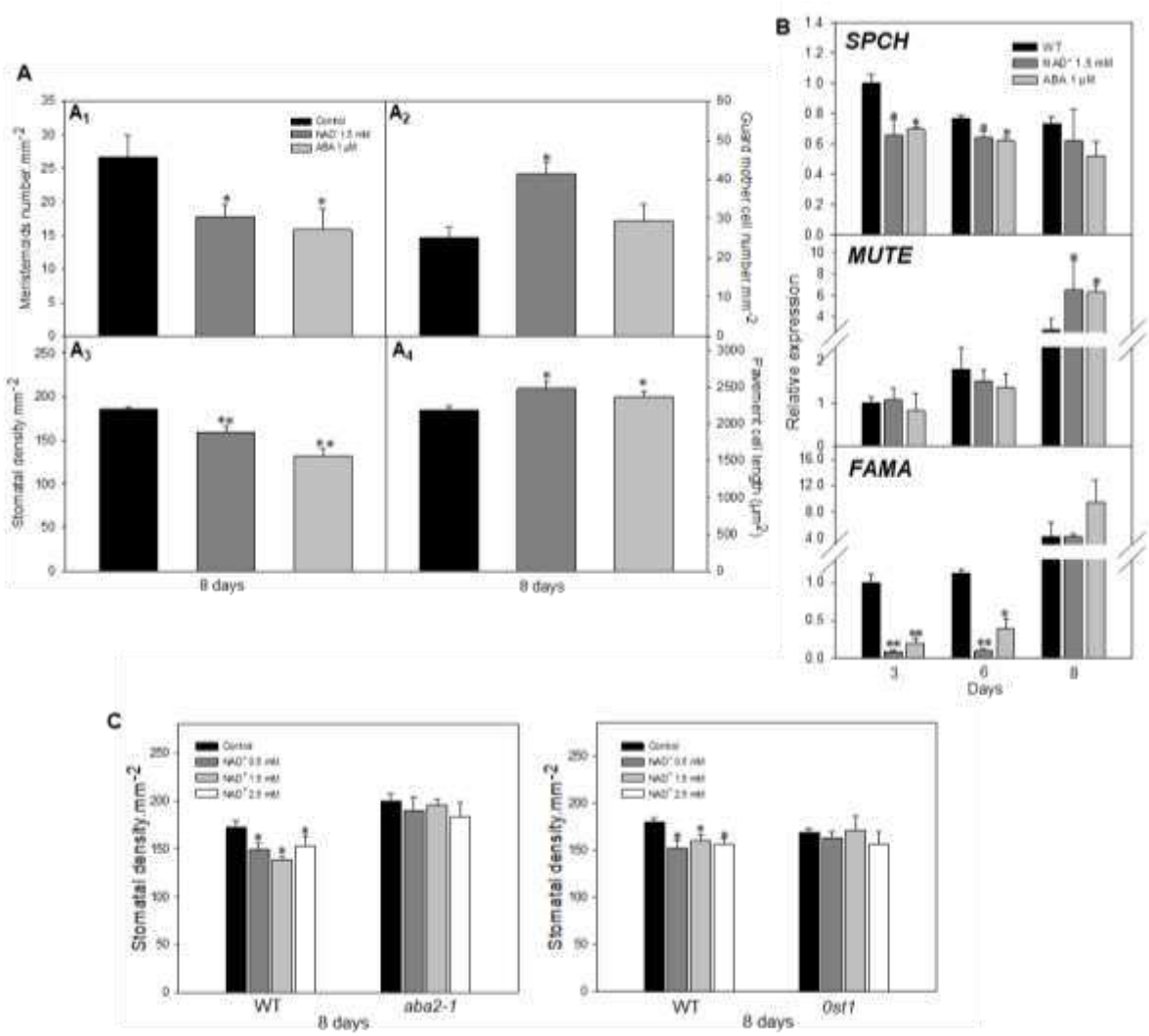

Figure 6: Crosstalk between NAD⁺ and ABA metabolism regulating stomatal development

A) Density of stomatal forming cells and guard cells of seedlings treated with 1.5 mM NAD^+ and 1 µM ABA for 8 days, **A_1)** Meristemoid number, **A_2)** Guard mother cell number, **A_3)** Guard cell number, **A_4)** Pavement cell length. Seedlings grown for 8 days in medium culture containing 1.5 mM NAD^+ or 1 µM ABA had their abaxial surfaces photographed by optical microscopy and analyzed. Values are compared with the control and presented as means SE (n=10). **B)** Relative transcript content of *SPCH*, *MUTE* and *FAMA* at day 3, 6 and 8 days after NAD^+ and ABA treatments. Gene expression was determined by quantitative reverse transcription polymerase (RT-PCR). Samples were normalized to *ACT2* and values are compared with the WT control of each time and presented as means SE (n=4). **C)** Guard cell number of WT, *aba2-1* and *ost1* seedlings after 8 days of NAD^+ treatment. Values are compared with the control and presented as means SE (n=10) demarcate values that were judged to be significantly different from the control (*$p < 0.05$; **$p < 0.01$).

To analyze whether the phenotype of reduced stomatal density in plants treated with exogenous NAD^+ was due to an interaction with ABA metabolism, we next applied NAD^+ in a mutant unable to produce high endogenous ABA content (*aba2-1*) (Yoshida et al., 2019) and also in a mutant impaired in ABA signaling (*ost1*) (Jalakas et al., 2018). Three NAD^+ concentrations were used and WT, *aba-2* and *ost1* seedlings were grown for 8 days as previously described (Figure 6C). The stomatal density decreased only in WT seedlings, while no differences were observed in the treated seedlings of *aba2-1* and *ost1* mutants in comparison to their respective not treated controls, which thus corroborates the hypothesis that NAD^+ may influence both ABA biosynthesis and ABA signaling in Arabidopsis.

DISCUSSION

NAD^+ dynamics regulate stomatal density in Arabidopsis cotyledons

Several studies have described the components of the signal transduction mechanism responsible for determining stomatal number and distribution (Lee and Bergmann, 2019; Zoulias et al., 2018). Despite the number of studies linking internal and external factors to stomatal development, at the onset of this work a deep study investigating NAD^+ dynamics and stomatal production had yet to be performed. In the present work, we combined genetic and pharmacological approaches to manipulate cellular and subcellular NAD^+ dynamics to demonstrate that NAD^+ negatively regulates stomatal development in Arabidopsis cotyledons. Accordingly, NAD^+ mutants along with NAD^+-treated WT seedlings displayed reduced stomatal number (Figure 1F, 2C and 2D). Although NAD^+ administration impacted the stomatal number in cotyledons of WT seedlings, NAD^+ carrier mutants were insensitive to this treatment (Supplemental Figure 65). We hypothesized that, given that NAD^+ transporter mutants are inefficient in NAD^+ uptake to their mitochondria (*ndt1* and *ndt2*) and peroxisomes (*pxn*), they likely display elevated cytosolic NAD^+ levels. It is conceivable the observed decrease in the stomatal number caused by the disturbed NAD^+ homeostasis might have reached a threshold in mutant lines beyond which further stomatal density reduction is not possible due to the upregulation of as yet uncharacterized compensatory mechanisms. Accordingly, the mitochondrial NAD^+ content in *NDT2* mutant plants were shown to be reduced, thus confirming that, at least the mutation in *AtNDT2*, leads to a decreased mitochondrial NAD^+ uptake activity (Luo et al., 2019).

This finding thus corroborates our previous hypothesis of elevated NAD^+ in the cytosol and possibly redirection toward others subcellular compartments in the mutants.

Our work also confirmed that NAD^+ is taken up by the cell. WT seedlings treated with NAD^+ displayed higher levels of the metabolite after 8 days (Figure 5A) and seedlings transformed with Peredox-mCherry sensor (Hung et al., 2011) revealed a higher cytosolic NADH/NAD^+ ratio when treated with exogenous NAD^+ (Figure 5B). What is known so far is the existence of Nrt1 and TNA1 carriers responsible to incorporate nicotinamide and quinolinate, respectively, in yeasts (Ohashi et al., 2013; Belenky et al., 2011). However, the existence of NAD^+ carrier proteins in the plasma membrane is still unrevealed in Arabidopsis. More recently, a lectin receptor kinase was identified as a sensor for extracellular NAD^+ in *A. thaliana* (Wang et al., 2017). However, the mechanisms underlying NAD^+ uptake in plants require further investigation.

We additionally demonstrated that mutations in NAD^+ transporters interfere with biometric parameters of stomata and pavement cells (Table 1). Mutant lines, mainly *ndt1*$^-$*:ndt1*$^-$ and *ndt2*$^-$*:ndt2*$^-$, showed increases in stomatal area and stomatal width. Additionally, these mutations resulted in the enlargement of pavement cells, which were characterized by higher area, length and width in comparison to the WT. Interestingly, stomatal density negatively correlates with stomatal size to control stomatal movements (Doheny-Adams et al., 2012; Lawson and Blatt, 2014; Hetherington and Woodward, 2003). In agreement, de Souza Chaves et al. (2019) demonstrated that plants with reduced *NDT1* expression displayed lower values of transpiration rate and stomatal conductance.

High expression of nicotinate/nicotinamide mononucleotide adenyltransferase (NMNAT) along with several other genes in the NAD^+ biosynthesis pathway was previously observed in guard cells but not in developing stomata and pavement cells (Hashida et al., 2010). This is in accordance with the publicly available transcriptome data (Arabidopsis eFP Browser) which indicates higher expression of *de novo* and salvage NAD^+ biosynthetic genes in guard cells. Furthermore, it has been demonstrated that the expression of *ASPARTATE OXIDASE* and *QUINOLINATE PHOSPHORIBOSYLTRANSFERASE* is higher in guard cells than in mesophyll cells (Yang et al., 2008). Collectively, these results indicate that NAD^+ biosynthesis occurs in mature stomata and that this coenzyme is important for regulating stomatal function.

Our data, therefore demonstrates that NAD^+ is not only important to modulate stomatal function but also to regulate stomatal development.

NAD^+ homeostasis affects the expression of genes that regulate stomatal development

The cell fate transitions from protodermal cell to mature guard cell are mainly directed by the action of transcription factors belonging to basic-helix-loop-helix (bHLH), SPEECHLESS, MUTE and FAMA (MacAlister et al., 2007; Ohashi-Ito and Bergmann, 2006; Pillitteri et al., 2007; Simmons and Bergmann, 2016). In the present study, we found that the expression of *SPCH*, *MUTE* and *FAMA* were effected in NAD^+ carrier mutants and in WT seedlings treated with exogenous NAD^+ (Figure 2A, 2B, 2C and Figure 6B). Two other genes with redundant functions, namely *SCRM1/ICE1* and *SCRM2*, act together with *SPCH*, *MUTE* and *FAMA* as heterodimers throughout the steps of stomatal development (Kanaoka et al., 2008). The expression of *SCRM1/ICE1* (Figure 2D) and *SCRM2* (Figure 2E) was shown to be increased in mutant lines. On the other hand, the correct number and distribution of stomata are controlled by a range of peptides such as the EPIDERMAL PATTERNING FACTOR 1 and 2 (EPF1/EPF2), ERECTA (ER), ER-LIKE1and 2 (ERL1/ERL2) and TOO MANY MOUNTHS (TMM) (Hara et al., 2007, 2009; Hunt and Gray, 2009b; Nadeau and Sack, 2002; Shpak et al., 2005). These proteins are widely known for their role in inhibiting stomatal development. Overall, the transcript abundance of these genes was shown to be increased in NAD^+ carrier mutants (Figure 2). Another gene required to regulate stomatal patterning is *SDD1* (STOMATAL DENSITY AND DISTRIBUTION1) (Berger and Altmann, 2000). Mutation in *SDD1* gene led to an increased stomatal index, which implies that it plays a negative role in stomatal development. Accordingly, the expression of *SDD1* gene in NAD^+ carrier mutant lines was shown to be increased at day 4 for *ndt1*$^-$*:ndt1*$^-$ and *ndt2*$^-$*:ndt2*$^-$ (Figure 2I). Taken together, these results provide evidence that NAD^+ dynamics are important to modulate the expression of the master genes belonging to stomatal biogenesis pathway. Despite to requirements for further studies to fully comprehend the NAD^+ action over these genes, this study expand our knowledge about the regulation of stomatal development and proposes a link between NAD^+ homeostasis and earlier developmental process.

NAD^+ distribution affects redox homeostasis in seedlings

Despite the fact that studies have shown that NAD^+ may regulate the transcription of several genes, to date NAD^+ regulating its own synthesis at transcriptional levels has yet to be elucidated (Schippers et al., 2008; Wang et al., 2017). In the present work and in agreement with our previous study (Feitosa-Araujo et al. (2020), we demonstrated that genes of *de novo* and salvage pathways were deregulated in seedlings of NAD^+ carrier mutants (Figure 3A). Addtionally to gene deregulation, reduced NAD^+ levels were also observed in *NDT1* and *NDT2* mutants (Figure 3B), a response previously shown for NAD^+ related mutants (Schippers et al., 2008; Jambunathan et al., 2010). This altered NAD pools found in the present and in previous studies points to the role of NAD^+ in producing and scavenging activity of ROS (Gakière et al., 2018). Furthermore, unbalanced NAD^+ levels has been previously linked to oxidative stress (Chai et al., 2006; Katoh et al., 2006; Schippers et al., 2008; Luo et al., 2019). Given the upregulation of the superoxide and H_2O_2 marker gene *At*ZAT12 (Xu et al., 2017) in the mutant lines (Figure 3C), we thus conclude that NAD^+ transporter mutants may be suffering from increased oxidative stress.

The changes associated with the processes occurring at early seed germination and at the first stages of seedling establishment are usually characterized by the production of large quantities of ROS (Wojtyla et al., 2016; Barba-Espin et al., 2010; Bailly, 2019). Much of this is caused by the generation of ROS as byproducts of the fatty acid β-oxidation, albeit additional sources of ROS do exist in germinating seeds, notably the NADPH oxidases (Kwak et al., 2003). Indeed, Bernhardt et al., 2012 showed that the levels of the *β*-oxidation marker eicosenoic acid (C20:1) were strongly reduced (77%) in WT seedlings at 4 days after imbibition, showing complete depletion in 6-day-old seedlings. In addition to the requirement of NAD^+ for proper *β*-oxidation in peroxisomes (Bernhardt et al., 2012), NAD^+ import into peroxisomes mediated by PXN is also pivotal to detoxify the H_2O_2 generated during *β* -oxidation (Eastmond, 2007). In agreement, our results show that *ZAT12* is higher expressed in *pxn-1* line, in comparison to the other genotypes, at day 4 (Figure 3C), as well as elevated expression of *PXN* is clearly observed in 4-day-old WT seedlings (Supplemental Figure 7), thus showing the importance of NAD^+ transport into peroxisomes for optimal *β* -oxidation and H_2O_2 detoxification. Interestingly, the much higher expression of *PXN* at the first stages of development, compared with the expression patterns of *NDT1* and

NDT2 (Supplemental Figure 7 and Bernhardt et al., 2012), is in accordance with the stronger stomatal phenotype herein observed for some parameters in *pxn-1* line (Figure 1, Figure 3 and Supplemental Figure 2). Collectively, the results presented here provide additional evidence that unbalanced NAD^+ compartmentation, besides of impacting redox homeostasis, further contributes to the stomatal phenotype observed.

Interaction between NAD^+ and ABA regulates stomatal development in Arabidopsis

Different studies have supported the relation of NAD^+ and ABA metabolism (Hunt and Gray, 2009a; Zeng et al., 2014; Wei et al., 2019; Vanderauwera et al., 2007). NAD^+ is required as NADH for zeaxanthin epoxidase (ABA1) and as NADPH for xanthoxin dehydrogenase (ABA2) activities, both belonging to the pathway of ABA biosynthesis (González-Guzmán et al., 2002; Barrero et al., 2005). It has been proposed that higher levels of NAD^+ leading to decreased seed germination and increased seed dormancy were linked to higher levels of ABA (Hunt and Gray, 2009a). Recently, it was described that NAD^+ is pivotal for ABA and proline accumulation under salt stress condition (Wei et al., 2019). Furthermore, NADK2 was shown to participate in stomatal function by modulating ABA-induced stomatal closure (Sun et al., 2017). Additionally, ADP-ribosyl cyclases use NAD^+ as substrate to produce cyclic ADP ribose (cADPR) which can in turn lead to increases in the concentration of cytosolic free Ca^{2+} thus influencing ABA signaling (Hetherington and Brownlee, 2004a; Zhang and Li, 2006).

Given that the functional characterization of *NDT1* and *NDT2* mutants showed that these plants present a reduced and delayed seed germination, a well-known ABA phenotype, we hypothesized that NAD^+ transport, as well as NAD^+ itself, could impact ABA metabolism (de Souza Chaves et al., 2019). Accordingly, ABA-biosynthesis (*ABA1, ABA2*) and ABA-responsive genes (*ABF3, RD29A, RD29B, ICK1*) were up-regulated in NAD^+ carrier mutants (Figure 3A). Additionally, increased levels of ABA were observed in a NAD-dependent manner in seedlings carrying the sensor ABAleon (Waadt et al., 2014) grown on medium containing three different concentrations of NAD^+ (Figure 5F). We further assessed the expression of two cytosolic calcium-responsive genes (Whalley et al., 2011) to verify whether ABA signaling would be increased in NAD^+ carrier mutants. As shown in Supplemental Figure 4 the expression

of both genes is increased in the mutant lines. Collectively, these results indicate a direct involvement of NAD^+ dynamics to regulate ABA levels and signaling.

It has been shown that ABA acts as a stress-related hormone helping plants to cope with different environmental conditions (Yoshida et al., 2014). Besides its several functions, ABA was demonstrated to regulate early developmental process such as stomatal development (Tanaka et al., 2013). ABA negatively regulates stomatal production in Arabidopsis by reducing the expression of the genes *SPCH* and *MUTE,* thus inhibiting the development of stomatal-lineage cells(Tanaka et al., 2013) . In the present study, we demonstrated that NAD^+ transporter mutants presented decreased expression of *SPCH* and *MUTE* (Figure 2A and 2B). Furthermore, Col-0 seedlings treated with ABA and NAD^+ presented similar expression of *SPCH*, *MUTE* and *FAMA* genes (Figure 6B). Interestingly, NAD^+-treated seedlings presented the same pattern of stomatal development as shown for ABA mutants (Figure 6A) (Tanaka et al., 2013). To extend our knowledge about NAD^+ dynamics and ABA metabolism regulating stomatal development, we chemically inhibited ABA production in seedlings (Chae et al., 2004). As shown in Figure 4C, the difference in stomatal number between WT and NAD^+ carrier mutants disappeared in treated seedlings. Further genetic analyses demonstrated that NAD^+ treatment in a mutant impaired in ABA biosynthesis (*aba2-1*) (Yoshida et al., 2019) and in ABA signaling (*ost1*) (Jalakas et al., 2018) do not alter stomatal number (Fig. 6, C). Together, these results provide a direct link between NAD^+ pool and ABA metabolism to modulate stomatal development in Arabidopsis cotyledons. This hypothesis is illustrated in Figure 7 and would hence explain why NAD^+ dynamics affect ABA metabolism leading to a negative regulation of stomatal development in cotyledons. This model further suggests that reduced mitochondrial or peroxisomal NAD^+ import (*ndt1*, *ndt2* and *pxn* mutants), as well as inefficient NAD^+ breakdown (*parp1*, *parp2* and *parp3* mutants) and exogenous NAD^+ feeding contributes to increases in cytosolic NAD^+ content. Altered NAD^+ distribution affects the cytosolic redox homeostasis, thus enhancing ABA response, which directly impact the expression of genes belonging to stomatal biogenesis pathway. Collectively, these results demonstrate that NAD^+ acts upstream of ABA responses and that interaction involving NAD^+ and ABA signaling regulates stomatal development in Arabidopsis cotyledons.

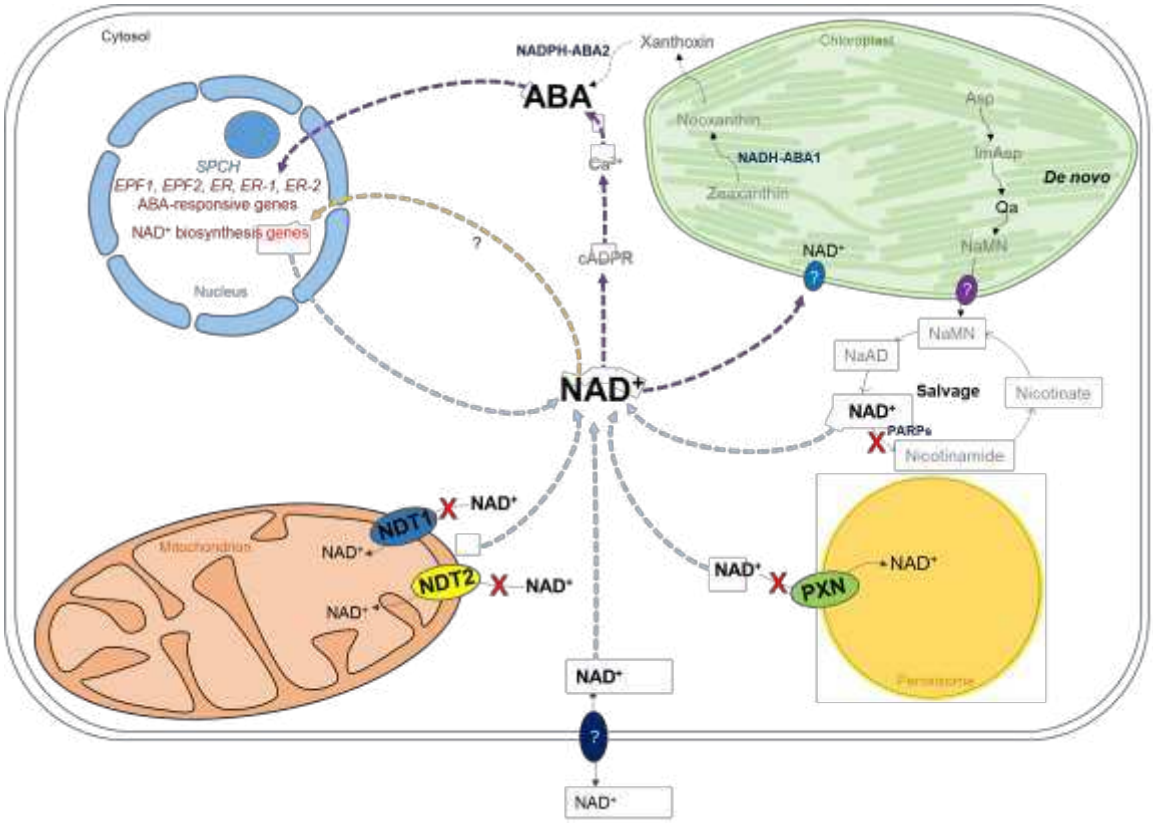

Figure 7: Hypothetical model connecting NAD⁺ dynamics with ABA metabolism regulating stomatal development.
Changes in cytosolic NAD⁺ content displayed by reduced mitochondrial and peroxisomal NAD⁺ import, exogenous NAD⁺ application and decreased NAD⁺ breakdown by PARP enzymes contribute to enhance both ABA biosynthesis and signaling. Increased internal ABA content and ABA signaling lead to deregulation of genes belonging to stomatal biogenesis pathway. In our hypothetical model, increases in cytosolic NAD⁺ perturb the redox homeostasis enhancing ABA synthesis and signaling which negatively regulates stomatal development. Blue arrows indicate processes contributing to increases in cytosolic NAD⁺ pool. Purple arrows indicate processes enhancing ABA biosynthesis, ABA signaling and ABA responses. Orange arrow means a possible feedback regulation of NAD⁺ over genes belonging to NAD⁺ biosynthesis. Impacted processes are highlighted with a red “x”. Up-regulated genes are in red while down-regulated genes are in blue. ABA pathway is underrepresented and NAD-dependent enzymes are highlighted.

CONCLUSIONS

Previous studies have broadened the knowledge concerning NAD⁺ functions in living organisms. In the present work, we established a new link between NAD⁺ and early developmental process in plants. We demonstrated that NAD⁺ dynamics regulates stomatal development in Arabidopsis cotyledons in an ABA-dependent manner. Our analysis revealed that NAD⁺ transport and metabolism are upstream of ABA synthesis and signaling, meaning that NAD⁺ homeostasis is essential to firstly balance the redox state of the cells, which impacts both ABA content and signaling.

Here we showed that enhanced ABA signaling promotes inhibition of stomata formation in Arabidopsis. That said, if NAD^+ affects ABA signaling it is likely to affect not only stomata formation but also stomatal physiology, meaning movements. This finding opens new perspectives for the studies of NAD^+ functions, and intriguingly demonstrates that NAD^+ compartmentalization represents a novel means to selectively influence stomatal signaling events in Arabidopsis.

EXPERIMENTAL PROCEDURES

Plant material

In all the experiments, *Arabidopsis thaliana* wild-type plants used were the *Columbia* ecotype (Col-0). *Arabidopsis* plants with reduced expression of genes encoding NAD^+ transporters from mitochondria - NDT1 (*At*2g47490), NDT2 (*At*1g25380) and peroxisome – PXN (*At*2g39970) were used. T-DNA mutants for NDT1 (*ndt1*$^-$*:ndt1*$^-$) and NDT2 (*ndt2*$^-$*:ndt2*$^-$) genes were derived from the GABI-KAT collection, GK–241G12 and GK-143G09, respectively and selected as described in Chaves et al., (2019) and Feitosa-Araujo (2020). Seeds of PXN mutant, *pxn-1* (GABI_046D01) was selected as described in Bernhardt et al., (2012). The poly(ADP-ribose)polymerase (PARP) T-DNA mutant lines *parp1* (SAIL_632_D07), *parp2* (SALK_111410) and *parp3* (SAIL_1250_B03) and *ost1* were obtained from Alisdair R. Fernie group. Seeds of *aba2.1* were obtained from Takuya Yoshida, ABAleon2.1 seeds were obtained from Rainer Waadt, seeds expressing Peredox-mCherry were obtained from Markus Schwarzländer group.

Growth conditions

Seeds of all genotypes were sown on standard greenhouse substrate (Tropstrato HT®) in plastic pots with a 0.1-L capacity or grown on half strength Murashige and Skoog medium without sucrose (Murashige and Skoog, 1962). After four days of stratification at 4 °C, pots and plates with seeds were taken into a growth chamber at 22 ± 2 °C, 60% relative humidity, 150 µmol photons m^{-2} s^{-1} irradiance, and 12 h of light and 12 h dark photoperiod. Subsequently, at 2, 4 and 8 days, cotyledons from all genotypes grown in pots were collected for morphological and gene expression analyses. In order to verify the influence of NAD^+, ABA and Norflurazon over stomatal development responses in seedlings, seeds were germinated on ½MS plates

containing the following concentrations of these chemicals, NAD^+ (0.5, 1.5, 2.5 mM), ABA (1µM) and Norflurazon (8µM). For each treatment seedlings were collected in different time points depending on the purpose of the analyses.

Epidermal cells analyses

Images of epidermis from cotyledons were taken by using an optical microscope ZEISS (model AX10) coupled with a digital camera (AxiocamMRc). Two cotyledons from six plants per genotype grown in pots had their abaxial surface photographed at 4 and 8 days after sowing. Cotyledons of seedlings grown on ½MS plates containing chemicals were photographed at day 8 after germination. Cotyledons were placed in a microscope slide containing a drop of water and subsequently pressed by using a coverslip to release the excess of chloroplasts inside the cells. Posteriorly eight areas of each cotyledon were photographed and analyzed using an open source image processing program named ImajeJ. The data concerning stomatal and pavement cell area, length and width were performed in at least 500 stomata and 500 pavement cells per genotype.

Gene expression analysis

Quantitative real time PCR (qRT-PCR) was used to perform assays of gene expression. Total RNA's were extracted from seedlings using Trizol® reagent (Ambion, Life Technologies, Carlsbad, CA, USA) following the manufacturer's instructions. Total RNA was quantified by spectrophotometer at 260 nm and subsequently treated with RNase-free DNase (Invitrogen™, Life Technologies Carlsbad, CA, USA). Nearly 2 µg of isolated RNA's were used to synthesize the complementary strand of DNA's (cDNA) employing the Improm-II™ Reverse Transcription System (Promega, Madison, WI, USA) and Oligo $(dT)_{15}$ according to manufacturer's recommendations. A 7300 Real time System (Applied Biosystems, Foster, CA, USA) and Power SYBR® Green PCR Master Mix (Life Technologies/Applied Biosystem, Foster, CA, USA) were used to perform quantitative RT-PCRs. Samples were collected, pooled and RT-PCR analysis were performed by following the steps: 94 °C for 10 min, 40 cycles of 94 °C for 15 s, 58 °C for 15, and 2 °C for 15 sec. Relative quantification was done with 3-4 biological replicates using actin as housekeeping gene. Gene expression measurement values

were normalized for the WT of each time. The list of primers used in this study is in Supplementary Table 1.

Coexpression analysis

Coexpression analysis using genes of ABA and NAD^+ metabolism along with stomatal biosynthesis-related genes was performed using the Pajek software. The data base used to perform transcriptional data mining was based on this link (http://prime.psc.riken.jp/?action=coexpression_index). The genes used as trap are listed in Supplementary Table 2. Analyses were performed with cut-off value of $r > 0.7$. Connections between each gene were prepared by "intersection of sets" search. The output files which were formatted with ".net" file from PRIMe database were later used to draw the networks using Pajek software (Batagelj and Mrvar et al. 1998).

NAD^+, NADH, $NADP^+$, NADPH measurements

To quantify the levels of NAD^+, NADH, $NADP^+$ and NADPH, aliquots of approximately 20 mg were used from seedlings collected in the middle of the light period at 4 and 8 days after germination in ½MS or after 8 days in medium containing 2.5 mM of NAD^+. The quantification was performed according to the protocol described by (Schippers et al., 2008).

ABA quantification

The phytohormone ABA was measured in dry seeds along with seedlings at 2, 4 and 8 days after stratification according to the protocol described by Pan et al., 2010 and adapted by Salem et al., 2017.

Plate reader experiments

Transparent 96-well plates (#82.1581; Sarstedt, Nümbrecht, Germany) were filled with 200 µl assay medium (10 mM 2-(N-morpholino)ethanesulfonic acid (MES), pH 5.8 (potassium hydroxide), 10 mM magnesium chloride, 10 mM calcium chloride, 5 mM potassium chloride). Seedlings of Peredox-mCherry and ABAleon2.1 lines were carefully prepared and placed in individual wells prefilled with assay medium using soft tweezers. After plate preparation, it was inserted into a CLARIOstar plate reader (BMG Labtech, Ortenberg, Germany) pre-equilibrated to 25°C. To avoid photosynthetic

effects, plates were kept in the dark for one hour before fluorescence was recorded. The excitation (Ex) and emission (Em) wavelength for the Peredox-mCherry sensor was: Ex: 400 ± 10 nm and 540 ± 20 nm; Em: 520 ± 10 nm and 615 ± 18 nm. The excitation (Ex) and emission (Em) wavelength for ABAleon2.1 sensor was: Ex: 430 ± 10 nm; Em: 480 ± 10 10 nm and 530 ± 10.

Statistical Analyses

All experiments were designed to be completely randomized. Data were submitted to ANOVA and tested for significant ($P < 0.05$ and $P < 0.01$) differences using Student's *t* tests or Tukey test. All the statistical analyses were performed using the algorithm embedded into Excel (Microsoft).

ACKNOWLEDGMENTS

Financial support was provided by Conselho Nacional de Desenvolvimento Científico e Tecnológico (CNPq), Fundação de Amparo à Pesquisa do Estado de Minas Gerais (FAPEMIG). Research fellowships granted by CNPq to EFA, ANN and WLA, Coordenação de Aperfeiçoamento de Pessoal de Nível Superior (CAPES PrInt program) to EFA are also gratefully acknowledged.

REFERENCES

Agrimi, G., Russo, A., Pierri, C.L., and Palmieri, F. (2012). The peroxisomal NAD+carrier of Arabidopsis thaliana transports coenzyme A and its derivatives. J. Bioenerg. Biomembr. **44**: 333–340.

Arias, C.L., Pavlovic, T., Torcolese, G., Badia, M.B., Gismondi, M., Maurino, V.G., Andreo, C.S., Drincovich, M.F., Gerrard Wheeler, M.C., and Saigo, M. (2018). NADP-dependent malic enzyme 1 participates in the abscisic acid response in arabidopsis thaliana. Front. Plant Sci. **871**: 1–11.

Bailly, C. (2019). The signalling role of ROS in the regulation of seed germination and dormancy. Biochem. J. **476**: 3019–3032.

Balcerowicz, M., Ranjan, A., Rupprecht, L., Fiene, G., and Hoecker, U. (2014). Auxin represses stomatal development in dark-grown seedlings via Aux/IAA proteins. Dev. **141**: 3165–3176.

Barba-Espin, G., Diaz-Vivancos, P., Clemente-Moreno, M.J., Albacete, A., Faize, L., Faize, M., Pérez-Alfocea, F., and Hernández, J.A. (2010). Interaction between hydrogen peroxide and plant hormones during germination and the early growth of pea seedlings. Plant, Cell Environ. **33**: 981–994.

Barrero, J.M., Piqueras, P., González-Guzmán, M., Serrano, R., Rodríguez, P.L., Ponce, M.R., and Micol, J.L. (2005). A mutational analysis of the ABA1 gene of Arabidopsis thaliana highlights the involvement of ABA in vegetative development. J Exp Bot **56**: 2071–2083.

Barron, J.T., Gu, L., and Parrillo, J.E. (2000). NADH/NAD redox state of cytoplasmic glycolytic compartments in vascular smooth muscle. Am. J. Physiol. - Hear. Circ. Physiol. **279**: 2872–2878.

Belenky, P., Stebbins, R., Bogan, K.L., Evans, C.R., and Brenner, C. (2011). Nrt1 and tna1-independent export of NAD+ precursor vitamins promotes NAD+ homeostasis and allows engineering of vitamin production. PLoS One **6**.

Berger, D. and Altmann, T. (2000). A subtilisin-like serine protease involved in the regulation of stomatal density and distribution in Arabidopsis thaliana. Genes Dev. **14**: 1119–1131.

Bergmann, D.C., Lukowitz, W., and Somerville, C.R. (2004). Stomatal development and pattern controlled by a MAPKK kinase. Science (80-.). **304**: 1494–1497.

Bergmann, D.C. and Sack, F.D. (2007). Stomatal Development. Annu. Rev. Plant

Biol. **58**: 163–181.

Bernhardt, K., Wilkinson, S., Weber, A.P.M., and Linka, N. (2012). A peroxisomal carrier delivers NAD + and contributes to optimal fatty acid degradation during storage oil mobilization. Plant J. **69**: 1–13.

Briggs, A.G. and Bent, A.F. (2011). Poly(ADP-ribosyl)ation in plants. Trends Plant Sci. **16**: 372–380.

Chae, S.H., Yoneyama, K., Takeuchi, Y., and Joel, D.M. (2004). Fluridone and norflurazon, carotenoid-biosynthesis inhibitors, promote seed conditioning and germination of the holoparasite Orobanche minor. Physiol. Plant. **120**: 328–337.

Chai, M.F., Wei, P.C., Chen, Q.J., An, R., Chen, J., Yang, S., and Wang, X.C. (2006). NADK3, a novel cytoplasmic source of NADPH, is required under conditions of oxidative stress and modulates abscisic acid responses in Arabidopsis. Plant J. **47**: 665–674.

Choudhury, F.K., Rivero, R.M., Blumwald, E., and Mittler, R. (2017). Reactive oxygen species, abiotic stress and stress combination. Plant J. **90**: 856–867.

Demarest, T.G., Babbar, M., Okur, M.N., Dan, X., Croteau, D.L., Fakouri, N.B., Mattson, M.P., and Bohr, V.A. (2019). NAD+ Metabolism in Aging and Cancer. Annu. Rev. Cancer Biol. **3**: 105–130.

Doheny-Adams, T., Hunt, L., Franks, P.J., Beerling, D.J., and Gray, J.E. (2012). Genetic manipulation of stomatal density influences stomatal size, plant growth and tolerance to restricted water supply across a growth carbon dioxide gradient. Philos. Trans. R. Soc. B Biol. Sci. **367**: 547–555.

Eastmond, P.J. (2007). Monodehyroascorbate reductase4 is required for seed storage oil hydrolysis and postgerminative growth in Arabidopsis. Plant Cell **19**: 1376–1387.

Engineer, C.B., Ghassemian, M., Anderson, J.C., Peck, S.C., Hu, H., and Schroeder, J.I. (2014). Carbonic anhydrases, EPF2 and a novel protease mediate CO2 control of stomatal development. Nature **513**: 246–250.

Feitosa-Araujo, E., de Souza Chaves, I., Florian, A., Fonseca-Pereira, P., Apfata, JAC., Heyneke, E., Medeiros, D. B., Pires, M.V., Mettler-Altmann, T., Neuhaus, H.E., Palmieri, F., Araújo, W.L., Obata, T., Weber, A.P.M., Linka, N., Fernie, A.R., Nunes-Nesi, A. (2020). Down-regulation of a mitochondrial NAD+ transporter (NDT2) alters seed production and germination in Arabidopsis. Plant

Cell Physiol.

Gadjev, I., Vanderauwera, S., Gechev, T.S., Laloi, C., Minkov, I.N., Shulaev, V., Apel, K., Inzé, D., Mittler, R., and Van Breusegem, F. (2006). Transcriptomic footprints disclose specificity of reactive oxygen species signaling in Arabidopsis. Plant Physiol **141**: 436–445.

Gakière, B., Fernie, A.R., and Pétriacq, P. (2018). More to NAD+ than meets the eye: A regulator of metabolic pools and gene expression in Arabidopsis ☆. Free Radic. Biol. Med. **122**: 86–95.

Galon, Y., Finkler, A., and Fromm, H. (2010). Calcium-regulated transcription in plants. Mol. Plant **3**: 653–669.

González-Guzmán, A.M., Apostolova, N., Bellés, J.M., Barrero, J.M., Belles, J.M., Barrero, J.M., Piqueras, P., Ponce, M.R., Micoi, J.L., Serrano, R., and Rodnguez, P.L. (2002). The short-chain alcohol dehydrogenase ABA2 catalyzes the conversion of xanthoxin to abscisic aldehyde. Plant Cell **14**: 1833–1846.

González, D., Fuentes, S., and Serna, L. (2017). Interactions among gibberellins, brassinosteroids and genes regulate stomatal development in the arabidopsis hypocotyl. Int. J. Dev. Biol. **61**: 383–387.

Von Groll, U., Berger, D., and Altmann, T. (2002). The subtilisin-like serine protease SDD1 mediates cell-to-cell signaling during Arabidopsis stomatal development. Plant Cell **14**: 1527–1539.

Gudesblat, G.E., Schneider-Pizoń, J., Betti, C., Mayerhofer, J., Vanhoutte, I., Van Dongen, W., Boeren, S., Zhiponova, M., De Vries, S., Jonak, C., and Russinova, E. (2012). SPEECHLESS integrates brassinosteroid and stomata signalling pathways. Nat. Cell Biol. **14**: 548–554.

Guse, A.H. (2015). Calcium mobilizing second messengers derived from NAD. Biochim. Biophys. Acta - Proteins Proteomics **1854**: 1132–1137.

Han, X., Hu, Y., Zhang, G., Jiang, Y., Chen, X., and Yu, D. (2018). Jasmonate negatively regulates stomatal development in arabidopsis cotyledons. Plant Physiol. **176**: 2871–2885.

Hara, K., Kajita, R., Torii, K.U., Bergmann, D.C., and Kakimoto, T. (2007). The secretory peptide gene EPF1. Genes Dev.: 1720–1725.

Hara, K., Yokoo, T., Kajita, R., Onishi, T., Yahata, S., Peterson, K.M., Torii, K.U., and Kakimoto, T. (2009). Epidermal cell density is autoregulated via a secretory

peptide, EPIDERMAL PATTERNING FACTOR 2 in Arabidopsis leaves. Plant Cell Physiol. **50**: 1019–1031.

Hashida, S., Itami, T., Takahashi, H., Takahara, K., and Nagano, M. (2010). Nicotinate/nicotinamide mononucleotide adenyltransferase- mediated regulation of NAD biosynthesis protects guard cells from reactive oxygen species in ABA-mediated stomatal movement in Arabidopsis. J. Exp. Bot. **61**: 3813–3825.

Hashida, S., Takahashi, H., Kawai-yamada, M., and Uchimiya, H. (2007). Arabidopsis thaliana nicotinate / nicotinamide mononucleo- tide adenyltransferase (AtNMNAT) is required for pollen tube growth.: 694–703.

Hashida, S.N., Takahashi, H., and Uchimiya, H. (2009). The role of NAD biosynthesis in plant development and stress responses. Ann. Bot. **103**: 819–824.

Hetherington, A.M. and Brownlee, C. (2004a). The generation of Ca2+ signals in plants. Annu. Rev. Plant Biol. **55**: 401–427.

Hetherington, A.M. and Brownlee, C. (2004b). The Generation of Ca2+ signals in plants. Annu. Rev. Plant Biol. **55**: 401–427.

Hetherington, A.M. and Woodward, F.I. (2003). The role of stomata in sensing and driving environmental change. Nature **424**: 901–908.

Hung, Y.P., Albeck, J.G., Tantama, M., and Yellen, G. (2011). Imaging cytosolic NADH-NAD+ redox state with a genetically encoded fluorescent biosensor. Cell Metab. **14**: 545–554.

Hunt, L., Bailey, K.J., and Gray, J.E. (2010). The signalling peptide EPFL9 is a positive regulator of stomatal development. New Phytol. **186**: 609–614.

Hunt, L. and Gray, J.E. (2009a). The relationship between pyridine nucleotides and seed dormancy. New Phytol. **181**: 62–70.

Hunt, L. and Gray, J.E. (2009b). The signaling peptide EPF2 controls asymmetric cell divisions during stomatal development. Curr. Biol. **19**: 864–869.

Hunt, L., Holdsworth, M.J., and Gray, J.E. (2007). Nicotinamidase activity is important for germination. Plant J. **51**: 341–351.

Jalakas, P., Merilo, E., Kollist, H., and Brosché, M. (2018). ABA-mediated regulation of stomatal density is OST1-independent. Plant Direct **2**: e00082.

Jambunathan, N., Penaganti, A., Tang, Y., and Mahalingam, R. (2010). Modulation of redox homeostasis under suboptimal conditions by Arabidopsis nudix hydrolase 7. BMC Plant Biol. **10**: 173.

Kanaoka, M.M., Pillitteri, L.J., Fujii, H., Yoshida, Y., Bogenschutz, N.L., Takabayashi, J., Zhu, J.K., and Torii, K.U. (2008). SCREAM/ICE1 and SCREAM2 specify three cell-state transitional steps leading to Arabidopsis stomatal differentiation. Plant Cell **20**: 1775–1785.

Kang, C.Y., Lian, H.L., Wang, F.F., Huang, J.R., and Yang, H.Q. (2009). Cryptochromes, phytochromes, and COP1 regulate light-controlled stomatal development in arabidopsis. Plant Cell **21**: 2624–2641.

Katoh, A., Uenohara, K., Akita, M., and Hashimoto, T. (2006). Early steps in the biosynthesis of NAD in Arabidopsis start with aspartate and occur in the plastid. Plant Physiol. **141**: 851–857.

Kim, T.-W., Michniewicz, M., Bergmann, D.C., and Wang, Z.-Y. (2012). Brassinosteroid regulates stomatal development by GSK3-mediated inhibition of a MAPK pathway. Nature **482**: 419–422.

Kulkarni, C.A. and Brookes, P.S. (2019). Cellular compartmentation and the redox/Non-redox functions of NAD+. Antioxid Redox Signal **31**: 623–642.

Lampard, G.R., MacAlister, C.A., and Bergmann, D.C. (2008). Arabidopsis stomatal initiation is controlled by MAPK-mediated regulation of the bHLH SPEECHLESS. Science (80-.). **322**: 1113–1116.

Lau, O.S., Davies, K.A., Chang, J., Adrian, J., Rowe, M.H., Ballenger, C.E., and Bergmann, D.C. (2014). Direct roles of SPEECHLESS in the specification of stomatal self-renewing cells. Science (80-.). **345**: 1605–1609.

Lau, O.S., Song, Z., Zhou, Z., Davies, K.A., Chang, J., Yang, X., Wang, S., Lucyshyn, D., Tay, I.H.Z., Wigge, P.A., and Bergmann, D.C. (2018). Direct control of SPEECHLESS by PIF4 in the high-temperature response of stomatal development. Curr. Biol. **28**: 1273-1280.e3.

Lawson, T. and Blatt, M.R. (2014). Stomatal size, speed, and responsiveness impact on photosynthesis and water use efficiency. Plant Physiol. **164**: 1556–1570.

Lee, E., Lucas, J.R., and Sack, F.D. (2014). Deep functional redundancy between FAMA and FOUR LIPS in stomatal development. Plant J. **78**: 555–565.

Lee, J.H., Jung, J.H., and Park, C.M. (2017). Light inhibits COP1-mediated degradation of ICE transcription factors to induce stomatal development in arabidopsis. Plant Cell **29**: 2817–2830.

Lee, L.R. and Bergmann, D.C. (2019). The plant stomatal lineage at a glance. J. Cell

Sci. **132**: 1–6.

Liu, Y.-J., Nunes-Nesi, A., Wallström, S. V, Lager, I., Michalecka, A.M., Norberg, F.E.B., Widell, S., Fredlund, K.M., Fernie, A.R., and Rasmusson, A.G. (2009). A redox-mediated modulation of stem bolting in transgenic Nicotiana sylvestris differentially expressing the external mitochondrial NADPH dehydrogenase. Plant Physiol **150**: 1248–1259.

Luo, L., He, Y., Zhao, Y., Xu, Q., Wu, J., Ma, H., Guo, H., Bai, L., Zuo, J., Zhou, J.M., Yu, H., and Li, J. (2019). Regulation of mitochondrial NAD pool via NAD+ transporter 2 is essential for matrix NADH homeostasis and ROS production in Arabidopsis. Sci China Life Sci **62**: 991–1002.

MacAlister, C.A., Ohashi-Ito, K., and Bergmann, D.C. (2007). Transcription factor control of asymmetric cell divisions that establish the stomatal lineage. Nature **445**: 537–540.

Masle, J., Gilmore, S.R., and Farquhar, G.D. (2005). The ERECTA gene regulates plant transpiration efficiency in Arabidopsis. Nature **436**: 866–870.

Matos, J.L., Lau, O.S., Hachez, C., Cruz-Ramírez, A., Scheres, B., and Bergmann, D.C. (2014). Irreversible fate commitment in the Arabidopsis stomatal lineage requires a FAMA and RETINOBLASTOMA-RELATED module. Elife **3**: 1–15.

Mehterov, N., Balazadeh, S., Hille, J., Toneva, V., Mueller-Roeber, B., and Gechev, T. (2012). Oxidative stress provokes distinct transcriptional responses in the stress-tolerant atr7 and stress-sensitive loh2 Arabidopsis thaliana mutants as revealed by multi-parallel quantitative real-time PCR analysis of ROS marker and antioxidant genes. Plant Physiol. Biochem. **59**: 20–29.

Murashige, T. and Skoog, F. (1962). A revised medium for rapid growth and bio assays with tobacco tissue cultures. Physiol. Plant. **15**: 474–497.

Nadeau, J.A. and Sack, F.D. (2002). Control of stomatal distribution on the Arabidopsis leaf surface. Science (80-.). **296**: 1697–1700.

Noctor, G. and Foyer, C.H. (2016). Intracellular redox compartmentation and ROS-related communication in regulation and signaling. Plant Physiol. **171**: 1581–1592.

Noctor, G., Queval, G., and Gakière, B. (2006). NAD(P) synthesis and pyridine nucleotide cycling in plants and their potential importance in stress conditions. J. Exp. Bot. **57**: 1603–1620.

Ohashi-Ito, K. and Bergmann, D.C. (2006). Arabidopsis FAMA controls the final

proliferation/differentiation switch during stomatal development. Plant Cell **18**: 2493–2505.

Ohashi, K., Kawai, S., and Murata, K. (2013). Secretion of quinolinic acid, an intermediate in the kynurenine pathway, for utilization in NAD+ biosynthesis in the yeast Saccharomyces cerevisiae. Eukaryot. Cell **12**: 648–653.

Palmieri, F. et al. (2009). Molecular identification and functional characterization of Arabidopsis thaliana mitochondrial and chloroplastic NAD+ carrier proteins. J. Biol. Chem. **284**: 31249–31259.

Pan, X., Welti, R., and Wang, X. (2010). Quantitative analysis of major plant hormones in crude plant extracts by high-performance liquid chromatography-mass spectrometry. Nat. Protoc. **5**: 986–992.

Pétriacq, P., Tcherkez, G., and Gakière, B. (2016a). Pyridine nucleotides induce changes in cytosolic pools of calcium in Arabidopsis. Plant Signal. Behav. **11**: 1–3.

Pétriacq, P., Ton, J., Patrit, O., Tcherkez, G., and Gakière, B. (2016b). NAD acts as an integral regulator of multiple defense layers. Plant Physiol. **172**: 1465–1479.

Pham, P.A., Wahl, V., Tohge, T., de Souza, L.R., Zhang, Y., Do, P.T., Olas, J.J., Stitt, M., Araújo, W.L., and Fernie, A.R. (2015). Analysis of knockout mutants reveals non-redundant functions of poly(ADP-ribose)polymerase isoforms in Arabidopsis. Plant Mol. Biol. **89**: 319–338.

Pillitteri, L.J., Sloan, D.B., Bogenschutz, N.L., and Torii, K.U. (2007). Termination of asymmetric cell division and differentiation of stomata. Nature **445**: 501–505.

Pillitteri, L.J. and Torii, K.U. (2007). Breaking the silence: Three bHLH proteins direct cell-fate decisions during stomatal development. BioEssays **29**: 861–870.

Pillitteri, L.J. and Torii, K.U. (2012). Mechanisms of Stomatal Development. Annu. Rev. Plant Biol. **63**: 591–614.

Van Roermund, C.W.T., Schroers, M.G., Wiese, J., Facchinelli, F., Kurz, S., Wilkinson, S., Charton, L., Wanders, R.J.A., Waterham, H.R., Weber, A.P.M., and Linka, N. (2016). The peroxisomal NAD carrier from Arabidopsis imports NAD in exchange with AMP. Plant Physiol. **171**: 2127–2139.

Saibo, N.J.M., Vriezen, W.H., Beemster, G.T.S., and Van Der Straeten, D. (2003). Growth and stomata development of Arabidopsis hypocotyls are controlled by gibberellins and modulated by ethylene and auxins. Plant J. **33**: 989–1000.

Salem, M.A., Li, Y., Wiszniewski, A., and Giavalisco, P. (2017). Regulatory-associated protein of TOR (RAPTOR) alters the hormonal and metabolic composition of Arabidopsis seeds, controlling seed morphology, viability and germination potential. Plant J. **92**: 525–545.

Schippers, J.H.M., Nunes-Nesi, A., Apetrei, R., Hille, J., Fernie, A.R., and Dijkwel, P.P. (2008). The Arabidopsis onset of leaf death5 mutation of quinolinate synthase affects nicotinamide adenine dinucleotide biosynthesis and causes early ageing. Plant Cell **20**: 2909–2925.

Shpak, E.D., Lakeman, M.B., and Torii, K.U. (2003). Dominant-negative receptor uncovers redundancy in the Arabidopsis ERECTA leucine-rich repeat receptor-like kinase signaling pathway that regulates organ shape. Plant Cell **15**: 1095–1110.

Shpak, E.D., McAbee, J.M., Pillitteri, L.J., and Torii, K.U. (2005). Plant science: Stomatal patterning and differentiation by synergistic interactions of receptor kinases. Science (80-.). **309**: 290–293.

Siegel, R.S., Xue, S., Murata, Y., Yang, Y., Nishimura, N., Wang, A., and Schroeder, J.I. (2009). Calcium elevation-dependent and attenuated resting calcium-dependent abscisic acid induction of stomatal closure and abscisic acid-induced enhancement of calcium sensitivities of S-type anion and inward-rectifying K+ channels in Arabidopsis guard cells. Plant J. **59**: 207–220.

Simmons, A.R. and Bergmann, D.C. (2016). Transcriptional control of cell fate in the stomatal lineage. Curr. Opin. Plant Biol. **29**: 1–8.

de Souza Chaves, I. et al. (2019). The mitochondrial NAD+ transporter (NDT1) plays important roles in cellular NAD+ homeostasis in Arabidopsis thaliana. Plant J. **100**: 487–504.

Strømland, Ø., Niere, M., Nikiforov, A.A., VanLinden, M.R., Heiland, I., and Ziegler, M. (2019). Keeping the balance in NAD metabolism. Biochem. Soc. Trans. **47**: 119–130.

Sugano, S.S., Shimada, T., Imai, Y., Okawa, K., Tamai, A., Mori, M., and Hara-Nishimura, I. (2010). Stomagen positively regulates stomatal density in Arabidopsis. Nature **463**: 241–244.

Sun, L., Li, Y., Miao, W., Piao, T., Hao, Y., and Hao, F.S. (2017). NADK2 positively modulates abscisic acid-induced stomatal closure by affecting accumulation of

H2O2, Ca2+ and nitric oxide in Arabidopsis guard cells. Plant Sci. **262**: 81–90.

Takahashi, H., Takahara, K., Hashida, S.N., Hirabayashi, T., Fujimori, T., Kawai-Yamada, M., Yamaya, T., Yanagisawa, S., and Uchimiya, H. (2009). Pleiotropic modulation of carbon and nitrogen metabolism in Arabidopsis plants overexpressing the NAD kinase2 gene. Plant Physiol. **151**: 100–113.

Tanaka, Y., Nose, T., Jikumaru, Y., and Kamiya, Y. (2013). ABA inhibits entry into stomatal-lineage development in Arabidopsis leaves. Plant J. **74**: 448–457.

Vanderauwera, S., Block, M. De, Steene, N. Van De, Cotte, B. Van De, Metzlaff, M., and Breusegem, F. Van (2007). Silencing of poly(ADP-ribose) polymerase in plants alters abiotic stress signal transduction. PNAS **104**: 15150-.

Waadt, R., Hitomi, K., Nishimura, N., Hitomi, C., Adams, S.R., Getzoff, E.D., and Schroeder, J.I. (2014). FRET-based reporters for the direct visualization of abscisic acid concentration changes and distribution in Arabidopsis. Elife **2014**: 1–28.

Wang, C., Zhou, M., Zhang, X., Yao, J., Zhang, Y., and Mou, Z. (2017). A lectin receptor kinase as a potential sensor for extracellular nicotinamide adenine dinucleotide in arabidopsis thaliana. Elife **6**: 1–23.

Wang, H., Ngwenyama, N., Liu, Y., Walker, J.C., and Zhang, S. (2007). Stomatal development and patterning are regulated by environmentally responsive mitogen-activated protein kinases in Arabidopsis. Plant Cell **19**: 63–73.

Webb, A.A.R., Larman, M.G., Montgomery, L.T., Taylor, J.E., and Hetherington, A.M. (2001). The role of calcium in ABA-induced gene expression and stomatal movements. Plant J. **26**: 351–362.

Wei, M., Zhuang, Y., Li, H., Li, P., Huo, H., Shu, D., Huang, W., and Wang, S. (2019). The cloning and characterization of hypersensitive to salt stress mutant, affected in quinolinate synthase, highlights the involvement of NAD in stress-induced accumulation of ABA and proline. Plant J.: 0–2.

Whalley, H.J., Sargeant, A.W., Steele, J.F.C., Lacoere, T., Lamb, R., Saunders, N.J., Knight, H., and Knight, M.R. (2011). Transcriptomic analysis reveals calcium regulation of specific promoter motifs in Arabidopsis. Plant Cell **23**: 4079–4095.

Wojtyla, Ł., Lechowska, K., Kubala, S., and Garnczarska, M. (2016). Different modest of hydrogen peroxide action during seed germination. Front Plant Sci. **7**:

1–16.

Xu, J., Tran, T., Padilla Marcia, C.S., Braun, D.M., and Goggin, F.L. (2017). Superoxide-responsive gene expression in Arabidopsis thaliana and Zea mays. Plant Physiol. Biochem. **117**: 51–60.

Yang Ming and Sack, F.D. (1995). The too many mouths and four lips mutations affect stomatal production in Arabidopsis. Plant Cell **7**: 2227–2239.

Yang, Y., Costa, A., Leonhardt, N., Siegel, R.S., and Schroeder, J.I. (2008). Isolation of a strong Arabidopsis guard cell promoter and its potential as a research tool. Plant Methods **4**: 1–15.

Yoo, C.Y., Mano, N., Finkler, A., Weng, H., Day, I.S., Reddy, A.S.N., Poovaiah, B.W., Fromm, H., Hasegawa, P.M., and Mickelbart, M. V. (2019). A Ca2+/CaM-regulated transcriptional switch modulates stomatal development in response to water deficit. Sci. Rep. **9**: 1–15.

Yoshida, T., Mogami, J., and Yamaguchi-Shinozaki, K. (2014). Omics approaches toward defining the comprehensive abscisic acid signaling network in plants. Plant Cell Physiol. **56**: 1043–1052.

Yoshida, T., Obata, T., Feil, R., Lunn, J.E., Fujita, Y., Yamaguchi-Shinozaki, K., and Fernie, A.R. (2019). The role of abscisic acid signaling in maintaining the metabolic balance required for Arabidopsis growth under nonstress conditions. Plant Cell **31**: 84–105.

Zeng, X., Li, Y.F., and Mahalingam, R. (2014). Arabidopsis nudix hydrolase 7 plays a role in seed germination. Planta **239**: 1015–1025.

Zhang, A.Y. and Li, P.L. (2006). Vascular physiology of a Ca2+ mobilizing second messenger - Cyclic ADP-ribose. J. Cell. Mol. Med. **10**: 407–422.

Zoulias, N., Harrison, E.L., Casson, S.A., and Gray, J.E. (2018). Molecular control of stomatal development. Biochem. J. **475**: 441–454.

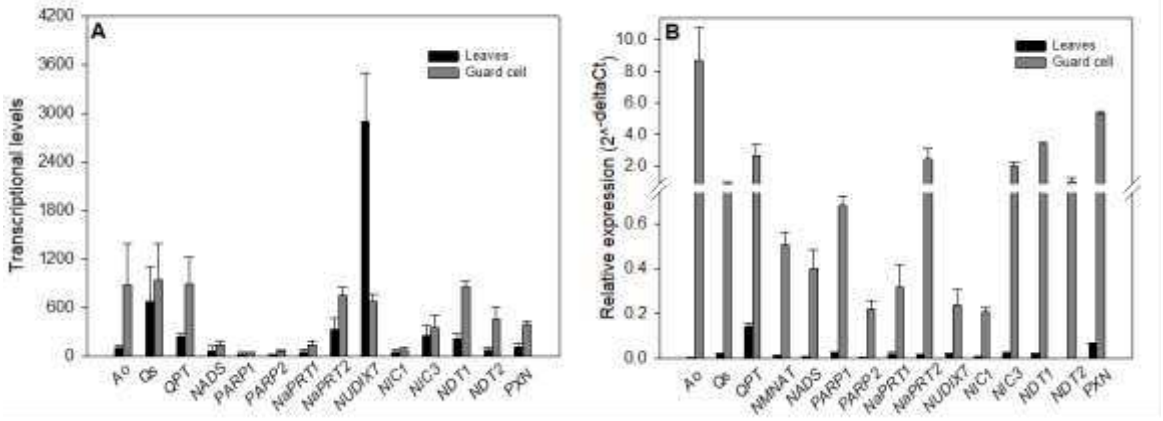

Supplemental Figure 1: Relative gene expression analysis of genes belonging to NAD⁺ biosynthetic pathway along with NAD⁺ transporters in leaves and guard cells of Arabidopsis plants.
A) Publically available transcriptome data. **B)** NAD-related transcripts from whole leave extracts and isolated epidermis fragments. Total RNA of leaves and isolated epidermis fragments was extracted from 4-week-old plants. Relative transcript abundance was measured by qPCR. ACT2 and F-box were used as housekeeping genes and values are presented as means ± SE (n = 3).

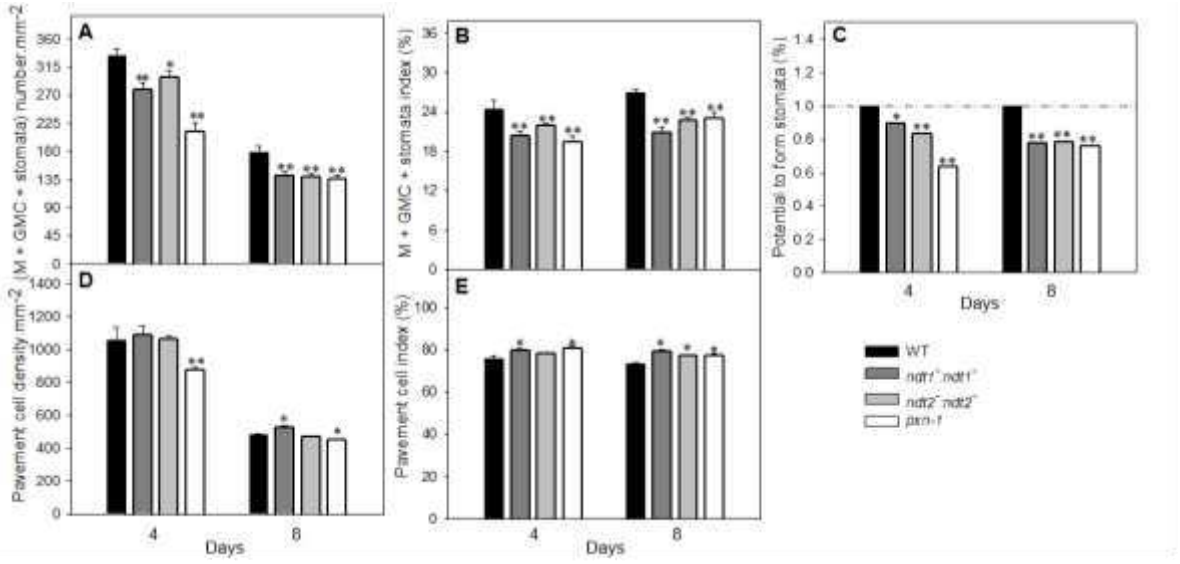

Supplemental Figure 2: NAD⁺ transport into mitochondria and peroxisomes impacts stomata and pavement cell number in *Arabidopsis thaliana* cotyledons.
Abaxial epidermal layer of cotyledons were photographed at 4 and 8 days after sowing on soil and analyzed by optical microscopy. **A)** (M + GMC + Stomata).mm^{-2}. **B)** M + GMC + Stomata index. **C)** Potential to forma stomata (%). **D)** Pavement cell density.mm^{-2}. **E)** Pavement cell index. Values are presented as means ± SE (n=12). Asterisks represents values that were judged to be significantly different from the WT (*p < 0.05, **p <0.01). WT: black bars, *ndt1^{-}:ndt1^{-}* : dark gray bars, *ndt2^{-}:ndt2^{-}*: gray bars and *pxn-1*: white bars.

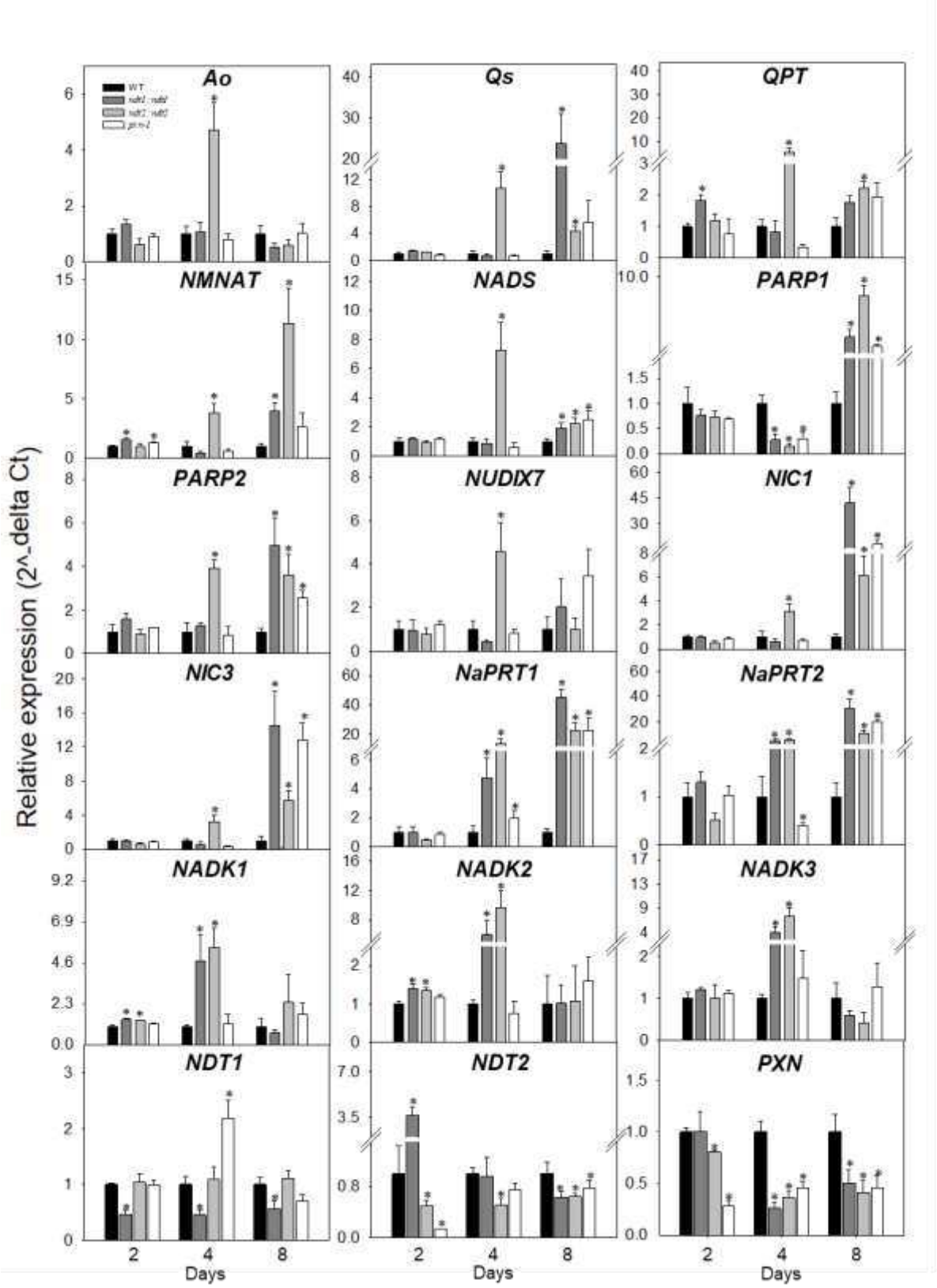

Supplemental Figure 3: Relative transcript levels of genes involved in NAD⁺ and NADP⁺ biosynthesis.

Transcript abundance of *Arabidopsis thaliana* NAD biosynthesis genes belonging to the *de novo Aspartate oxidase (AO), Quinolinate synthase (QS), Quinolinate phosphoribosyltransferase (QPT), Nicotinamide mononucleotide adenylyltransferease*

(NMNAT), NAD synthetase (NADS) and salvage pathway Poly(ADP-ribose)polymerase 1 (PARP1), Poly(ADP-ribose)polymerase 2 (PARP2), Nudix hydrolase 7 (NUDIX7), Nicotinamidase 1 (NIC1), Nicotinamidase 3 (NIC3), Nicotinate phosphoribosyltransferase 1 (NaPRT1), Nicotinate phosphoribosyltransferase 2 (NaPRT2) together with NADP biosynthesis genes *NAD kinase 1 (NADK1), NAD kinase 2 (NADK2), NAD kinase 3 (NADK3)* and NAD^+ transporters was determined. RNA was isolated from seedlings at 2, 4 and 8 days after sowing. Actin was used as endogenous control. Values are compared with the WT of each time and presented as means SE (n=4). Asterisks indicate that the values from mutant lines were determined by Student's t test to be significantly different (P< 0.05) from WT.

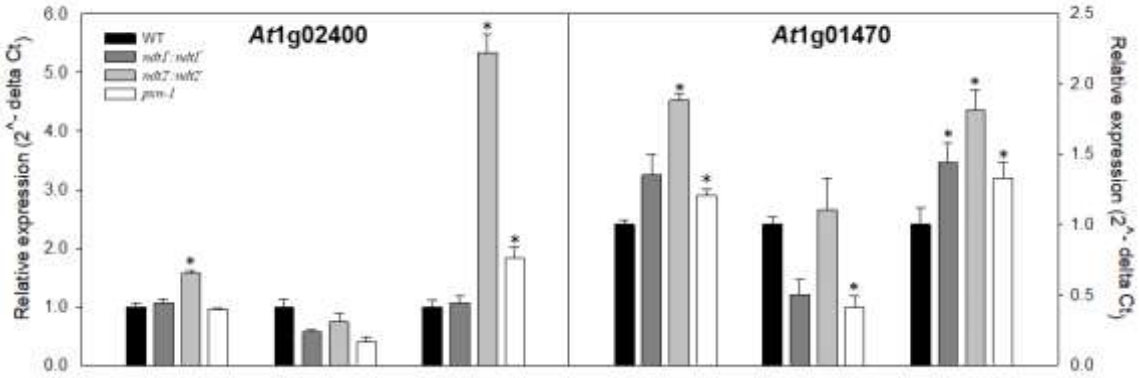

Supplemental Figure 4: Relative gene expression of calcium responsive genes in seedlings of WT and NAD^+ transporter mutants at 2, 4 and 8 days after sowing. Total RNA of seedlings was extracted and relative transcript abundance was measured for *At*g02400 and *At1*g01470 by qPCR. *ACT2* was used as housekeeping gene and values are presented as means ± SE (n = 3).

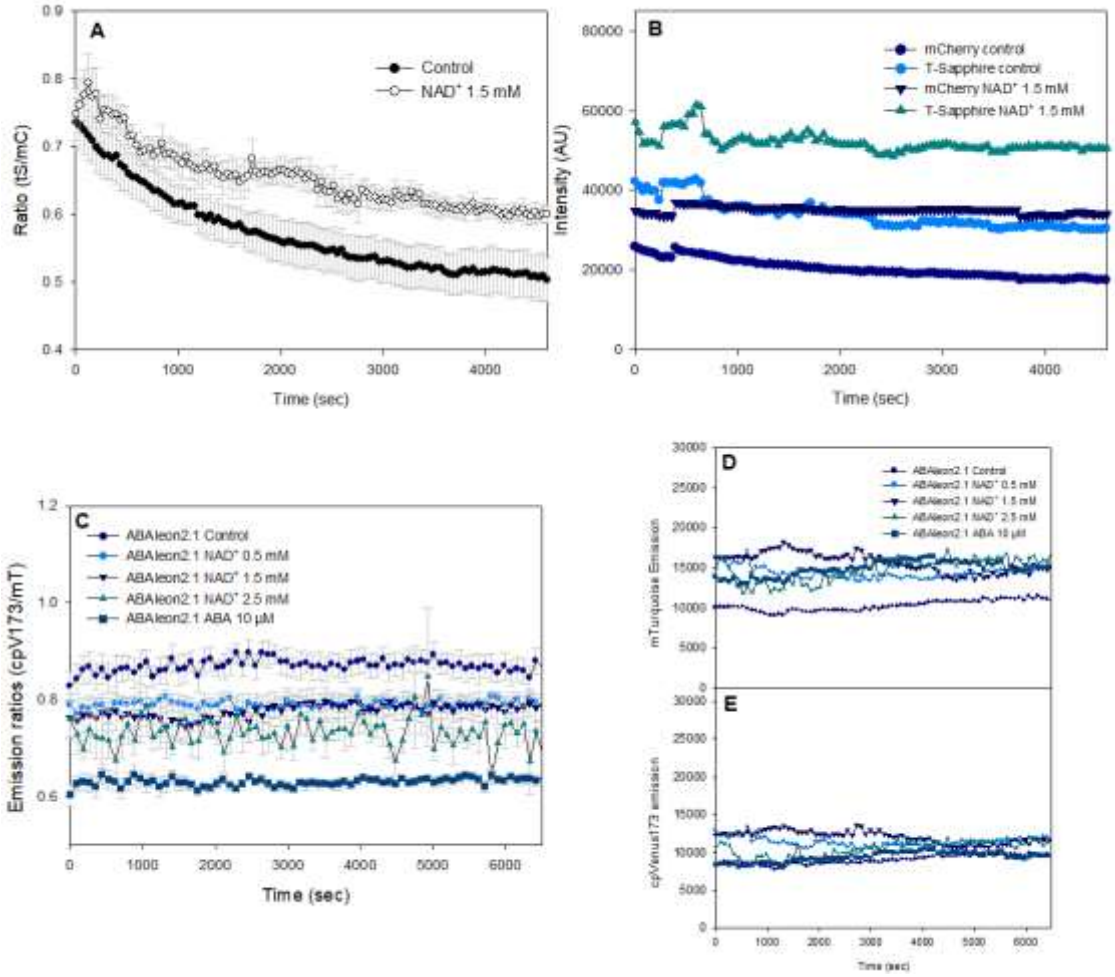

Supplemental Figure 5: Time course responses of Peredox-mCherry and ABAleon2.1 seedlings treated with NAD⁺.
A) Fluorescence emission of Peredox-mCherry seedlings grown for 8 days in medium containing NAD⁺ 1.5 mM. Peredox-mCherry sensor reports the NADH/NAD⁺ ratio. **B)** Emission intensities of T-Sapphire and mCherry. **C)** Fluorescence emission of 8-days-old ABAleon2.1 seedlings treated with NAD⁺ (0, 0.5, 1.5, 2.5 mM) and ABA 10µM for 5 days. ABAleon is a sensor protein able to detect changes in ABA *in vivo*. **D)** and **E)** Emission intensities of mTurquoise and cpVenus173. Values are means ± SE (n=7).

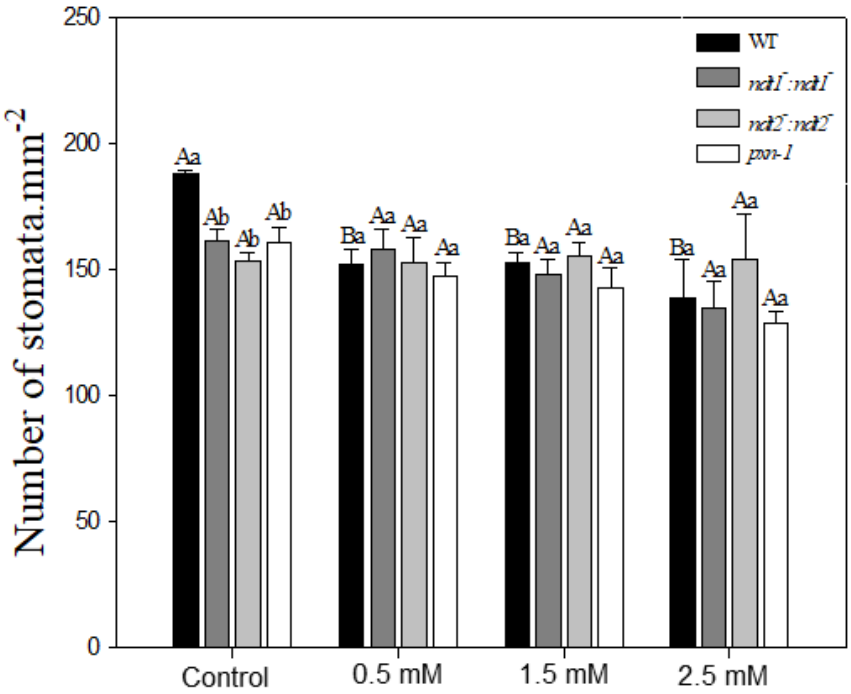

Supplemental Figure 6: Effects of Exogenous NAD⁺ treatment in stomatal number in WT and NAD⁺ carrier mutants

Stomatal density of seedlings treated with exogenous NAD⁺. Seedlings of WT and NAD⁺ carrier mutants were grown in culture medium containing 0, 0.5, 1.5 and 2.5 mM of NAD⁺ for 8 days. Abaxial surfaces of 10 cotyledons per genotype were photographed and analyzed by optical microscopy. Lower case letters: statistical difference between genotypes within the same treatment / dose. Capital letter: statistical difference of the same genotype at different doses performed by Tukey test ($p < 0.05$). WT: black bars, *ndt1⁻:ndt1⁻* : dark gray bars, *ndt2⁻:ndt2⁻*: gray bars and *pxn-1*: white bars.

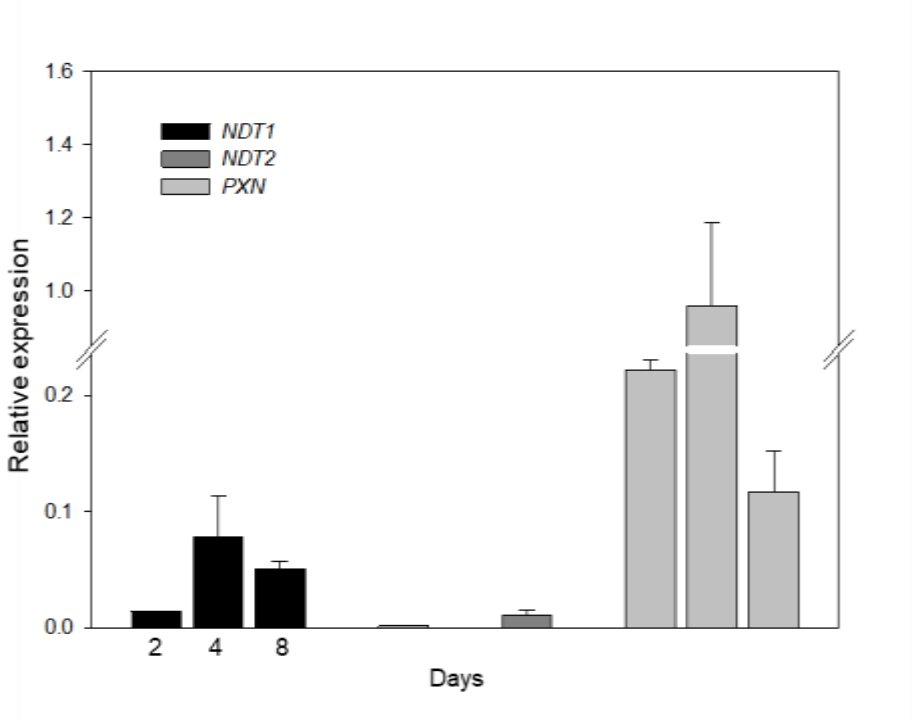

Supplemental Figure 7: Relative gene expression of NAD⁺ transporters in WT plants at 2, 4 and 8 days after sowing.
Total RNA of seedlings was extracted and relative transcript abundance was measured for *NDT1, NDT2* and *PXN* genes by qPCR. ACT2 was used as housekeeping gene and values are presented as means ± SE (n = 3).

Supplementary Table 1: List of primers used in this work to perform qPCR.

Gene code	Name	Foward	Reverse
At2G39970	PXN	ACAACGTTACCGCTTTGGAGAC	TGACTGTAGCTCCGAGTTTCGC
At1g25380	NDT2	CGATGCCATGTTCCAACTAC	CATCAAAAGGGCCAAAAAGT
At2g47490	NDT1	GGGAATTCGCGGATTGTACAGTGG	TGGGAAACTGAATGGCAACATGAC
At5g14760	Ao	TGGTCGCTGGTGCTCATCTTTG	AGGCCCTTCAGTACACACAACTC
At5g50210	Qs	TAGCAGGTGGTGAAGGTTGCTC	AGCGAGCTAAGCGAGTTCATCTTC
At2g01350	QPT	TTGGGAAAGTATCAGGGAATGCAC	TGCAGCATCTGCCATTAACTTGG
At5g55810	NMNAT	TGGCAACTGGGAGTTTCAATCCTC	TCTCTCGCCAGCTCAAACATGC
At1g55090	NADs	CAACAGCTGAGCTTGAGCCCATTC	CCATGTCGACTTCATCGAGCTGAG
At4g36940	NAPRT1	AGAACGAACCACCTCCAAAGGTC	AGCTCTTCCCTAGCTTCATCTGC
At2g23420	NAPRT2	AGTGCCACAACGTGTCGAAGAG	TTCTCTTGCTTCATCTGCACTTCC
At2G22570	NIC1	CGGCAATATGGCTCCAACAAAGC	GCAAGCTTTGCACTTTCCTCCAC
At5G23220	NIC3	ACTCGTCATCGACATGCAGAAC	CCTTTCACTTGCGTCACAGCAC
At4g12720	NUDIX7	AATTCTCTCCAAGGTACACACAGC	CCATAGGTTCCACCATGGTTACAG
At2g31320	PARP1	ATCGTCTACGATACAGCCCAGGTG	TGGTTCAGGCTCATCTCTTGTGC
At4g02390	PARP2	ATGCTACTCTGGCACGGTTCAC	AGGAGGAGCTATTCGCAGACCTTG
At2g37620	Actin	CTTGCACCAAGCAGCATGAA	CCGATCCAGACACTGTACTTCCTT
At5g53210	SPEECHLESS	TCCTTCACCGCCTGTTCTAAGC	TGAATCTGGTGGTGGTTGATGCG
At3g06120	MUTE	AACGTCGAAAGACCCTAAACCG	TGGATGGCTCGATTGTCTGGTG
At3g24140	FAMA	TTACTCGGCACCAAACTTCTTAGG	CGGAAGGAGAGAGTTGATGTTGC
At2g20875	EPF1	ACCAACATCCTCCCATCCAAGTC	ACAAGACGGCATGGAGAACACG
At1g34245	EPF2	AGCTCAAACGCACCACAAGAAG	CACGTTTACACGGCGAACATGC
At2g26330	ER (Erecta)	AGCCTCTGGGATCTTCTTCATGGC	AGCCGTGTGTCCCAATCAAGAG
At5g62230	ERL1	AGCTAACCGGTTTGTGGTACTTTG	ATTTCCGATGCTCTCCGGGATG
At5g07180	ERL2	TCACTGGTCCAATACCAGCAACC	AGCTGGTTTCTTGCGAGGTCAAG
At1g80080	TMM	AACAGTCTTCGGGTCCTTCACC	TTCACGTCCCGGAACTCCAAAG
At3g26744	SCRM1	AGGCCAGCAAGCTAGAGTTGAG	TCATGGTAGCGAGCAACAGACC
At1g12860	SCRM2	AGTTGTGTCCATCTTCCTCCTTGC	TAACCTCAACTCTTGGTTGTTGGC
At1g04110	SDD1	TGTACGATCGTCAAGGGAAAGCG	TTCACATGCCCTGCTCCAATCG
At3g21070	NADK1	GTCAATGGTCCATCCTCAGGTTCC	TGGGCGGAATGATAGAGAATGCG
At1g21640.	NADK2	GGCAAAGCAATGCCTGGTAAAGTG	ACTCCATCGCCTTGTACCTTCG
At1g78590	NADK3	ACTCTGTTCCGGTTCTAGGAGTC	TGATCGCTCAGTTCTTCGACCTC
At5g52310	RD29A	TGGACAAAGCAATGAGCATGAGC	AGGTTTACCTGTTACGCCTGGTG
At5g52300	RD29B	ACTGATCCCACGCATAAAGGTG	CTCGTCGGAAAGTCTTCTTCGC
At5g67030	ABA1	TGGGCTTGGTCCTCTGTCTTTC	CACCAACTCTTCCTGGATGTGG
At3g24220	ABA2	TGCAGTGGCATTGCGAAGGTAG	ACCGGCTCGGTCCGTAATTAAAC
At5g59820	ZAT12	TGCGAGTCACAAGAAGCCTA	GTGTCCTCCCAAAGCTTGTC
At2g23430	ICK1	GTA TCG ACG GGG TAC GAA GA	TTA ACC GCC GAT TCA AAT TC
At4g34000	ABF3	GTT CTC AAC CTG CAA CAC AGT GC	TCC AGG AGA TAC TGC TGC AAC C
At1g02400	Calcium responsive 1	CCCATCTGACCCTACATGCT	TGGCTTCTTTGCTGTGTTTG
At1g01470	Calcium responsive 2	ATCAAGAGCCGTCATGTCCT	TCATTCGATTCCGATCTGTG

Supplementary Table 2: List of primers used to perform coexpression analysis

NAD metabolism

At5g14760	At4g36940	At1g25380	At2g04430
At5g50210	At2g23420	At2g39970	At2g04450
At1g21640	At5g55810	At1g55090	At4g12720
At1g78590	At2g01350	At5g09230	At5g47240
At3g21070	At2g22570	At1g68760	At3g46200
At5g22470	At5g23230	At5g47650	At4g25434
At2g31320	At5g23220	At1g79690	At5g45940
At4g02390	At2g47490	At1g18300	At1g30110
At2g31865	At3g46200	At5g55760	At2g31870

Stomatal biogenesis

At5g53210	At3g26744	At1g0080	At1g14350
At3g06120	At4g21750	At2g26330	At4g12970
At3g24140	At4g04890	At1g34245	At1g20160
At3g12280	At1g05230	At1g06390	At1g12860

ABA metabolism

At4g15560	At3g04870	At4g25700	At1g67080
At4g36810	At1g06820	At5g52570	At1g30100
At5g17230	At5g57030	At5g67030	At4g18350
At4g14210	At3g10230	At1g08550	At3g14440
At3g24220	At1g52340	At1g16540	At5g45340
At1g78390	At2g27150	At4g19230	At2g29090
At1g52400			

Chapter 2: The importance of NAD transporters in responses to elevated CO_2

Elias Feitosa Araujo[1], Mateus Miranda Pena[1], Wagner L. Araújo[1], Adriano Nunes-Nesi[1]

[1] Departamento de Biologia Vegetal, Universidade Federal de Viçosa, 36570-900 Viçosa, Minas Gerais, Brazil

*Correspondence:

Adriano Nunes-Nesi
Departamento de Biologia Vegetal,
Universidade Federal de Viçosa,
36570-900 Viçosa, Minas Gerais, Brazil
Phone: +55-31-3612-5357
Email: nunesnesi@ufv.br

ABSTRACT

Nicotinamide adenine dinucleotide (NAD^+) is considered a cornerstone of plant metabolism due to its pivotal role in biological processes, mainly maintaining the redox homeostasis in subcellular compartments. As sessile organisms plants must adapt their metabolism, physiology and developmental processes to face challenge environmental cues such as elevated atmospheric CO_2 concentrations. As a central molecule in metabolism, it is expected that changes in CO_2 concentration would lead to changes in both NAD(P)(H) pool and dynamics of redox related processes. With the aim to study the relationship between high CO_2 concentration and NAD^+ distribution and its consequences for plant physiology, plants with reduced expression of mitochondrial (*NDT1, NDT2*) and peroxisomal (*PXN*) NAD^+ transporter genes were grown under elevated CO_2. Mutant plants exhibited reduced rosette dry weight and leaf number under high CO_2 compared to wild-type. Furthermore, the levels of photorespiratory intermediates, glutamate and glycine, accumulated in mutant lines under elevated CO_2. Moreover, NADPH/$NADP^+$ ratio was higher in mutant lines than in wild-type under elevated CO_2 concentration. Interestingly, while wild-type plants grown under high CO_2 increased seed production, the mutants were insensitive to increases in CO_2 concentration during reproductive phase, producing less seeds under both CO_2 conditions. These results suggest that the positive effects of CO_2 fertilization in plants is partially abolished in mutants with altered NAD^+ homeostasis. The compromised responses to CO_2 may also be linked to reduced stomatal number of NAD^+ carrier plants alongside reduced stomatal conductance under elevated CO_2. Together, these results demonstrate the importance of the correct NAD^+ distribution to control proper plant development, seed production and stomatal conductance under elevated CO_2 condition.

Key-words: NAD^+, NAD^+ carriers, high CO_2, Arabidopsis

INTRODUCTION

Several studies have demonstrated that changes in atmospheric CO_2 concentration affect plant performance and productivity (Thompson et al., 2017). It has been widely shown that elevated CO_2 concentrations alter plant responses related with photosynthesis (Ainsworth et al., 2008), photorespiration (Bishop et al., 2014), stomatal movements (Tian et al., 2015a), stomatal development (Woodward et al., 2002), seed yield (Meehl et al., 2007), harvest index (Meehl et al., 2007), seed quality (Taub et al., 2008), shoot and root growth (Masle, 2000; Takatani et al., 2014; Hachiya et al., 2014) along with metabolism (Ribeiro et al., 2012). Although the relationship between high CO_2 and redox status is still scarce, elevated CO_2 concentrations triggers biotic stress defenses through redox-linked pathways (Mhamdi and Noctor, 2016).

Given the absence of studies addressing the possible crosstalk between the main components of the redox pathways and elevated CO_2 concentrations in the environment, it seems reasonable that much attention has to be given to this topic in future studies. The nicotinamide adenine dinucleotide (NAD^+) and its derivative forms NAD(P)(H) are largely known as being important to regulate the cellular redox state in ambient CO_2 conditions (Noctor et al., 2006). High atmospheric CO_2 concentration enhance photosynthetic rates because the carboxylase activity of Rubisco is increased (Thompson et al., 2017). That said, a higher amount of NADPH is expected to be required to run the Calvin-Benson cycle at higher rates under high CO_2. Furthermore, the reduced oxygenase activity of Rubisco in elevated CO_2 conditions drastically diminishes the photorespiration, a process known as highly demanding on NAD^+ content inside chloroplasts, mitochondria and peroxisomes (Peterhansel et al., 2010). Additionally, a great body of studies have shown that increased CO_2 levels positively affects carbohydrates accumulation (Ribeiro et al., 2012; Thompson et al., 2017) which consequently would need NAD^+ as electron acceptor during their oxidation process over glycolysis and mitochondrial respiration. Therefore, it is plausible that the content and distribution of NAD(P)/NAD(P)(H) redox couples in subcellular compartments may have a role in plant performance under high CO_2.

Plants synthetize NAD^+ through two pathways, *de novo* and salvage pathway (Hashida et al., 2009; Gakière et al., 2018). The *de novo* pathway starts in plastids being aspartate or tryptophan the precursors, while the salvage pathway begins with nicotinamide (NAM) or nicotinic acid (NA). Both pathways converge to the formation of

the mononucleotide nicotinic acid (NaMN), which will posteriorly form NAD^+. The final steps of NAD^+ biosynthesis take place in cytosol and to perform its biological functions inside organelles it must be imported by them (Noctor et al., 2006). Biological membranes are impermeable to NAD^+, thus, specific membrane proteins are necessary to import and export NAD^+ through this barrier (Palmieri et al., 2011; Toleco et al., 2020). In Arabidopsis three genes encoding NAD^+ carriers have been found and characterized (Palmieri et al., 2009; Bernhardt et al., 2012). These genes named *NDT1*, *NDT2* and *PXN* encode proteins located in the mitochondria inner membrane and peroxisomes, respectively (Palmieri et al., 2009; Bernhardt et al., 2012; de Souza Chaves et al., 2019). The functional characterization of *NDT1* and *NDT2* genes demonstrated that correct NAD^+ transport into mitochondria is important to regulate stomatal development, stomatal conductance, photosynthesis, seed production and quality (de Souza Chaves et al, 2019; Feitosa-Araujo et al., 2020). Furthermore, the impaired NAD^+ import by peroxisomes negatively influenced fatty acids degradation in seedlings of *A. thaliana*, which led to a reduced lipid mobilization during the first steps of seedling development (Bernhardt et al., 2012).

The fact that disturbed NAD^+ transport (de Souza Chaves et al., 2019; Feitosa-Araujo et al., 2020) affected processes that are also regulated by CO_2 concentrations such as seed production, stomatal conductance and stomatal development along with photosynthesis led us to investigate how plants deficient in the transport of NAD^+ would behave in ambient with elevated CO_2 concentrations. For this, *NDT1*, *NDT2* and *PXN* mutant plants were submitted to two different atmospheric CO_2 concentrations and their metabolic and reproductive phase responses were analyzed. Overall, the results obtained demonstrated that the redox homeostasis impacted in NAD^+ carrier mutants, the reduced stomatal number and lower stomatal conductance did not allow them to efficiently respond to elevations on CO_2 content in terms of growth and increases in seed production as verified in WT plants.

RESULTS

Kinetics of stomatal aperture in plants with reduced expression of NAD transporters

We have demonstrated that plants with reduced *NDT1* expression exhibit decreased stomatal density and stomatal conductance compared to wild-type plants

(de Souza Chaves et al., 2019). Furthermore, we showed that stomatal development is negatively affected in cotyledons of *NDT1*, *NDT2* and *PXN* (previous Chapter of this thesis). In order to better understand the stomatal behavior in leaves of plants with reduced expression of NAD^+ transporters, we measured their water loss from detached 4-week-old rosettes (Figure 1A). Surprisingly, despite having less stomata per area *ndt1⁻:ndt1⁻ and pxn-3* mutant lines did not exhibit clear reduction in fresh weight loss in comparison with wild-type (Figure 1A). However, clear reduction was observed for *as-1-ndt1*, *ndt2⁻:ndt2⁻*, *as-1-ndt2* and *pxn-1* mutant plants regarding leaf water lost over the time in comparison with wild-type plants (Figure 1A).

Stomatal aperture is highly regulated by light, CO_2 concentration and the hormone ABA (Kinoshita et al., 2001; Kim et al., 2010; Munemasa et al., 2015; Jezek and Blatt, 2017). To study the kinetics of stomatal closing and opening, 40-day-old NAD^+ transporter mutants and wild-type plants were submitted to light-dark-light and ambient CO_2 – elevated CO_2 – ambient CO_2 transitions by using an infrared gas analyzer. The *ndt1⁻:ndt1⁻* , *as-1-ndt1*, *ndt2⁻:ndt2⁻* , *as-1-ndt2* and *pxn-3* lines kept the stomata more closed in high CO_2 concentrations while the *pxn-1* line behaved similarly to wild-type plants (Figure 1B). When plants were submitted to light-dark transitions no statistical differences were observed in stomatal conductance between lines (Supplementary Figure 1).

Expression analysis of ABA-responsive genes and NAD^+ biosynthetic genes in epidermal fragments of leaves from plants with reduced expression of NAD transporters

In the first chapter, we demonstrated a crosstalk between NAD^+ transport and ABA metabolism. To verify whether the guard cells of *NDT1*, *NDT2* and *PXN* mutants would have differential response to internal ABA, gene expression of three ABA-responsive genes *RD29A*, *RD29B* and *ABF3* was assessed in epidermal fragments, which is enriched with intact guard cells (Figure 1C). The peroxisomal line *pxn-1* showed reduced expression for the three ABA-responsive genes, while *ndt2⁻:ndt2⁻* presented the same transcription abundance only for the genes *RD29B* and *ABF3*.

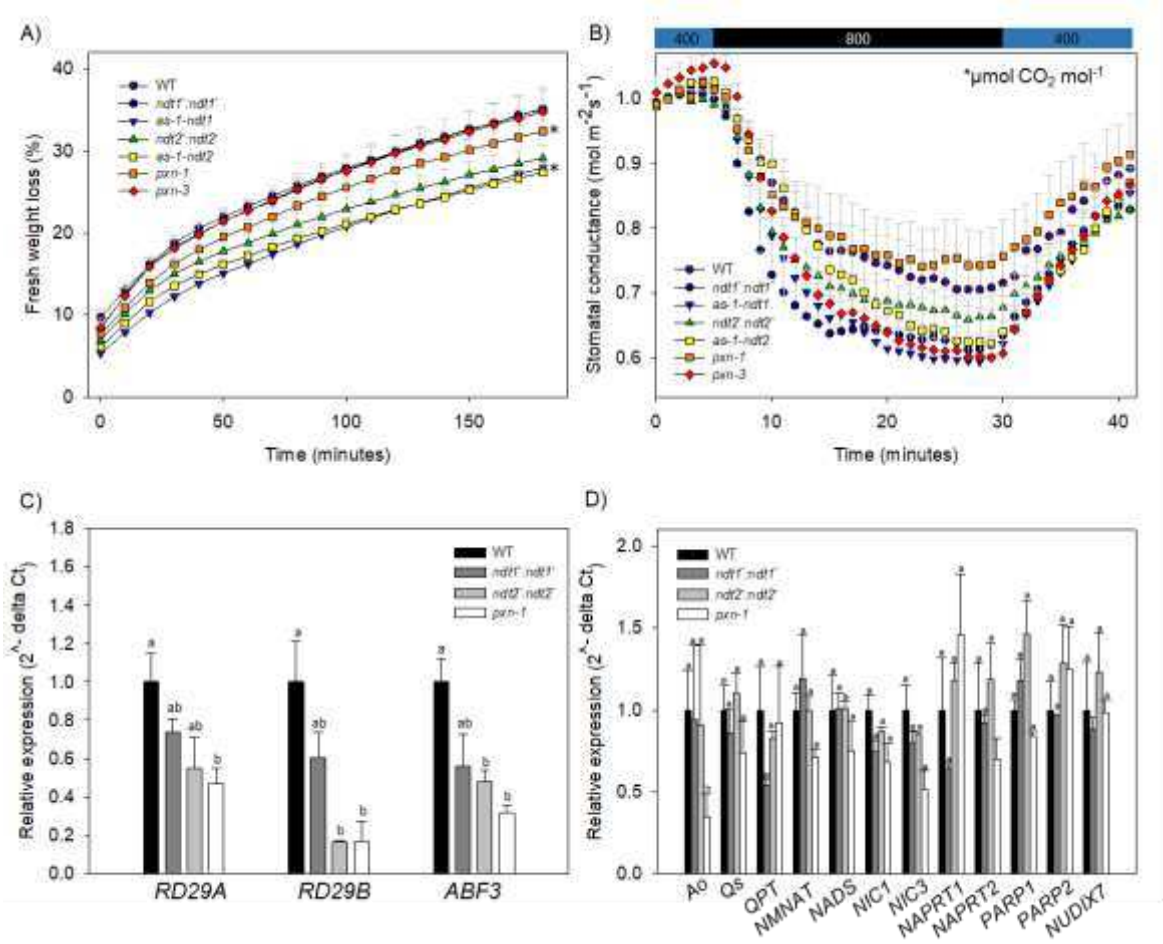

Figure 1: Stomatal movements and gene expression in plants with reduced expression of NAD⁺ carrier genes.
A) Fresh weight loss from detached 32-old-day rosettes. **B)** Stomatal conductance kinetics under CO_2 concentration transitions. **C)** Gene expression of ABA-responsive genes in epidermal fragments enriched with guard cells. **D)** Gene expression of NAD⁺ biosynthesis genes in epidermal fragments enriched with guard cells. Asterisks represent values that were judged to be statistically different from WT by T test ($p < 0.05$). Different letters represent values that were judged to be statistically different between lines by Tukey's test multiple comparison test ($p < 0.05$).

Even though the expression of *RD29A*, *RD29B* and *ABF3* followed a trend to be diminished in *NDT1* mutant line, it did not show statistical differences compared to wild-type plants. We also assessed the expression of genes belonging to NAD⁺ biosynthesis pathway and no differences in gene expression were found in epidermal fragments of NAD⁺ carrier mutants compared to wild-type, with exception of aspartate oxidase encoding gene (AO) that was significantly reduced in *PXN* mutant line (Figure 1D).

Growth parameters of NAD^+ carrier mutants under elevated atmospheric CO_2 concentrations

To obtain more insights into the physiological roles of NAD^+ distribution under high CO_2 concentrations, we grew NAD^+ carrier mutant plants in ambient CO_2 (400 μmol CO_2 mol^{-1}) for 16 days. Afterwards, we submitted all plants to elevated CO_2 (800 μmol CO_2 mol^{-1}) during 16 days. After CO_2 treatment, no remarkable differences in terms of growth phenotype among lines were observed between plants grown under atmospheric and high CO_2 conditions (Figure 2A). Under atmospheric CO_2 condition, the rosette dry weight was shown to be reduced only in *ndt1⁻:ndt1⁻* and *pxn-3* lines compared with the wild type while in higher CO_2 *ndt2* and *pxn* mutant lines presented diminished rosette dry weight in comparison with wild-type (Figure 2B). The mutant lines *ndt1⁻:ndt1⁻*, *as-1-ndt2* and *pxn-3* presented reduced rosette area under ambient CO_2 while in high CO_2 no differences were observed between wild-type and mutant lines (Figure 2C). The wild-type plants exhibited in both conditions a total leaf area higher than all mutant lines (Figure 2D). However, the specific rosette area and the specific leaf area were unchanged between mutants and wild-type plants in both conditions (Figure 2E and 2F). As shown for rosette dry weight, *ndt1⁻:ndt1⁻* and *pxn-3* lines presented a lower accumulation of root biomass in ambient CO_2 whereas only *pxn-1* line showed a low root dry weight in high CO_2 (Figure 2G). Any difference was observed for root/shoot ratio parameter in both conditions between the tested lines (Figure 2H). Nevertheless, the number of leaves per rosette was shown to be higher in wild-type plants under high CO_2 concentration than in mutant lines whereas no differences were observed between lines in ambient CO_2 (Figure 2I).

Changes in primary metabolism of NAD^+ carrier mutants submitted to high CO_2 concentration

In order to provide further information about the behavior of NAD^+ carrier mutants under high CO_2 we next performed detailed analyses of the primary metabolism in plants grown under elevated CO_2 for 16 days**.** The growth of plants with reduced expression of *NDT1*, *NDT2* and *PXN* genes along with WT plants under high CO_2 concentrations resulted in no changes in the levels of chlorophylls, amino acids, total protein and nitrate in leaves (Supplementary Figure 2A-G).

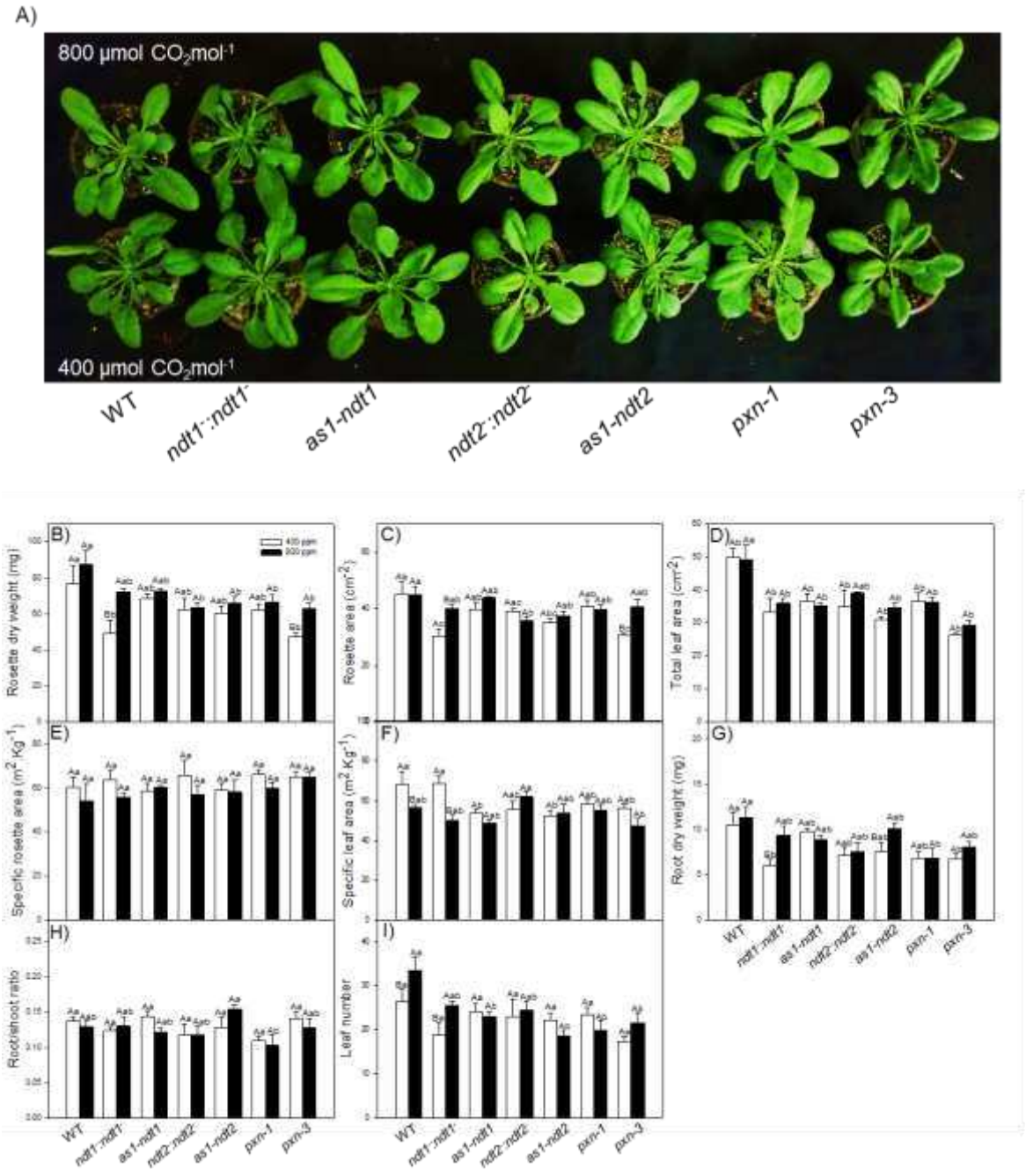

Figure 2: Growth parameters of plants with reduced expression of NAD⁺ carrier genes grown under ambient and elevated CO_2.

A) Phenotypic characterization of 32-day-old plants grown at 400 or 800 µmol CO_2mol^{-1}. **B)** Rosette dry weight (mg), **C)** Rosette area (cm^2), **D)** Total leaf area (cm^2), **E)** Specific rosette area ($m^2\ Kg^{-1}$), **F)** Specific leaf area ($m^2\ Kg^{-1}$), **G)** Root dry weight (mg), **H)** Root/Shoot ratio, **I)** Leaf number. Values are means ± SE of five independent replicates. Different capital letters represent values that were judged to be statistically different between treatments by Tukey's test multiple comparison test ($p < 0.05$). Different lower case letters represent values that were judged to be statistically different between lines in each treatment by Tukey's test multiple comparison test ($p < 0.05$).

To understand the importance of NAD^+ distribution in plants under high CO_2 concentration, we further performed a metabolite profiling analysis in leaves at the middle of the light period in non-flowering plants of NAD^+ carrier mutants and wild-type submitted to elevated CO_2 concentration for 16 days. No major changes were observed between NAD^+ carrier mutants and wild-type plants in terms of glucose, fructose, sucrose, starch, malate and fumarate contents at ambient and elevated CO_2 (Supplementary Figure 3A-F). The only exception was found for the higher sucrose content in *as-1-ndt2* line in elevated CO_2 (Supplementary Figure 3C).

We next measured a broad number of compounds from different classes of metabolites by GC-MS approach. This analysis revealed that, among 38 successfully annotated compounds, considerable changes in both TCA cycle and photorespiratory intermediates and amino acids were observed (Figure 3 and Supplementary table 1). The levels of alanine, aspartate, cysteine and glutamate were shown to be increased in leaves of NAD^+ transporter mutants under high CO_2 while the levels of glycine and cysteine were reduced under this condition compared to wild-type (Figure 3). The mutant lines presented higher levels of GABA and gluconate in high CO_2 condition when compared to wild-type plants (Figure 3). No major changes were observed for sugar and sugar alcohols except for raffinose levels that were reduced in all mutant lines under high CO_2 condition. The levels of shikimate and putrescine behaved in opposite ways. While the shikimate content of wild-type was reduced compared to NAD^+ transporter lines the levels of putrescine were reduced in NAD^+ carrier mutants under high CO_2 concentrations (Figure 3). The photorespiratory intermediates glycine, serine and glycerate were reduced in all lines, a common response for plants grown under high CO_2. However, *as-1-ndt2*, *pxn-1* and *pxn-3* lines accumulated more glycine while *ndt1*$^-$*:ndt1*$^-$ and *ndt2*$^-$*:ndt2*$^-$ lines accumulated more glycerate compared to wild-type plants (Figure 3).

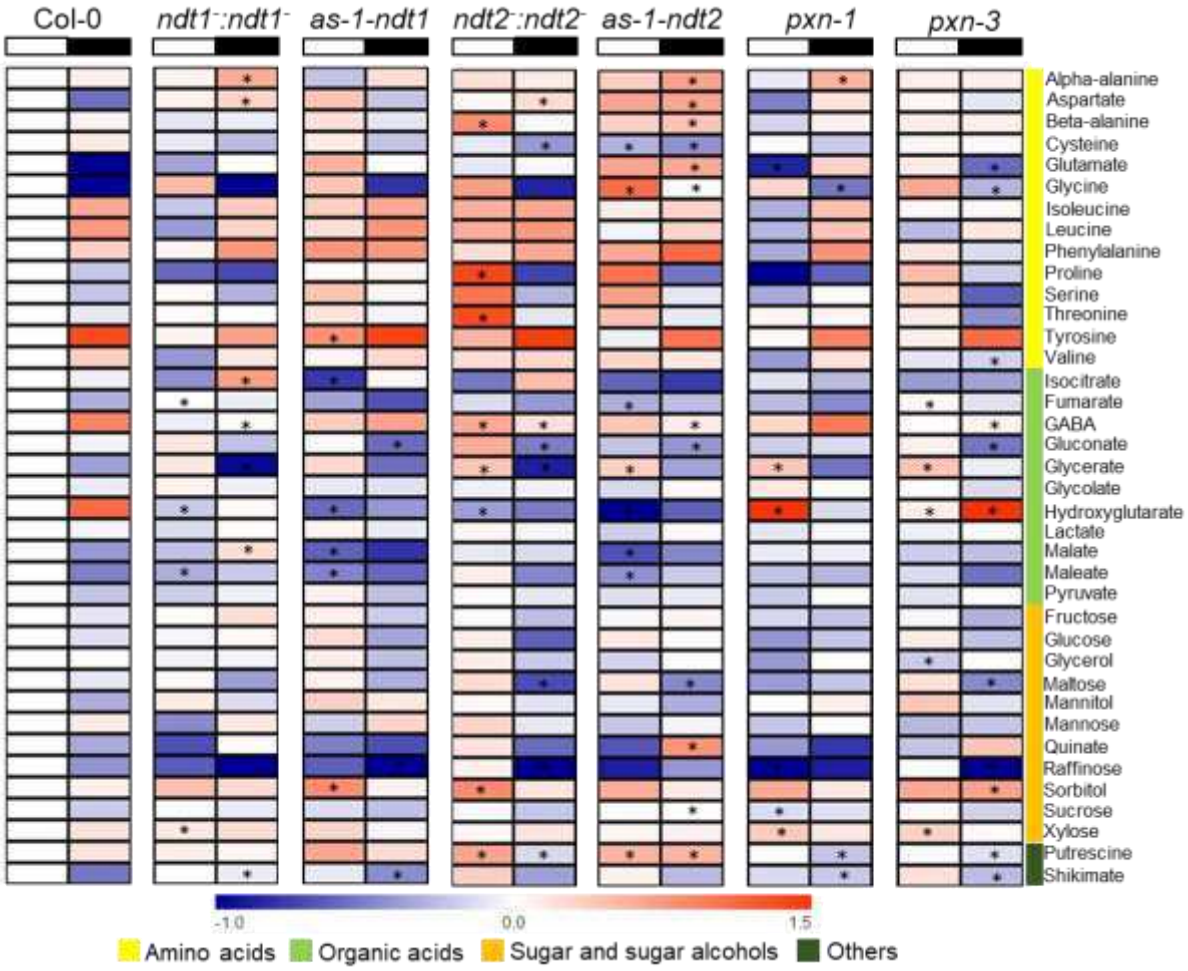

Figure 3: Heat map showing the changes in relative abundance of metabolite levels measured by GC-MS in WT and NAD⁺ carrier mutants submitted to high CO_2 concentration.
WT, *ndt1⁻:ndt1⁻*, *as-1-ndt1*, *ndt2⁻:ndt2⁻*, *as-1-ndt2*, *pxn-1* and *pxn-3* plants were grown under high CO_2 concentration for 16 days. Relative log_2-transformed values of signal intensities were normalized with respect to the mean response calculated for the wild type at ambient CO_2 concentration. Values are means ± SE of five independent samplings. Asterisks represent values that were judged to be statistically different between lines compared to WT in each treatment by Tukey's test multiple comparison test ($p < 0.05$).

Changes in pyridine nucleotide levels in leaves of NAD⁺ carrier mutants submitted to high CO_2 concentrations

To verify the influence of elevated CO_2 on the redox balance, the content of pyridine nucleotides was assessed in leaves of plants submitted to high CO_2 during 16 days. In ambient CO_2 only *pxn-1* line presented lower content of NAD^+ while in high CO_2 *ndt1⁻:ndt1⁻*, *as-1-ndt2* and *pxn-3* lines showed increases in NAD^+ (Figure 4A). The reduced form NADH did not show any difference among lines under both CO_2 conditions (Figure 4B). The contents of $NADP^+$ were shown to be increased in *ndt1⁻*

:ndt1^{-}, *ndt2*$^{-}$*:ndt2*$^{-}$ and *as-1-ndt2* lines in ambient CO_2 while in high CO_2 *as-1-ndt2* and pxn-3 lines presented higher amounts compared to wild-type (Figure 4C). In ambient CO_2 the levels of NADPH were unchanged between lines while in elevated CO_2 *ndt1*$^{-}$*:ndt1*$^{-}$, *as-1-ndt1 and ndt2*$^{-}$*:ndt2*$^{-}$ presented higher levels of NADPH (Figure 4D).

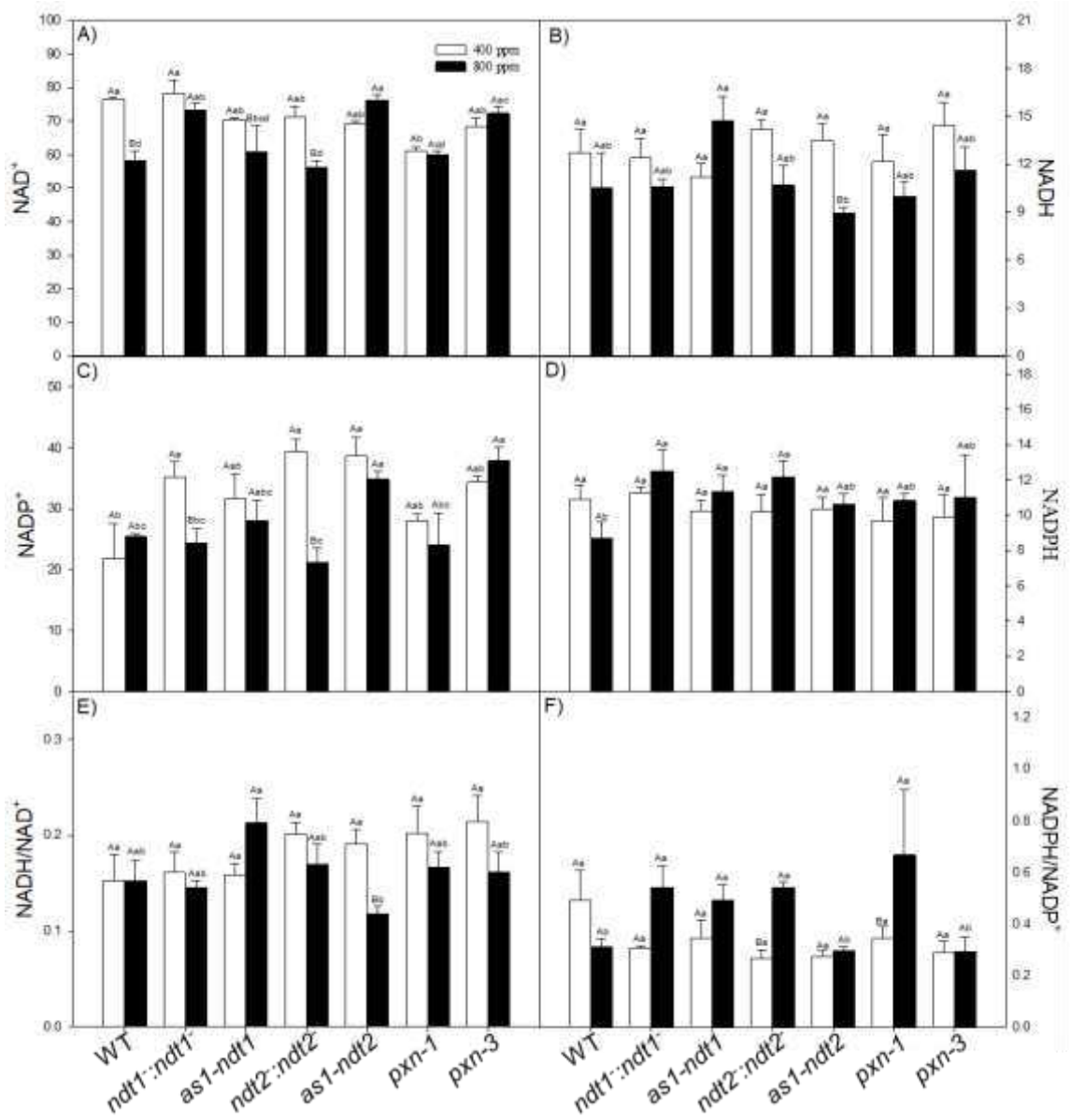

Figure 4: Pyridine nucleotide levels in rosette leaves of WT and NAD^{+} carrier mutants grown under ambient and elevated CO_2.
The levels of pyridine nucleotides were measured at the middle of the light period from plants submitted to 400 ppm or 800 ppm CO_2 for 16 days. **A)** NAD^{+}, **B)** NADH, **C)** NADP^{+}, **D)** NADPH, **E)** NADH/NAD^{+} ratio and **F)** NADPH/NADP^{+} ratio. Values are means ± SE of five independent samplings. Different capital letters represent values that were judged to be statistically different between treatments by Tukey's test multiple comparison test ($p < 0.05$). Different lower case letters represent values that were judged to be statistically different between lines in each treatment by Tukey's test multiple comparison test ($p < 0.05$).

Consequently, the NADPH/NADP$^+$ was increased for *ndt1$^-$:ndt1$^-$*, *as-1-ndt1, ndt2$^-$:ndt2$^-$* and *pxn-1* lines under high CO_2 condition while no differences in NADH/NAD$^+$ were found between lines at the same condition (Figure 4E, F). The results suggest that increased CO_2 concentration leads the mutant lines to be in a more reduced state compared to wild-type plants under the same condition.

Effects of deficient NAD$^+$ transport in reproductive phase of plants under elevated CO_2

Plants grown under elevated CO_2 conditions present differential seed production compared to the ones cultivated under ambient CO_2 concentration (Baker and Rosenqvist, 2004; Ainsworth et al., 2008). Previous studies demonstrated that NAD$^+$ transport into mitochondria played by NDT1 and NDT2 proteins is important for proper seed production and seed quality (de Souza Chaves et al., 2019; Feitosa-Araujo et al., 2020). To study the importance of NAD$^+$ distribution in reproductive phase under elevated CO_2 condition, plants were grown for 16 days under ambient CO_2 and posteriorly submitted to high CO_2 concentration until seeds were harvested. In ambient CO_2 condition, *ndt1$^-$:ndt1$^-$*, *ndt2$^-$:ndt2$^-$*, *as-1-ndt2* and *pxn-1* lines produced less siliques per plant than the control (Figure 5A). When submitted to high CO_2, wild-type plants increased their number of siliques per plant compared to wild-type plants cultivated in ambient CO_2 concentration (Fig. 5A). Additionally, all NAD$^+$ carrier mutant lines presented reduced silique production under high CO_2 concentrations in comparison to the control (Figure 5A). The silique length of *ndt1$^-$:ndt1$^-$*, *as-1-ndt1*, *ndt2$^-$:ndt2$^-$*and *pxn-1* under ambient CO_2 condition was smaller than wild-type plants while in high CO_2 this differences were not observed (Figure 5B). The silique width of NAD$^+$ transporter mutants in both CO_2 conditions presented a smaller size than the control (Figure 5C). In ambient CO_2 concentration, the number of seeds per silique were smaller than for all NAD$^+$ carrier mutant lines while in high CO_2 only *ndt1$^-$:ndt1$^-$* line presented a small number of seeds per silique (Figure 5D). Wild-type plants produced higher number of seeds under high CO_2 concentration than all NAD$^+$ carrier mutant lines, which led these mutants to have a lower total seed weight (Figure 5, E, F). Interestingly, the NAD carrier mutant plants were not able to recover the wild-type phenotype, in terms of seed production, even under high CO_2 concentration.

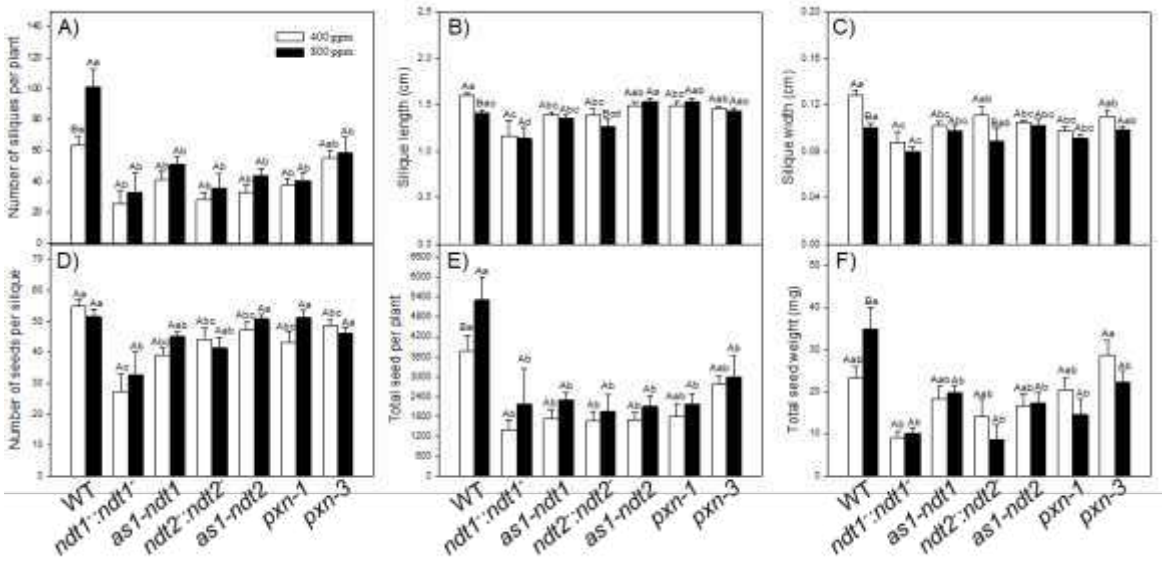

Figure 5: Reproductive parameters of WT and NAD+ carrier mutants submitted to ambient and elevated CO_2.
The number of siliques per plant **(A)**, silique length (cm) **(B)**, silique width (cm) **(C)**, number of seeds per silique **(D)**, total seed per plant **(E)** and total seed weight (mg) **(F)** parameters were measured in Arabidopsis WT and NAD+ carrier mutant plants at the reproductive phase after being grown under high CO_2. Values are means ± SE of 12 independent samplings. Different capital letters represent values that were judged to be statistically different between treatments by Tukey's test multiple comparison test ($p < 0.05$). Different lower case letters represent values that were judged to be statistically different between lines in each treatment by Tukey's test multiple comparison test ($p < 0.05$).

Changes on seed quality of NAD+ carrier mutants submitted to high CO_2 concentrations

Given that NAD+ carrier mutant plants grown in elevated CO_2 concentrations exhibited a lower amount of seed production and knowing that mutants for *NDT1* and *NDT2* presented changes in seed metabolites (de Souza Chaves et al., 2019; Feitosa-Araujo et al., 2020), we next evaluated the main metabolites in seeds of plants grown in ambient and high CO_2. In ambient CO_2 condition, all mutant lines tended to have a higher content of malate in their seed being statistically different from the control the lines *ndt1-:ndt1-*, *as-1-ndt1* and *ndt2-:ndt2-* (Figure 6A). However, in high CO_2 significant differences were found only for *ndt2-:ndt2-* even with the other lines presented a trend to accumulate more malate (Figure 6A). The fumarate content in seeds grown under ambient CO_2 was not detected whereas seeds of NAD+ carrier mutants presented a trend to accumulate in high CO_2 condition (Figure 6B).

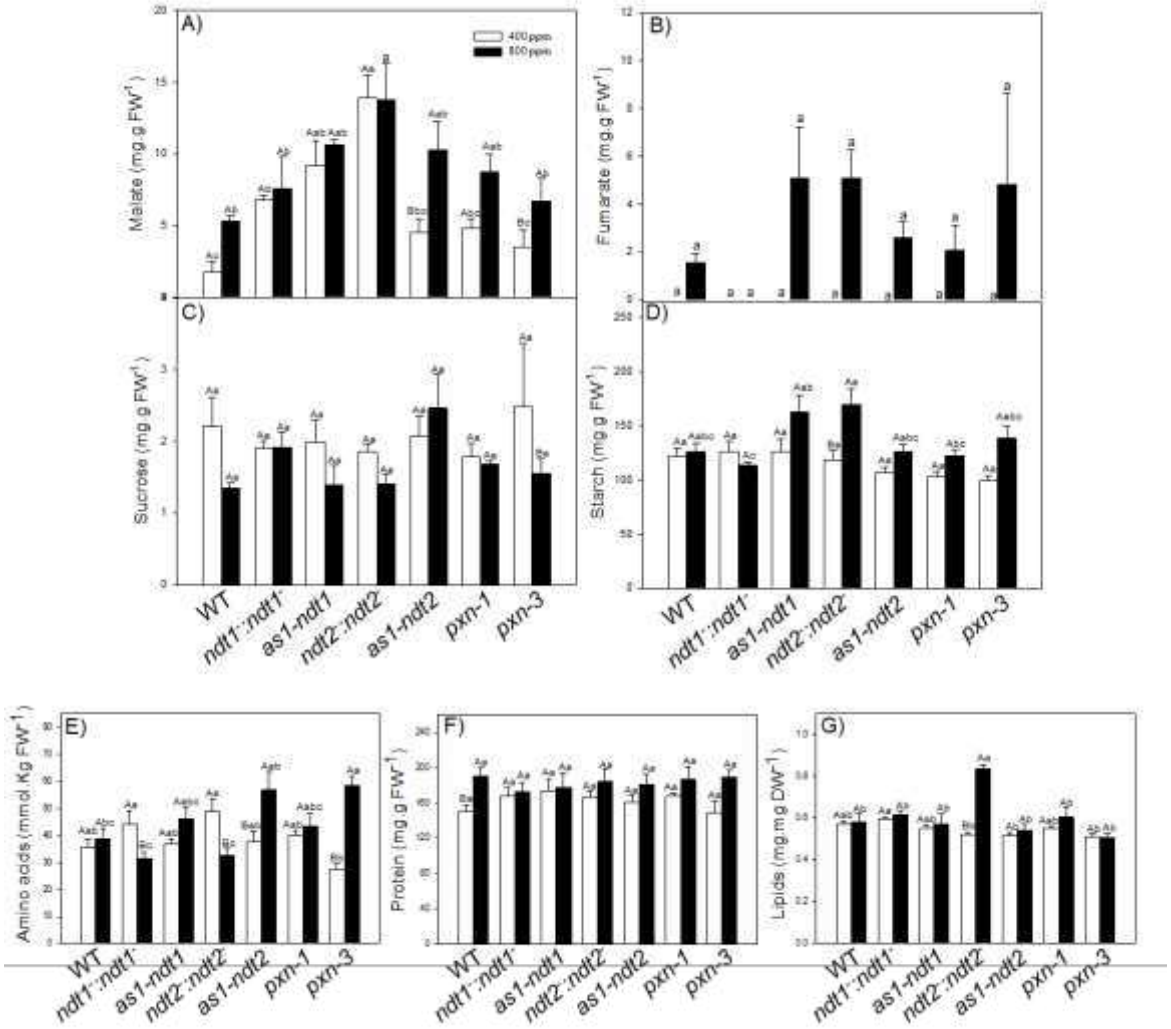

Figure 6: Metabolite levels in dry seeds of WT and NAD⁺ carrier mutants submitted to ambient and elevated CO_2.
WT and NAD⁺ carrier mutant plants were grown under ambient and elevated CO_2 untill the end of the reproductive phase. Seeds were collected and metabolites were measured in dry seeds. **A)** Malate, **B)** Fumarate, **C)** Sucrose, **D)** Starch, **E)** Amino acids, **F)** Protein and **G)** Lipids. Each replicate derived from a pool of five plants and values are means ± SE of five independent samplings. Different capital letters represent values that were judged to be statistically different between treatments by Tukey's test multiple comparison test ($p < 0.05$). Different lower case letters represent values that were judged to be statistically different between lines in each treatment by Tukey's test multiple comparison test ($p < 0.05$).

The levels of sucrose were shown to be diminished in seeds of wild-type plants grown under high CO_2 concentrations (Figure 6C). However, no differences were observed between NAD⁺ carrier mutants and the control in both conditions (Figure 6C). The content of starch was similar between lines in ambient and elevated CO_2 conditions (Figure 6D). Similarly, no significant changes were observed for the

contents of amino acids, proteins and lipids in seeds of wild-type and NAD^+ carrier mutant plants grown under ambient and high CO_2 concentrations (Figure 6E, F, G). To extend our analyses of seed quality, we posteriorly measured the root growth of seeds that were produced in both ambient and high CO_2 concentrations (Supplementary Figure 4). Seeds were placed in vertical plates on medium with and without sucrose 1%. After 8 days of growing the root length was measured and no differences were found between wild-type and NAD^+ transporter mutants independent of the CO_2 concentration and carbon availability in medium (Supplementary Figure 4).

DISCUSSION

Altered NAD transport does not impair stomatal behavior and plant growth in Arabidopsis plants

The effects of elevated CO_2 concentrations in plant performance have been extensively studied (Takatani et al., 2014; Hachiya et al., 2014; AbdElgawad et al., 2015; Bishop et al., 2015; Tian et al., 2015b). It has been demonstrated that CO_2 regulates the stomatal density and stomatal conductance (Chater et al., 2011). Arabidopsis plants submitted to elevated CO_2 concentrations presented a slight decrease in stomatal number (Woodward et al., 2002). Furthermore, Arabidopsis leaves close their stomata in response to elevated CO_2 concentrations (Tian et al., 2015b). Medeiros et al. (2016) demonstrated that fully expanded leaves of Arabidopsis respond to CO_2 transitions where increases in CO_2 reduce stomatal conductance and vice versa. Chaves et al., (2019) demonstrated that reduced expression of *NDT1* and *NDT2* genes lead to reduced stomatal density and stomatal conductance showing that stomata-related parameters are deregulated in mitochondrial NAD^+ carrier mutants. Indeed, we demonstrated here that the water loss from detached rosettes of NAD^+ carrier deficient mutants is reduced (Figure 1A), the mutant keep their stomata more closed under high CO_2 (Figure 1D), presented higher levels of malate in guard cells (Supplementary Figure 1B), a metabolite that negatively regulates stomatal opening (Araújo et al., 2011b), and decreased expression of ABA-responsive genes in guard cells (Figure 1C), a hormone known as a negative regulator of stomatal opening (Roelfsema et al., 2004) . Thus, we hypothesized that since NAD^+ carrier mutants present a lower stomatal density and increased malate levels in guard cells, the ABA

content in their guard cells must be kept in a low content compared to wild-type to allow these plants to open their stomata.

Posteriorly, we submitted plants to high CO_2 concentrations and biometrical and metabolic parameters were analyzed. It has been shown that Arabidopsis plants grown under elevated CO_2 present increases in leaf and root biomass, leaf number, leaf area and decreases in root/shoot ratio and specific leaf area (Ribeiro et al., 2012; Hachiya et al., 2014). These responses under high CO_2 are due to the promotion of carboxylase activity compared to the oxygenase activity of Rubisco leading to increases of CO_2 fixation relative to photorespiration process (Ehlers et al., 2015). However, the positive effects of elevated CO_2 are only pronounced in non-starved nitrogen plants (Takani et al., 2014). Accordingly, we demonstrated that wild-type plants grown under elevated CO_2 presented higher increases in biomass compared to mutant lines (Figure 2B) but not as pronounced as in previous studies (Ribeiro et al., 2012; Hachiya et al., 2014) (Ribeiro et al., 2012; Hachiya et al., 2014; Takani et al., 2014). In the present study, elevated CO_2 caused well known symptoms of nitrogen-starved plants (Takani et al., 2014) such as decreased contents of chlorophylls, amino acids, proteins and nitrate (Supplementary Figure 2) which might explain the lower increases in biomass upon CO_2 treatment (Figure 2A, B).

Under elevated CO_2 the oxygenation reaction of Rubisco is suppressed and the photorespiration process is reduced (Peterhansel et al., 2010). Consequently, the levels of glycine, serine and glutamate, intermediates in the photorespiratory pathway, are decreased. To better understand why NAD^+ mutant plants displayed reduced growth under elevated CO_2 we next performed a metabolite analyses in order to link growth and metabolism. Interestingly, in ambient CO_2 NAD^+ mutant lines tended to accumulate more glycine and serine compared to wild-type and under high CO_2 presented the same trend, being significant for *as-1-ndt2*, *pxn-1* and *pxn-3* lines (Figure 3). This is in agreement with the highly requirement of NAD^+ inside chloroplasts, mitochondria and peroxisomes for photorespiration (Peterhansel et al., 2010) . which could might explain why NAD^+ carrier mutant lines grown less than the wild-type. Furthermore, since NAD^+ carrier mutants produce less stomata this could create a barrier for CO_2 uptake which could enhance the photorespiration in these plants. Additionally, NAD^+ carrier mutants showed reduced levels of gluconate under elevated CO_2 (Figure 3). Gluconate has been linked to the oxidative pentose

phosphate pathway (OPPP) because it can enter in this pathway to form 6-phosphogluconate (Garlick et al., 2002). The OPPP is known as important source of reducing power, reducing $NADP^+$ to NADPH, and biosynthetic precursors in plants. Our data suggests that the OPPP pathway is enhanced under high CO_2 because the levels of gluconate decreased in all lines (Figure 3). However, the mutant lines presented lower levels of gluconate (Figure 3) and higher NADPH/$NADP^+$ ratio than wild-type under high CO_2 thus arguing in favor of an enhancement of OPPP in mutant lines (Figure 4). The NADPH from OPPP pathway has been implicated in responses to oxidative stress (Pugin, 1997).

Taking into account that NAD^+ carrier mutants accumulated photorespiratory intermediates under ambient and elevated CO_2 and that photorespiration serves as electron sink (Peterhansel et al., 2010), it is reasonable that these mutants are experiencing oxidative stress, thus leading to enhancement of reductant production (Figure 4). In agreement, H_2O_2 and superoxide marker genes are highly expressed in NAD^+ mutant lines (Chapter 1 of this thesis). These findings suggest that impaired NAD^+ homeostasis leads to both reduced stomatal density and stomatal conductance along with increases in photorespiratory intermediates that might explain the reduced biomass gain under elevated CO_2 in NAD^+ transporter mutants.

Elevated CO_2 does not rescue the lower seed production of NAD^+ carrier mutant plants

In the last decades several studies have shown the importance played by NAD^+ to modulate proper seed production (Chai et al., 2005; Katoh et al., 2006; Wang and Pichersky, 2007; Hashida et al., 2009). The levels of NAD^+ is assumed as pivotal to regulate pollen germination (Cárdenas et al., 2006; Hashida et al., 2007, 2013a, 2013b) because this process is dependent on energy produced by mitochondrial respiration and plastid glycolysis (Selinski and Scheibe, 2014). Additionally, a range of metabolic reactions such as the biosynthesis of lipids, components of cell walls, and amino acids, are highly dependent on NAD^+ levels during the maturation of pollen grains and pollen tube growth (Hashida et al., 2009). Recently it was demonstrated that not only NAD^+ contents but also mitochondrial NAD^+ transport performed by NDT1 and NDT2 proteins regulates pollen tube growth and seed production (de Souza Chaves et al., 2019). Interestingly, NADPH provision via the OPPP in peroxisomes is

required for gametophytic interaction during pollen tube guidance to ovules (Hölscher et al., 2016). Accordingly, in the present work, we demonstrated that the NAD^+ import into peroxisomes performed by PXN protein negatively impacted seed production under ambient CO_2 (Figure 5).

Increases in atmospheric CO_2 has been shown to have a positive effect on crop yield in C3 plants because they respond directly to rising CO_2 by increasing photosynthesis, biomass gain and reducing stomatal conductance and photorespiration (Jablonski et al., 2002; Long et al., 2006; Ziska and Bunce, 2007; Hikosaka et al., 2011). Accordingly, Miyagi et al. (2007) described that the ratio of seed mass per plant of plants grown under high CO_2 per plants grown under ambient CO_2 ranged from 0.54 to 4.45 in the literature. The gains in seed yield under high CO_2 is associated with the higher carbon assimilation derived from enhanced photosynthesis and that could be translocated to reproductive phase to ensure the full development of flowers and grains (Deng and Woodward, 1998; Rogers et al., 1996; Wu et al., 2004). In agreement, we observed that wild-type plants cultivated under high CO_2 significantly increased seed production compared to wild-type plants grown under ambient CO_2 (Figure 5). Surprisingly, NAD^+ carrier mutants were insensitive to CO_2 fertilization because no increases in seed yield was observed between both CO_2 conditions (Figure 5). As explained previously, during fertilization NAD^+ compartmentalization and dynamics are crucial to guide pollen tube growth. That said, the insensitiveness of NAD^+ carrier mutants in terms of seed production under elevated CO_2 could be explained by the fact that even though more carbon is available under this condition, without proper NAD^+ distribution seeds may not be effectively produced. Furthermore, during vegetative phase mutants tend to accumulate photorespiratory intermediates under both CO_2 conditions (Figure 3) which could enhance the lower seed phenotype due to a possible decrease in carbon translocation from vegetative to reproductive tissues. In addition, it has been shown that CO_2 impacts seed quality because plants grown under high CO_2 produce seeds with a lower content of nitrogen, amino acids, proteins and reduced seed germination (Andalo et al., 1996; Jablonski et al., 2002; Taub et al., 2008; Högy et al., 2009; Soba et al., 2019) Here we observed that wild-type seeds produced under elevated CO_2 presented increased levels of malate, fumarate and protein whereas the levels of sucrose were decreased (Figure 6A, B, F). Besides the trend of having increases in amino acids, malate and fumarate the mutant

lines did not show significantly differences with seeds of WT plants under high CO_2 (Figure 6A, B, E).

CONCLUSIONS

Several studies have described the pivotal role of NAD^+ to control plant metabolism, posttranslational regulation along with redox homeostasis. Recent studies revealed that NAD^+ transport performed by NDT1, NDT2 and PXN proteins is fundamental to modulate physiological and developmental processes alongside redox homeostasis. Proper NAD^+ distribution and metabolism are required to regulate stomatal development in an ABA-dependent manner, thus suggesting that NAD^+ dynamics may impact stomatal movements. Here we demonstrated that plants impaired in NAD^+ import into mitochondria and peroxisomes lost less water from detached leaves, accumulated malate in guard cells and kept their stomata more closed under high CO_2 condition. Consequently, NAD^+ transporter mutants do not efficiently respond to the benefits provided from CO_2 fertilization including biomass gain and increases in seed yield. Here we provided evidence that correct NAD^+ distribution directly impact biomass accumulation and seed production because NAD^+ dynamics is required to control photorespiration, stomatal conductance and stomatal development under ambient and elevated CO_2.

EXPERIMENTAL PROCEDURES

Plant material

In the experiments, *A. thaliana* wild-type plants (ecotype Col-0) and plants with reduced expression of genes encoding NAD^+ transporters from mitochondria - *NDT1* (*At*2g47490), *NDT2* (*At*1g25380) and peroxisome – *PXN* (*At*2g39970) were used. NDT1 and NDT2 mutant lines were isolated as described by Chaves et al., 2019 and Feitosa-Araujo., 2020, respectively. Seeds of *PXN* mutants, *pxn-1* (GABI_046D01) and *pxn-3* (SAIL_636F12) were kindly provided by Dr. Nicole Linka (Heinrich Heine University, Düsseldorf, Germany). The isolation of pxn mutant lines was performed as previously described (Bernhardt et al., 2012).

Growth conditions

Seeds of all genotypes were plated in petri dishes containing MS medium plus 1% sucrose. After four days of stratification at 4 °C, plates with seeds were transferred into a growth chamber at 22 ± 2 °C, 60% relative humidity, 150 µmol photons m^{-2} s^{-1} irradiance, and 12 h of light and 12 h dark photoperiod. After 10 days in light, seedlings were transferred to plastic pots with 0.1-L capacity filled with standard greenhouse substrate (Tropstrato HT®). Sixteen days after being placed in the light and under environmental CO_2 concentration, plants were submitted either ambient (400 µmol.mol^{-1}) or elevated (800 µmol.mol^{-1}) CO_2 concentration for 16 days or until the end of reproductive phase. CO_2 concentration inside the growth chambers were daily checked during the experiment and no fertilization was applied. Harvests of five independent samples per line were performed at the middle of light period for vegetative phase analyses and 12 independent samples per line were collected for reproductive phase analyses. Samples were grinded in liquid nitrogen and stored at -80°C until use.

Biometric analyses

Growth parameters of 32-days-old plants were evaluated as follow from five independent samples per line: rosette dry weight (RDW), root system dry weight (RSDW), root: shoot ratio (RSR), rosette leaf area (RLA), specific rosette area (SRA), leaf number (LN), total leaf area (TLA) and specific leaf area (SLA). RLA and TLA were determined by the digital image method, where leaves were scanned (Hewlett Packard Scanjet G2410, Palo Alto, California, USA) and the images obtained processed with the aid of ImajeJ software. The SRA and SLA were estimated using the formula: SRA (or SLA) = RLA (or TLA) / RDW. During the reproductive phase, we determined the length and diameter of siliques using stereomicroscope. For that, six siliques from twelve plants of each line were photographed and measured and the length, diameter and number of seeds in each silique were determined. In addition, the total seed production and weight were determined.

We also evaluated seed growth and seedling development. For these analyses seeds were placed in plates containing ½ MS + MES supplied or not with 1% sucrose. The plates were kept open and in the vertical position and after 8 days, plates were scanned and analyzed by using ImajeJ software.

Epidermal fragment isolation

Fully expanded leaves from five rosettes per plant were blended for 1 min plus 1 min (twice for 30 s) using a Waring blender with an internal filter to clarify the epidermal fragments of mesophyll and fibrous cells (Pandey et al., 2002). Subsequently, epidermal fragments were collected on a nylon membrane and washed to avoid apoplast contamination before being frozen in liquid nitrogen.

Biochemical analyses

Five rosettes per line were harvested from 32-days-old plants at the middle of the light period and snap frozen in liquid nitrogen. Subsequently, samples were homogenized and extracted in methanol as described (Gibon et al., 2004). Chlorophyll and nitrate were quantified according to Sulpice et al., 2009, while glucose, fructose and sucrose contents according to Fernie et al., 2001. Amino acids were determined as described by Gibon et al., 2004 and malate and fumarate as described in Nunes-Nesi et al. (2007). The levels of starch and protein were determined as previously described (Cross et al., 2006). Quantification of NAD^+, NADH, $NADP^+$ and NADPH was performed as detailed by Schippers et al. (2008).

Metabolite profiling was performed by Gas Chromatography-Mass Spectrometry (GC-MS) method according to the protocol described by (Lisec et al., 2006). Metabolites were manually annotated, and ion intensity was determined using the reference library mass spectra and retention indices from the Golm Metabolome Database (<http://gmd.mpimp-golm.mpg.de>; Kopka et al., 2005) and following the recommended reporting format for metabolic profiling (Fernie et al., 2011).

Stomatal opening and closing kinetics measurements

To perform kinetics of stomatal closing and opening in response to transitions in CO_2 concentrations, an open-flow infrared gas exchange analyzer system (LI-6400XT; LI-COR) equipped with an integrated fluorescence chamber (LI-6400-40; LI-COR) was used. The stomatal conductance (*gs*) values were recorded at intervals of 30 seconds. For *gs* responses to CO_2 transitions, leaves were exposed to 400/800/400 mmol CO_2 mol^{-1} air for 5/20/10 min under PPFD of 150 mmol m^{-2} s^{-1}. The *gs* responses to dark-light transitions were determined in plants acclimated in light for at least two

hours. The light in the chamber was kept turned on-off-on for 5-20-20 minutes, respectively and the *gs* was recorded over the time.

Water Loss Measurements

For water loss measurements, the weight of detached rosettes was determined over three hours. Rosettes were placed in dried petri dishes with their abaxial side up. Water loss was calculated as a percentage of the initial fresh weight (Araújo et al., 2011b).

Gene expression analysis

Quantitative real time PCR (qRT-PCR) was used to perform assays of gene expression. Total RNA's were extracted from epidermal fragments enriched with guard cells from 32-days-old plants using Trizol® reagent (Ambion, Life Technologies, Carlsbad, CA, USA) following the manufacturer's instructions. A 7300 Real time System (Applied Biosystems, Foster, CA, USA) and Power SYBR® Green PCR Master Mix were used to perform quantitative RT-PCRs. Relative quantification was performed with four biological replicates using actin as housekeeping gene. The list of primers used in this study is in Supplementary Table 2.

Statistical analyses

The experiments were performed in a randomized complete block design. The data was submitted to analysis of variance (ANOVA) two-way ANOVA. In this, two factors were considered corresponding to two environments: ambient and elevated [CO_2] (Supplementary Table 3). In order to verify the statistical difference between the genotypes, the means were compared using Tukey test ($P < 0.05$) using the GENES program (Cruz, 2013).

ACKNOWLEDGMENTS

Financial support was provided by Conselho Nacional de Desenvolvimento Científico e Tecnológico (CNPq), Fundação de Amparo à Pesquisa do Estado de Minas Gerais (FAPEMIG). Research fellowships granted by CNPq to EFA, ANN and WLA, Coordenação de Aperfeiçoamento de Pessoal de Nível Superior (CAPES PrInt program) to EFA are also gratefully acknowledged.

REFERENCES

AbdElgawad, H., Farfan-Vignolo, E.R., Vos, D. de, and Asard, H. (2015). Elevated CO2 mitigates drought and temperature-induced oxidative stress differently in grasses and legumes. Plant Sci. **231**: 1–10.

Ainsworth, E.A., Leakey, A.D.B., Ort, D.R., and Long, S.P. (2008). FACE-ing the facts: inconsistencies and interdependence among field, chamber and modeling studies of elevated [CO2] impacts on crop yield and food supply. New Phytol. **179**: 5–9.

Andalo, C., Godelle, B., Lefranc, M., Mousseau, M., and Till-Bottraud, I. (1996). Elevated CO2 decreases seed germination in Arabidopsis thaliana. Glob. Chang. Biol. **2**: 129–135.

Araújo, W.L. et al. (2011b). Antisense inhibition of the iron-sulphur subunit of succinate dehydrogenase enhances photosynthesis and growth in tomato via an organic acid–mediated effect on stomatal aperture. Plant Cell **23**: 600–627.

Baker, N.R. and Rosenqvist, E. (2004). Applications of chlorophyll fluorescence can improve crop production strategies: An examination of future possibilities. J. Exp. Bot. **55**: 1607–1621.

Bernhardt, K., Wilkinson, S., Weber, A.P.M., and Linka, N. (2012). A peroxisomal carrier delivers NAD + and contributes to optimal fatty acid degradation during storage oil mobilization. Plant J. **69**: 1–13.

Bishop, K.A., Betzelberger, A.M., Long, S.P., and Ainsworth, E.A. (2015). Is there potential to adapt soybean (Glycine max Merr.) to future [CO2]? An analysis of the yield response of 18 genotypes in free-air CO2 enrichment. Plant, Cell Environ. **38**: 1765–1774.

Bishop, K.A., Leakey, A.D.B., and Ainsworth, E.A. (2014). How seasonal temperature or water inputs affect the relative response of C3 crops to elevated [CO2]: A global analysis of open top chamber and free air CO2 enrichment studies. Food Energy Secur. **3**: 33–45.

Cárdenas, L., McKenna, S.T., Kunkel, J.G., and Hepler, P.K. (2006). NAD(P)H oscillates in pollen tubes and is correlated with tip growth. Plant Physiol. **142**: 1460–1468.

Chai, M.F., Chen, Q.J., An, R., Chen, Y.M., Chen, J., and Wang, X.C. (2005). NADK2, an Arabidopsis chloroplastic NAD kinase, plays a vital role in both

chlorophyll synthesis and chloroplast protection. Plant Mol. Biol. **59**: 553–564.

Chater, C., Kamisugi, Y., Movahedi, M., Fleming, A., Cuming, A.C., Gray, J.E., and Beerling, D.J. (2011). Regulatory mechanism controlling stomatal behavior conserved across 400 million years of land plant evolution. Curr. Biol. **21**: 1025–1029.

Cross, J.M., Korff, M. Von, Altmann, T., Bartzetko, L., Sulpice, R., Gibon, Y., Palacios, N., and Stitt, M. (2006). Variation of enzyme activities and metabolite levels in 24 Arabidopsis accessions growing in carbon-limited conditions. Plant Physiol. **142**: 1574–1588.

Cruz, C.D. (2013). GENES - Software para análise de dados em estatística experimental e em genética quantitativa. Acta Sci. - Agron. **35**: 271–276.

Deng, X. and Woodward, F.I. (1998). The growth and yield responses of Fragaria ananassa to elevated CO2 and N supply. Ann. Bot. **81**: 67–71.

Ehlers, I., Augusti, A., Betson, T.R., Nilsson, M.B., Marshall, J.D., and Schleucher, J. (2015). Detecting long-term metabolic shifts using isotopomers: CO2-driven suppression of photorespiration in C3 plants over the 20th century. Proc. Natl. Acad. Sci. U. S. A. **112**: 15585–15590.

Feitosa-Araujo, E., de Souza Chaves, I., Florian, A., Fonseca-Pereira, P., Apfata, JAC., Heyneke, E., Medeiros, D. B., Pires, M.V., Mettler-Altmann, T., Neuhaus, H.E., Palmieri, F., Araújo, W.L., Obata, T., Weber, A.P.M., Linka, N., Fernie, A.R., Nunes-Nesi, A. (2020). Down-regulation of a mitochondrial NAD+ transporter (NDT2) alters seed production and germination in Arabidopsis. Plant Cell Physiol.

Fernie, A.R., Aharoni, A., Willmitzer, L., Stitt, M., Tohge, T., Kopka, J., Carroll, A.J., Saito, K., Fraser, P.D., and Deluca, V. (2011). Recommendations for reporting metabolite data. Plant Cell **23**: 2477–2482.

Fernie, A.R., Roscher, A., Ratcliffe, R.G., and Kruger, N.J. (2001). Fructose 2,6-bisphosphate activates pyrophosphate: Fructose-6-phosphate 1-phosphotransferase and increases triose phosphate to hexose phosphate cycling heterotrophic cells. Planta **212**: 250–263.

Gakière, B. et al. (2018). NAD biosynthesis and signaling in plants. CRC. Crit. Rev. Plant Sci. **37**: 259–307.

Garlick, A.P., Moore, C., and Kruger, N.J. (2002). Monitoring flux through the

oxidative pentose phosphate pathway using [1-14C] gluconate. Planta **216**: 265–272.

Gibon, Y., Blaesing, O.E., Hannemann, J., Carillo, P., Ho, M., Palacios, N., Cross, J., Selbig, J., and Stitt, M. (2004). A Robot-Based platform to measure multiple enzyme activities in Arabidopsis using a set of cycling assays : Comparison of changes of enzyme activities and transcript levels during diurnal cycles and in prolonged darkness. Plant Cell **16**: 3304–3325.

Hachiya, T., Sugiura, D., Kojima, M., Sato, S., Yanagisawa, S., Sakakibara, H., Terashima, I., and Noguchi, K. (2014). High CO2 triggers preferential root growth of arabidopsis thaliana via two distinct systems under low pH and low N stresses. Plant Cell Physiol. **55**: 269–280.

Hashida, S., Takahashi, H., Kawai-yamada, M., and Uchimiya, H. (2007). Arabidopsis thaliana nicotinate / nicotinamide mononucleo- tide adenyltransferase (AtNMNAT) is required for pollen tube growth.: 694–703.

Hashida, S.N., Kawai-Yamada, M., and Uchimiya, H. (2013a). NAD+ accumulation as a metabolic off switch for orthodox pollen. Plant Signal. Behav. **8**.

Hashida, S.N., Takahashi, H., Takahara, K., Kawai-Yamada, M., Kitazaki, K., Shoji, K., Goto, F., Yoshihara, T., and Uchimiya, H. (2013b). NAD+ accumulation during pollen maturation in Arabidopsis regulating onset of germination. Mol. Plant **6**: 216–225.

Hashida, S.N., Takahashi, H., and Uchimiya, H. (2009). The role of NAD biosynthesis in plant development and stress responses. Ann. Bot. **103**: 819–824.

Hikosaka, K., Kinugasa, T., Oikawa, S., Onoda, Y., and Hirose, T. (2011). Effects of elevated CO2 concentration on seed production in C3 annual plants. J. Exp. Bot. **62**: 1523–1530.

Högy, P., Wieser, H., Köhler, P., Schwadorf, K., Breuer, J., Franzaring, J., Muntifering, R., and Fangmeier, A. (2009). Effects of elevated CO2 on grain yield and quality of wheat: Results from a 3-year free-air CO2 enrichment experiment. Plant Biol. **11**: 60–69.

Holscher, C., Lutterbey, M.C., Lansing, H., Meyer, T., Fischer, K. Von Schaewen, A. (2016) Defects in peroxisomal 6-phosphogluconate dehydrogenase isoform PGD2 prevent gametophytic interaction in Arabidopsis thaliana. Plant Physiol. **171**, 192–205.

Jablonski, L.M., Wang, X., and Curtis, P.S. (2002). Plant reproduction under elevated CO2 conditions: A meta-analysis of reports on 79 crop and wild species. New Phytol. **156**: 9–26.

Jezek, M., Blatt, M. R. (2017). The membrane transport system of the guard cell and its integration for stomatal dynamics. Plant Physiology, **174**(2), 487-519.

Katoh, A., Uenohara, K., Akita, M., and Hashimoto, T. (2006). Early steps in the biosynthesis of NAD in Arabidopsis start with aspartate and occur in the plastid. Plant Physiol. **141**: 851–857.

Kim, T.-H., Böhmer, M., Hu, H., Nishimura, N., and Schroeder, J.I. (2010). Guard Cell Signal Transduction Network: Advances in Understanding Abscisic Acid, CO 2 , and Ca 2+ Signaling . Annu. Rev. Plant Biol. **61**: 561–591.

Kinoshita, T., Doi, M., Suetsugu, N., Kagawa, T., Wada, M., Shimazaki, K. I. (2001). Phot1 and phot2 mediate blue light regulation of stomatal opening. Nature, **414**(6864), 656-660.

Lisec, J., Schauer, N., Kopka, J., Willmitzer, L., and Fernie, A.R. (2006). Gas chromatography mass spectrometry–based metabolite profiling in plants. Nat. Protoc. **1**: 387–396.

Long, S.P., Ainsworth, E.A., Leakey, A.D.B., Nosberger, J., and Ort, D.R. (2006). Food for thought: Lower-Than-Expected Crop Yield Simulation with Rising CO2 Concentrations. Science (80-.). **27**: 1965–1970.

Masle, J. (2000). The effects of elevated CO2 concentrations on cell division rates, growth patterns, and blade anatomy in young wheat plants are modulated by factors related to leaf position, vernalization, and genotype. Plant Physiol. **122**: 1399–1415.

Medeiros, D.B., Martins, S.C.V., Cavalcanti, J.H.F., Daloso, D.M., Martinoia, E., Nunes-Nesi, A., DaMatta, F.M., Fernie, A.R., and Araújo, W.L. (2016). Enhanced photosynthesis and growth in atquac1 knockout mutants are due to altered organic acid accumulation and an increase in both stomatal and mesophyll conductance. Plant Physiol. **170**: 86–101.

Meehl GA, Stocker TF, Collins WD, Friedlingstein P, Gaye AT, Gregory JM, Kitoh A, Knutti R, Murphy JM, Noda A, et al. (2007). Global climate projections. In S Solomon, D Qin, M Manning, Z Chen, M Marquis, KB Averyt, M Tignor, HL Miller, eds, Climate Change 2007: The Physical Science Basis. Contribution of Working

Group I to the Fourth Assessment Report of the Intergovernmental Panel on Climate Change. Cambridge University Press, New York.

Mhamdi, A. and Noctor, G. (2016). High CO2 primes plant biotic stress defences through redox-linked pathways. Plant Physiol. **172**: 929–942.

Miyagi, K.M., Kinugasa, T., Hikosaka, K., and Hirose, T. (2007). Elevated CO2 concentration, nitrogen use, and seed production in annual plants. Glob. Chang. Biol. **13**: 2161–2170.

Munemasa, S., Hauser, F., Park, J., Waadt, R., Brandt, B., Schroeder, J. I. (2015). Mechanisms of abscisic acid-mediated control of stomatal aperture. Current opinion in plant biology, **28**: 154-162.

Noctor, G., Queval, G., and Gakière, B. (2006). NAD(P) synthesis and pyridine nucleotide cycling in plants and their potential importance in stress conditions. J. Exp. Bot. **57**: 1603–1620.

Nunes-Nesi, A., Carrari, F., Gibon, Y., Sulpice, R., Lytovchenko, A., Fisahn, J., Graham, J., Ratcliffe, R.G., Sweetlove, L.J., and Fernie, A.R. (2007). Deficiency of mitochondrial fumarase activity in tomato plants impairs photosynthesis via an effect on stomatal function. Plant J. **50**: 1093–1106.

Palmieri, F. et al. (2009). Molecular identification and functional characterization of Arabidopsis thaliana mitochondrial and chloroplastic NAD+ carrier proteins. J. Biol. Chem. **284**: 31249–31259.

Palmieri, F., Pierri, C.L., Grassi, A. De, Nunes-Nesi, A., Fernie, A.R., Group, M.P., Vic, U.F. De, Mu, A., De Grassi, A., Nunes-Nesi, A., and Fernie, A.R. (2011). Evolution, structure and function of mitochondrial carriers: A review with new insights. Plant J. **66**: 161–181.

Pandey, S., Wang, X. Q., Coursol, S. A., Assmann, S. M. (2002). Preparation and applications of Arabidopsis thaliana guard cell protoplasts. New Phytologist. **153**(3): 517-526.

Peterhansel, C., Horst, I., Niessen, M., Blume, C., Kebeish, R., Kürkcüoglu, S., and Kreuzaler, F. (2010). Photorespiration. Arab. B. **8**: e0130.

Pugin, A. (1997). Early events induced by the elicitor cryptogein in tobacco cells: Involvement of a plasma membrane NADPH oxidase and activation of glycolysis and the pentose phosphate pathway. Plant Cell **9**: 2077–2091.

Ribeiro, D.M., Araujo, W.L., Fernie, a. R., Schippers, J., and Mueller-Roeber, B.

(2012). Action of gibberellins on growth and metabolism of Arabidopsis thaliana plants associated with high concentration of carbon dioxide. Plant Physiol. **160**: 1781–1794.

Roelfsema, M.R.G., Levchenko, V., and Hedrich, R. (2004). ABA depolarizes guard cells in intact plants, through a transient activation of R- and S-type anion channels. Plant J. **37**: 578–588.

Rogers, G.S., Milham, P.J., Gillings, M., and Conroy, J.P. (1996). Sink strength may be the key to growth and nitrogen responses in N-deficient wheat at elevated CO2. Aust. J. Plant Physiol. **23**: 253–264.

de Souza Chaves, I. et al. (2019). The mitochondrial NAD+ transporter (NDT1) plays important roles in cellular NAD+ homeostasis in Arabidopsis thaliana. Plant J. **100**: 487–504.

Selinski, J. and Scheibe, R. (2014) Pollen tube growth: where does the energy come from? Plant Signal. Behav. **9**.

Soba, D., Ben Mariem, S., Fuertes-Mendizábal, T., Méndez-Espinoza, A. M., Gilard, F., González-Murua, C., Irigoyen, J.J., Tcherkez, G., Aranjuelo, I. (2019). Metabolic effects of elevated CO2 on wheat grain development and composition. Journal of agricultural and food chemistry, **67**(31), 8441-8451.

Sulpice, R. et al. (2009). Starch as a major integrator in the regulation of plant growth. PNAS **106**: 10348–10353.

Takatani, N., Ito, T., Kiba, T., Mori, M., Miyamoto, T., Maeda, S.I., and Omata, T. (2014). Effects of high CO2 on growth and metabolism of arabidopsis seedlings during growth with a constantly limited supply of nitrogen. Plant Cell Physiol. **55**: 281–292.

Taub, D.R., Miller, B., and Allen, H. (2008). Effects of elevated CO2 on the protein concentration of food crops: A meta-analysis. Glob. Chang. Biol. **14**: 565–575.

Thompson, M., Gamage, D., Hirotsu, N., Martin, A., and Seneweera, S. (2017). Effects of elevated carbon dioxide on photosynthesis and carbon partitioning: A Perspective on root sugar sensing and hormonal crosstalk. Front. Physiol. **8**: 1–13.

Tian, W. et al. (2015a). A molecular pathway for CO2 response in Arabidopsis guard cells. Nat. Commun. **6**: 1–10.

Tian, W. et al. (2015b). A molecular pathway for CO2 response In Arabidopsis guard

cells. Nat. Commun. **6**.

Toleco, M.R., Naake, T., Zhang, Y., Heazlewood, J.L., and Fernie, A.R. (2020). Plant mitochondrial carriers: Molecular gatekeepers that help to regulate plant central carbon metabolism. Plants **9**: 117.

Wang, G. and Pichersky, E. (2007). Nicotinamidase participates in the salvage pathway of NAD biosynthesis in Arabidopsis. Plant J. **49**: 1020–1029.

Woodward, F.I., Lake, J.A., and Quick, W.P. (2002). Stomatal development and CO2: Ecological consequences. New Phytol. **153**: 477–484.

Wu, D.X., Wang, G.X., Bai, Y.F., and Liao, J.X. (2004). Effects of elevated CO 2 concentration on growth, water use, yield and grain quality of wheat under two soil water levels. Agric. Ecosyst. Environ. **104**: 493–507.

Ziska, L.H. and Bunce, J.A. (2007). Predicting the impact of changing CO2 on crop yields: Some thoughts on food. New Phytol. **175**: 607–618.

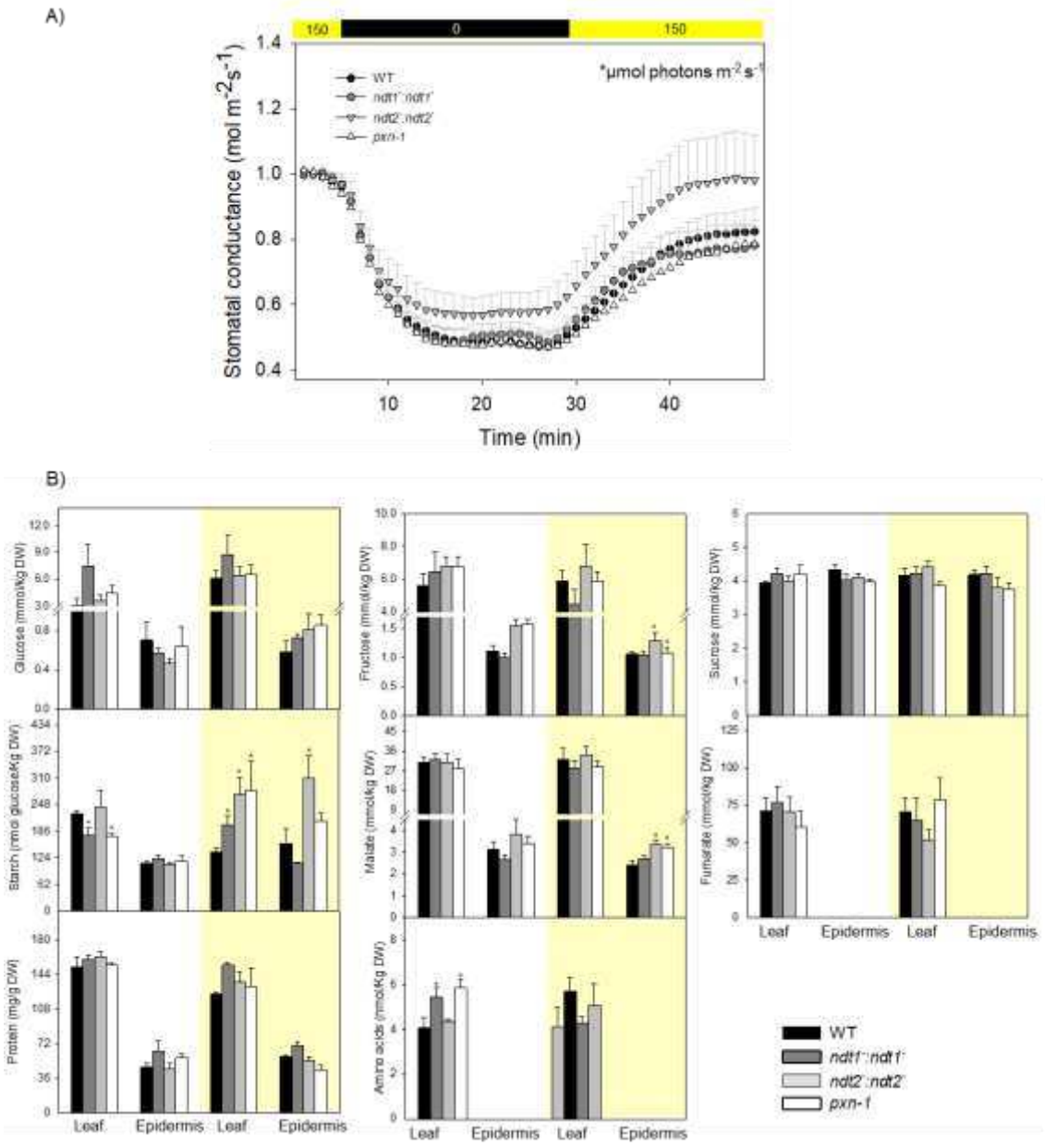

Supplementary Figure 1: Stomatal movement and metabolites in guard-cell enriched epidermal fragments.

A) Stomatal conductance kinetics under light-dark transitions. **B)** Leaf and guard cell metabolites of plants deficient in NAD^+ uptake into mitochondria and peroxisomes. Asterisks represent values that were judged to be statistically different from WT by T test ($p < 0.05$).

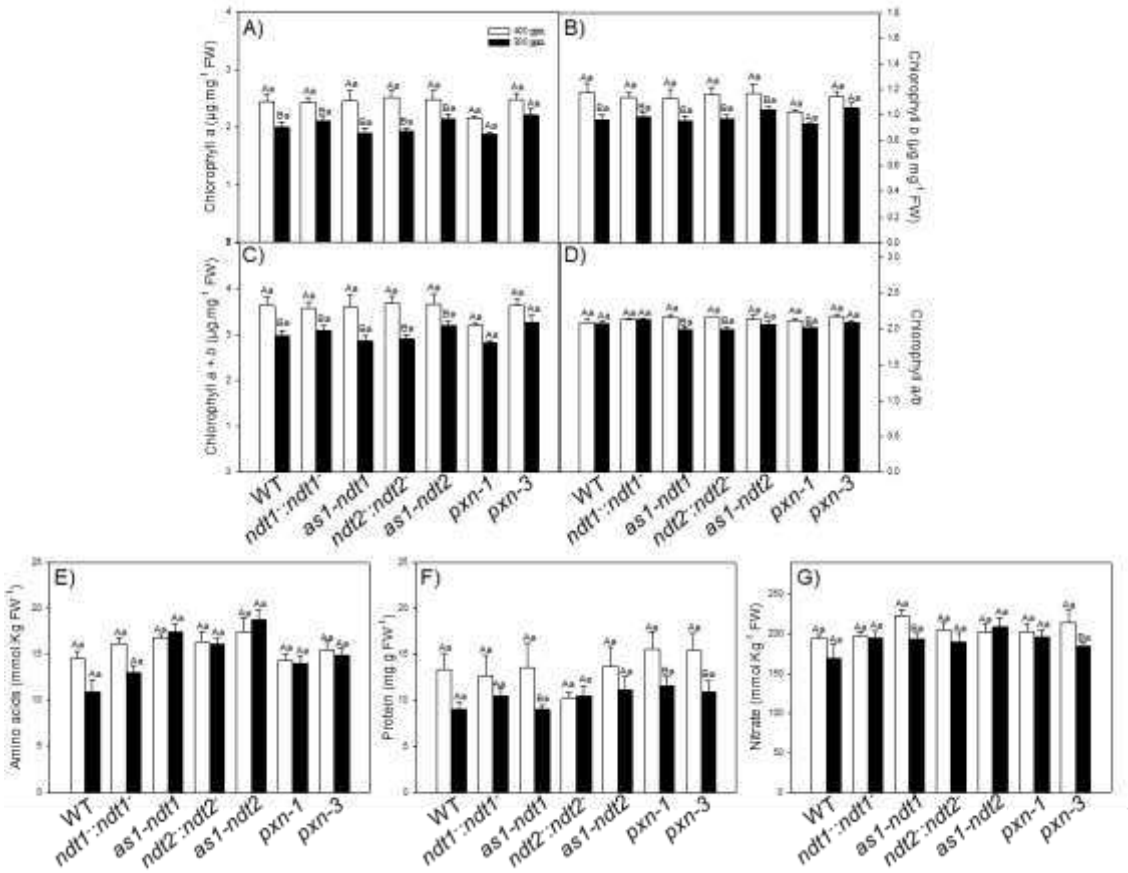

Supplementary Figure 2: Levels of chlorophylls, amino acids, proteins and nitrate in rosettes of WT and NAD⁺ carrier mutant plants submitted to elevated CO_2 concentration.

Metabolites were measured at the middle of the light period from plants grown at 400 ppm or 800 ppm CO_2 during 16 days. **A)** chlorophyll *a*, **B)** chlorophyll *b*, **C)** chlorophyll *a* + *b*, **D)** chlorophyll *a/b* ratio, **E)** amino acids, **F)** Proteins and **G)** Nitrate. Plants were harvested and the middle of light period and metabolites were measured. Values are means ± SE of five independent replicates. Different capital letters represent values that were judged to be statistically different between treatments by Tukey's test multiple comparison test ($p < 0.05$). Different lower case letters represent values that were judged to be statistically different between lines in each treatment by Tukey's test multiple comparison test ($p < 0.05$).

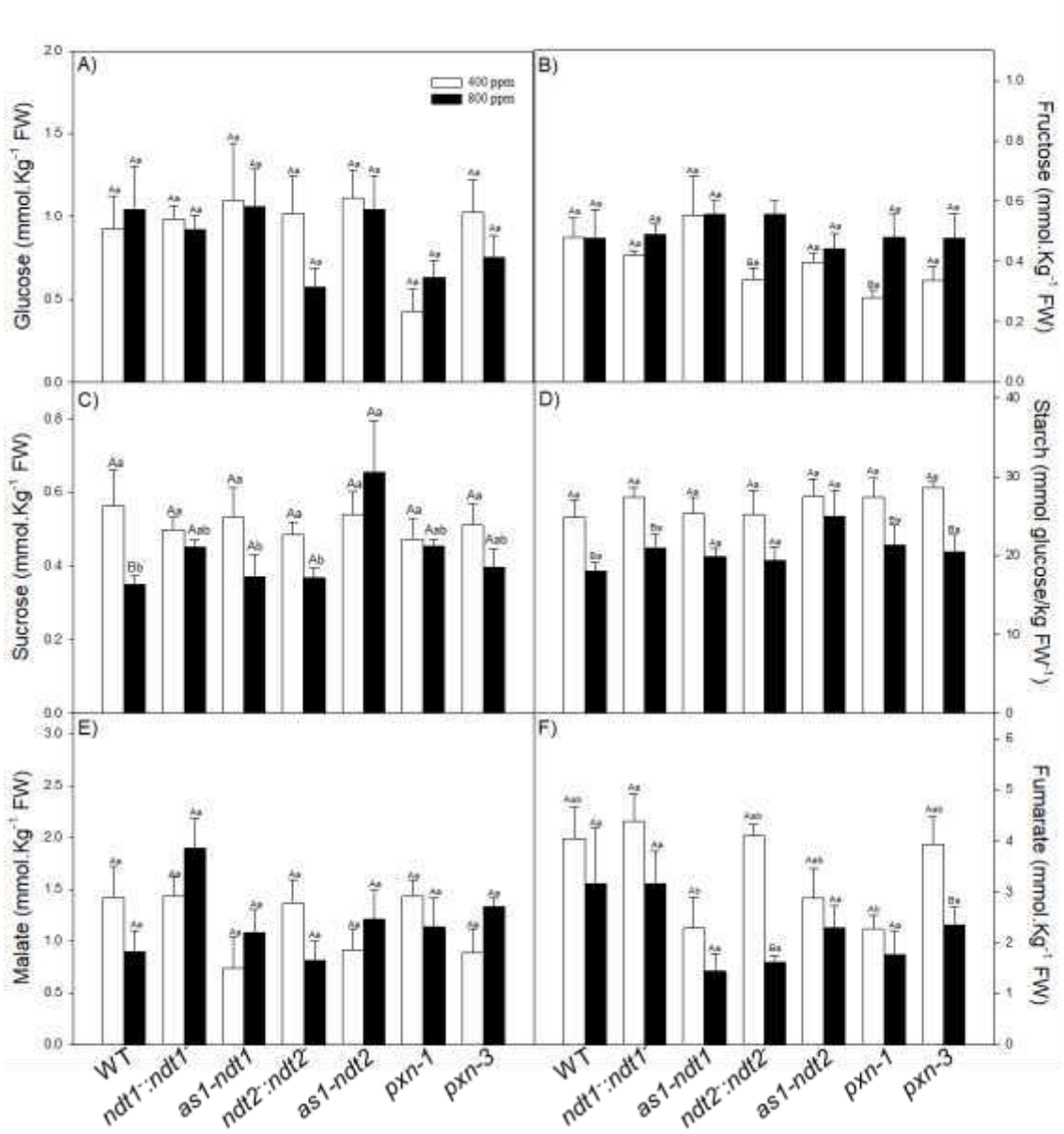

Supplementary Figure 3: Levels of sugars, starch, malate and fumarate in rosettes of WT and NAD⁺ carrier mutant plants submitted to elevated CO_2 concentration.

Metabolites were measured at the middle of the light period from plants grown at 400 ppm or 800 ppm CO_2 during 16 days. **A)** Glucose, **B)** Fructose, **C)** Sucrose, **D)** Starch, **E)** Malate and **F)** Fumarate. Values are means ± SE of five independent replicates. Different capital letters represent values that were judged to be statistically different between treatments by Tukey's test multiple comparison test ($p < 0.05$). Different lower case letters represent values that were judged to be statistically different between lines in each treatment by Tukey's test multiple comparison test ($p < 0.05$).

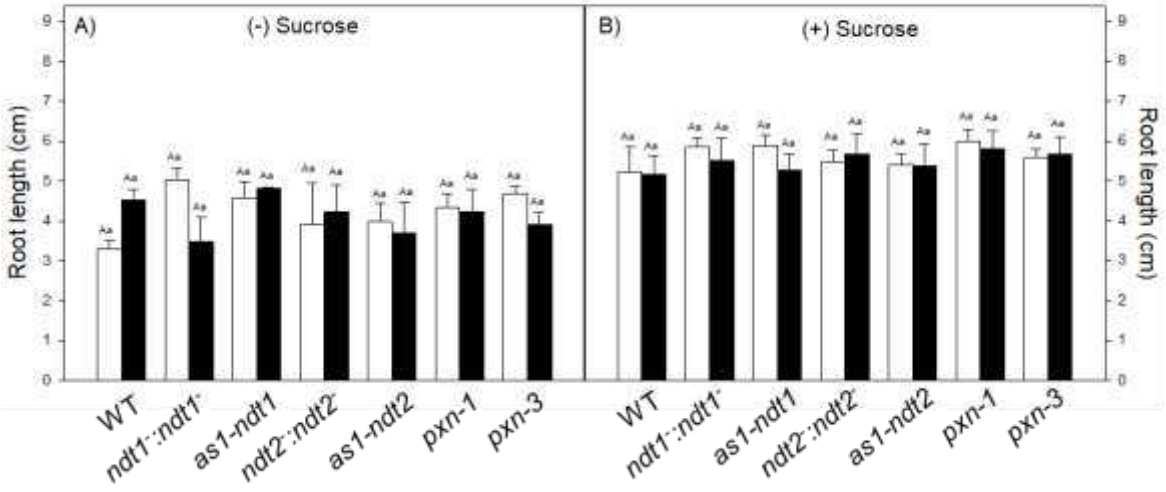

Supplementary Figure 4: Root growth of WT and NAD⁺ carrier mutant seedlings in vertical plates.

The root growth of WT and NAD⁺ carrier mutant seedlings were recorded for seedlings derived from seeds produced in plants grown in high CO_2 concentration. **A)** root growth from seeds produced in ambient and elevated CO_2 in medium without sucrose and **B)** root growth from seeds produced in ambient and elevated CO_2 in medium containing sucrose. Values were derived from 6 replicates each containing 6 plants per genotype. Different capital letters represent values that were judged to be statistically different between treatments by Tukey's test multiple comparison test ($p < 0.05$). Different lower case letters represent values that were judged to be statistically different between lines in each treatment by Tukey's test multiple comparison test ($p < 0.05$).

	WT		*ndt1⁻:ndt1⁻*		*as-1-ndt1*		*ndt2⁻:ndt2⁻*		*as-1-ndt2*		*pxn-1*		*pxn-3*	
	Control	High CO_2	Control	High CO_2	Control	High CO_2	Control	High CO_2	Control	High CO_2	Control	High CO_2	Control	High CO_2
Alpha-alanine	1.00 ± 0.14 Aab	1.09 ± 0.06 Ad	1.06 ± 0.07 Bab	**1.52 ± 0.14 Aab**	0.85 ± 0.02 Ab	1.19 ± 0.16 Abc	1.18 ± 0.09 Aab	1.11 ± 0.02 Acd	1.29 ± 0.20 Aa	**1.63 ± 0.15 Aa**	0.94 ± 0.08 Bb	**1.48 ± 0.19 Aab**	1.09 ± 0.12 Aab	1.09 ± 0.15 Acd
Aspartate	1.00 ± 0.23 Aab	0.68 ± 0.20 Ac	1.07 ± 0.25 Aab	**1.24 ± 0.21 Aab**	1.36 ± 0.13 Aab	0.85 ± 0.05 Abc	1.04 ± 0.22 Aab	**1.19 ± 0.11 Aab**	1.59 ± 0.48 Aa	**1.58 ± 0.20 Aa**	0.71 ± 0.17 Ab	1.15 ± 0.19 Aabc	1.05 ± 0.18 Aab	0.93 ± 0.20 Abc
Beta-alanine	1.00 ± 0.08 Ab	1.06 ± 0.10 t	0.93 ± 0.11 Ab	0.95 ± 0.06 Ab	1.18 ± 0.09 Aab	0.93 ± 0.05 Ab	**1.82 ± 0.53 Aab**	0.98 ± 0.10 Bb	1.29 ± 0.22 Aab	**1.37 ± 0.05 Aa**	0.89 ± 0.06 Ab	1.08 ± 0.05 Aa	1.10 ± 0.06 Ab	1.08 ± 0.06 Aa
Cysteine	1.00 ± 0.03 Aab	1.12 ± 0.15 Aa	0.94 ± 0.07 Aab	0.84 ± 0.06 Aab	1.11 ± 0.22 Aab	0.85 ± 0.16 Aab	0.94 ± 0.06 Aab	**0.76 ± 0.08 Ab**	0.81 ± 0.05 Ab	0.74 ± 0.05 Ab	0.99 ± 0.04 Aab	0.86 ± 0.06 Aab	1.05 ± 0.11 Aab	1.02 ± 0.12 Aab
Glutamate	1.00 ± 0.38 Aab	0.39 ± 0.15 Ac	0.78 ± 0.29 Aab	1.00 ± 0.25 Aab	1.48 ± 0.37 Aab	1.01 ± 0.07 Aab	0.94 ± 0.26 Aab	0.99 ± 0.17 Aab	**1.59 ± 0.56 Ba**	**1.56 ± 0.21 Aa**	0.55 ± 0.21 Bb	1.27 ± 0.38 Aab	1.11 ± 0.25 Bab	0.67 ± 0.20 Abc
Glycine	1.00 ± 0.09 Ab	0.34 ± 0.03 Bd	1.42 ± 0.16 Aab	0.38 ± 0.02 Bcd	1.34 ± 0.20 Ab	0.58 ± 0.07 Bbc	1.65 ± 0.25 Aab	0.55 ± 0.08 Bbc	2.12 ± 0.49 Aa	**1.02 ± 0.19 Ba**	**1.23 ± 0.25 Ab**	0.69 ± 0.07 Bbc	1.57 ± 0.13 Aab	**0.82 ± 0.20 Bab**
Isoleucine	1.00 ± 0.10 Bab	1.57 ± 0.32 Aa	0.86 ± 0.10 Ab	1.31 ± 0.27 Aa	1.29 ± 0.12 Aab	1.57 ± 0.18 Aa	1.50 ± 0.40 Aab	1.56 ± 0.27 Aa	**1.11 ± 0.17 Aab**	**1.25 ± 0.04 Aa**	0.81 ± 0.05 Bb	**1.39 ± 0.10 Aa**	1.04 ± 0.02 Aab	**1.03 ± 0.05 Aa**
Leucine	1.00 ± 0.13 Bab	1.69 ± 0.34 Aa	0.77 ± 0.11 Ab	1.25 ± 0.23 Aa	1.18 ± 0.07 Aab	1.73 ± 0.24 Aa	1.52 ± 0.52 Aa	1.69 ± 0.36 Aa	0.97 ± 0.15 Aab	1.24 ± 0.07 Aa	0.82 ± 0.05 Ab	1.35 ± 0.11 Aa	0.83 ± 0.01 Ab	1.13 ± 0.08 Aa
Phenylalanine	1.00 ± 0.30 Aab	1.29 ± 0.50 Aab	1.06 ± 0.28 Aab	1.71 ± 0.14 Aab	1.72 ± 0.30 Aa	1.70 ± 0.14 Aab	1.21 ± 0.18 Aab	1.55 ± 0.23 Aab	1.57 ± 0.39 Aab	2.16 ± 0.37 Aa	0.79 ± 0.24 Ab	1.75 ± 0.41 Aab	1.15 ± 0.27 Aab	0.91 ± 0.24 Ab
Proline	1.00 ± 0.17 Abc	0.86 ± 0.23 Aab	0.66 ± 0.18 Acd	0.61 ± 0.04 Ab	1.00 ± 0.07 Abc	1.05 ± 0.13 Aa	**2.58 ± 0.96 Aa**	0.60 ± 0.10 Bb	2.06 ± 0.53 Aab	0.69 ± 0.13 Ba	0.39 ± 0.04 Ac	0.66 ± 0.04 Ab	1.41 ± 0.21 Aabc	0.88 ± 0.15 Aab
Serine	1.00 ± 0.06 Abc	0.85 ± 0.21 Aab	1.04 ± 0.06 Abc	0.81 ± 0.15 Aab	1.37 ± 0.08 Aabc	1.04 ± 0.13 Aa	2.04 ± 0.51 Aa	0.82 ± 0.08 Bab	1.65 ± 0.48 Aab	0.93 ± 0.06 Bab	0.79 ± 0.10 Ac	1.00 ± 0.13 Aab	1.24 ± 0.06 Abc	0.65 ± 0.08 Ab
Threonine	1.00 ± 0.05 Ab	0.94 ± 0.19 Aab	1.02 ± 0.02 Ab	1.00 ± 0.08 Aab	1.16 ± 0.07 Ab	0.97 ± 0.11 Aab	**2.52 ± 0.95 Aa**	0.93 ± 0.06 Bab	1.37 ± 0.32 Ab	0.95 ± 0.04 Aab	1.06 ± 0.17 Ab	1.06 ± 0.12 Aa	1.11 ± 0.05 Ab	0.74 ± 0.07 Ab
Tyrosine	1.00 ± 0.04 Bb	2.51 ± 0.55 Aa	1.06 ± 0.28 Ab	1.64 ± 0.43 Aa	**1.78 ± 0.26 Aa**	2.62 ± 0.40 Aa	1.47 ± 0.30 Bab	2.69 ± 0.64 Aa	0.96 ± 0.14 Bb	2.04 ± 0.21 Aa	1.03 ± 0.11 Ab	1.90 ± 0.08 Aa	1.08 ± 0.12 Bb	2.13 ± 0.36 Aa
Valine	1.00 ± 0.11 Aab	1.29 ± 0.21 Aa	0.76 ± 0.01 Bb	1.13 ± 0.17 Aab	1.04 ± 0.02 Aab	1.22 ± 0.15 Aab	1.20 ± 0.18 Aa	1.23 ± 0.16 Aab	1.25 ± 0.23 Aa	1.14 ± 0.03 Aab	0.76 ± 0.02 Bb	1.16 ± 0.09 Aab	0.94 ± 0.06 Aab	**0.89 ± 0.03 Ab**
Isocitrate	1.00 ± 0.11 Aa	0.96 ± 0.08 Abc	0.74 ± 0.08 Bab	**1.65 ± 0.07 Aa**	**0.58 ± 0.03 Bb**	1.04 ± 0.33 Abc	0.69 ± 0.21 Bab	1.39 ± 0.29 Aab	0.66 ± 0.09 Aab	0.59 ± 0.05 Ac	0.93 ± 0.15 Aab	0.83 ± 0.09 Ac	0.76 ± 0.10 Aab	0.78 ± 0.06 Ac
Fumarate	1.00 ± 0.04 Aa	0.80 ± 0.08 Bab	**1.00 ± 0.03 Aa**	0.95 ± 0.03 Aa	**0.78 ± 0.07 Ab**	0.63 ± 0.06 Bd	0.90 ± 0.08 Aab	0.76 ± 0.07 Abc	0.80 ± 0.02 Ab	0.83 ± 0.07 Aabc	0.83 ± 0.01 Ab	0.73 ± 0.04 Acd	**1.03 ± 0.05 Aa**	0.92 ± 0.02 Aab
Gaba	1.00 ± 0.16 Bb	1.90 ± 0.20 Aa	0.95 ± 0.12 Ab	**1.02 ± 0.07 Ab**	1.30 ± 0.13 Aab	1.60 ± 0.06 Aa	**1.56 ± 0.29 Aa**	**1.18 ± 0.17 Ab**	1.34 ± 0.19 Aab	**1.10 ± 0.14 Ab**	1.23 ± 0.03 Bab	1.98 ± 0.19 Aa	1.01 ± 0.08 Ab	**1.07 ± 0.09 Ab**
Gluconate	1.00 ± 0.06 Aab	0.96 ± 0.04 Aa	1.13 ± 0.15 Aab	0.85 ± 0.10 Aab	1.02 ± 0.13 Aab	**0.67 ± 0.05 Ad**	1.54 ± 0.42 Aa	**0.70 ± 0.01 Bcd**	0.85 ± 0.09 Ab	**0.75 ± 0.03 Abcd**	0.88 ± 0.14 Ab	0.91 ± 0.09 Aab	1.08 ± 0.05 Aab	**0.69 ± 0.02 Acd**
Glycerate	1.00 ± 0.01 Ab	0.77 ± 0.14 Aab	1.13 ± 0.01 Aab	**0.51 ± 0.02 Bc**	1.22 ± 0.12 Aab	0.67 ± 0.06 Bbc	1.34 ± 0.15 Aa	**0.55 ± 0.05 Bbc**	**1.27 ± 0.02 Aa**	0.78 ± 0.05 Bab	**1.33 ± 0.07 Aa**	0.68 ± 0.03 Bbc	**1.34 ± 0.05 Aa**	0.95 ± 0.16 Bab
Glycolate	1.00 ± 0.02 Aabc	0.95 ± 0.06 Aab	1.07 ± 0.01 Aab	0.96 ± 0.03 Aab	0.94 ± 0.02 Abc	0.92 ± 0.02 Ab	0.96 ± 0.13 Abc	0.97 ± 0.02 Aab	0.90 ± 0.02 Ac	1.04 ± 0.06 Aa	1.13 ± 0.04 Aa	1.00 ± 0.04 Aab	1.00 ± 0.03 Aabc	0.91 ± 0.01 Ab
Hydroxyglutarate	1.00 ± 0.16 Ab	2.15 ± 0.75 Ab	**0.86 ± 0.09 Ab**	1.03 ± 0.10 Ab	**0.67 ± 0.05 Ab**	0.76 ± 0.09 Ab	**0.77 ± 0.06 Abc**	0.70 ± 0.07 Ab	**0.50 ± 0.05 Ab**	0.65 ± 0.05 Ab	**3.33 ± 1.22 Ba**	0.90 ± 0.11 Bbc	**1.09 ± 0.25 Bb**	**4.84 ± 1.80 Ba**
Lactate	1.00 ± 0.04 Aabc	0.97 ± 0.09 Aa	0.91 ± 0.04 Abc	1.02 ± 0.04 Aa	1.06 ± 0.08 Aa	0.95 ± 0.05 Aa	1.05 ± 0.04 Aab	0.98 ± 0.07 Aa	0.88 ± 0.05 Bc	1.03 ± 0.02 Aa	0.93 ± 0.06 Aabc	0.99 ± 0.01 Aa	0.96 ± 0.01 Aabc	0.99 ± 0.04 Aa
Malate	1.00 ± 0.11 Aa	0.76 ± 0.05 Abc	0.85 ± 0.07 Bab	1.19 ± 0.15 Aa	**0.65 ± 0.03 Abc**	0.58 ± 0.13 Ac	0.94 ± 0.07 Aa	0.91 ± 0.07 Aab	**0.63 ± 0.05 Ac**	0.72 ± 0.13 Abc	0.95 ± 0.09 Aa	0.96 ± 0.08 Aab	0.87 ± 0.07 Aa	0.84 ± 0.06 Abc
Maleate	1.00 ± 0.04 Aab	0.71 ± 0.05 Bab	**0.81 ± 0.01 Acd**	0.87 ± 0.07 Aa	**0.71 ± 0.08 Ad**	0.67 ± 0.09 Ab	**1.10 ± 0.06 Aa**	0.72 ± 0.06 Bab	0.74 ± 0.09 Acd	0.87 ± 0.01 Aa	0.84 ± 0.09 Abcd	0.82 ± 0.10 Aab	0.91 ± 0.02 Abc	0.68 ± 0.06 Bab
Piruvate	1.00 ± 0.07 Aa	0.85 ± 0.02 Aa	0.87 ± 0.05 Aa	0.96 ± 0.00 Aa	1.08 ± 0.12 Aa	0.84 ± 0.07 Ba	1.02 ± 0.12 Aa	0.93 ± 0.04 Aa	0.92 ± 0.02 Aa	0.95 ± 0.06 Aa	0.86 ± 0.06 Aa	0.99 ± 0.08 Aa	0.92 ± 0.09 Aa	1.00 ± 0.08 Aa
Fructose	1.00 ± 0.17 Aa	0.93 ± 0.08 Aab	1.01 ± 0.10 Aa	1.18 ± 0.12 Aa	1.08 ± 0.16 Aa	0.87 ± 0.12 Aab	0.99 ± 0.09 Aa	0.84 ± 0.13 Ab	0.98 ± 0.19 Aa	1.05 ± 0.16 Aab	0.90 ± 0.17 Aa	0.85 ± 0.06 Ab	0.99 ± 0.02 Aa	0.81 ± 0.08 Ab
Glucose	1.00 ± 0.16 Aa	0.92 ± 0.10 Aab	0.98 ± 0.11 Aa	1.04 ± 0.10 Aa	1.20 ± 0.23 Aa	0.79 ± 0.07 Bab	1.10 ± 0.15 Aa	0.65 ± 0.10 Bb	1.13 ± 0.21 Aa	1.02 ± 0.13 Aa	0.75 ± 0.14 Aa	0.86 ± 0.16 Aab	1.11 ± 0.02 Aa	0.85 ± 0.14 Aab
Glycerol	1.00 ± 0.03 Aab	1.00 ± 0.17 Aa	0.97 ± 0.09 Aabc	0.97 ± 0.08 Aa	1.10 ± 0.06 Aa	0.84 ± 0.06 Ba	1.10 ± 0.10 Ad	0.86 ± 0.04 Aa	0.89 ± 0.09 Abc	1.02 ± 0.05 Aa	0.76 ± 0.04 Ac	1.00 ± 0.12 Aa	**0.87 ± 0.07 Abc**	1.00 ± 0.10 Aa
Maltose	1.00 ± 0.08 Aab	0.94 ± 0.07 Aa	1.03 ± 0.07 Aab	0.77 ± 0.02 Bab	1.07 ± 0.15 Aab	0.81 ± 0.07 Bab	1.21 ± 0.07 Aa	**0.62 ± 0.02 Bc**	1.16 ± 0.18 Aa	**0.72 ± 0.01 Bbc**	0.76 ± 0.09 Ab	0.85 ± 0.13 Aab	1.17 ± 0.08 Aa	**0.73 ± 0.02 Abc**
mannitol	1.00 ± 0.05	0.80 ± 0.02	1.11 ± 0.04	0.92 ± 0.08	1.29 ± 0.15	1.13 ± 0.10	1.04 ± 0.11	0.92 ± 0.09	0.94 ± 0.06	0.80 ± 0.06	1.01 ± 0.02	1.09 ± 0.02	1.34 ± 0.10	0.92 ± 0.07
Mannose	1.00 ± 0.13 Aab	1.11 ± 0.10 Aab	0.73 ± 0.06 Bb	1.13 ± 0.07 Aab	0.88 ± 0.09 Bab	1.25 ± 0.08 Aa	1.24 ± 0.24 Aa	0.94 ± 0.08 Aab	0.86 ± 0.08 Ab	0.97 ± 0.21 Aab	0.86 ± 0.12 Ab	1.02 ± 0.09 Aab	0.82 ± 0.07 Ab	0.86 ± 0.18 Ab
Quinate	1.00 ± 0.24 Aab	0.80 ± 0.14 Ab	0.62 ± 0.04 Ab	1.01 ± 0.25 Aab	0.71 ± 0.09 Ab	0.62 ± 0.03 Ab	1.15 ± 0.24 Aa	0.67 ± 0.05 Ab	0.63 ± 0.05 Bb	**1.73 ± 0.67 Aa**	0.76 ± 0.02 Aab	0.58 ± 0.06 Ab	0.85 ± 0.14 Aab	1.37 ± 0.33 Aab
Raffinose	1.00 ± 0.25 Aa	0.75 ± 0.16 Aa	0.64 ± 0.15 Aab	0.46 ± 0.02 Aab	0.65 ± 0.21 Aab	**0.34 ± 0.04 Ab**	1.08 ± 0.21 Aa	**0.39 ± 0.02 Bb**	0.54 ± 0.07 Aab	0.75 ± 0.16 Aa	**0.29 ± 0.02 Ab**	0.54 ± 0.12 Aab	0.99 ± 0.26 Aa	**0.40 ± 0.09 Bb**
Sorbitol	1.00 ± 0.06 Ab	1.08 ± 0.07 Ab	1.39 ± 0.19 Aab	1.22 ± 0.07 Ab	**1.80 ± 0.29 Aa**	1.07 ± 0.07 Bb	**1.83 ± 0.21 Aa**	1.16 ± 0.17 Bb	1.52 ± 0.38 Aab	1.11 ± 0.03 Ab	1.55 ± 0.22 Aab	1.14 ± 0.09 Ab	1.56 ± 0.23 Aab	**1.62 ± 0.23 Aa**
Sucrose	1.00 ± 0.04 Aab	0.87 ± 0.03 Bbc	0.99 ± 0.03 Aabc	0.94 ± 0.02 Aab	0.92 ± 0.03 Abc	0.84 ± 0.02 Ac	0.99 ± 0.02 Aabc	0.86 ± 0.05 Bc	0.99 ± 0.03 Aabc	**1.00 ± 0.02 Aa**	**0.91 ± 0.01 Ac**	0.92 ± 0.03 Aabc	1.03 ± 0.04 Aa	0.88 ± 0.02 Bbc
Xylose	1.00 ± 0.07 Ad	1.17 ± 0.06 Aa	**1.12 ± 0.06 Aabc**	1.19 ± 0.02 Aa	1.24 ± 0.09 Aabc	0.98 ± 0.11 Ba	1.04 ± 0.08 Acd	1.15 ± 0.06 Aa	1.06 ± 0.07 Abcd	1.08 ± 0.09 Aa	**1.31 ± 0.03 Aa**	1.13 ± 0.09 Aa	**1.26 ± 0.08 Aab**	1.03 ± 0.10 Aa
Putrescine	1.00 ± 0.05 Ab	1.14 ± 0.09 Ab	1.09 ± 0.07 Ab	1.06 ± 0.10 Abc	1.60 ± 0.19 Aa	1.20 ± 0.06 Bb	**1.58 ± 0.32 Aa**	**0.90 ± 0.06 Bc**	**1.46 ± 0.18 Aab**	**1.46 ± 0.08 Aa**	0.99 ± 0.13 Ab	**0.85 ± 0.06 Ac**	0.99 ± 0.02 Ab	**0.92 ± 0.04 Ac**
Schikimate	1.00 ± 0.05 Aab	0.69 ± 0.02 Bd	1.00 ± 0.06 Aab	**0.95 ± 0.04 Aa**	0.95 ± 0.07 Ab	**0.73 ± 0.04 Bcd**	1.28 ± 0.20 Aa	0.77 ± 0.03 Bbc	1.07 ± 0.09 Aab	0.83 ± 0.04 Bbc	0.91 ± 0.07 Ab	**0.86 ± 0.06 Aab**	1.18 ± 0.07 Aab	**0.83 ± 0.01 Bbc**

Supplementary Table 1: Relative abundance of primary metabolite levels in *Arabidopsis* mutants *ndt1⁻:ndt1⁻, as-1-ndt1, ndt2⁻:ndt2⁻, as-1-ndt2, pxn-1, pxn-3* and Columbia wild type plants (Col-0) grown at ambient (400 µmol mol^{-1} CO_2) and elevated CO_2 (800 µmol mol^{-1} CO_2) as measured by GC-MS. Relative log2-transformed values of signal intensities were normalized with respect to the mean response calculated for the wild type control. Values are means ± SE of five independent samplings; bold demarcate values judged to be statistically different between lines by Tukey's test multiple comparison test ($p < 0.05$).

Gene code	Name	Foward	Reverse
At2G39970	PXN	ACAACGTTACCGCTTTGGAGAC	TGACTGTAGCTCCGAGTTTCGC
At1g25380	NDT2	CGATGCCATGTTCCAACTAC	CATCAAAAGGGCCAAAAAGT
At2g47490	NDT1	GGGAATTCGCGGATTGTACAGTGG	TGGGAAACTGAATGGCAACATGAC
At5g14760	Ao	TGGTCGCTGGTGCTCATCTTTG	AGGCCCTTCAGTACACACAACTC
At5g50210	Qs	TAGCAGGTGGTGAAGGTTGCTC	AGCGAGCTAAGCGAGTTCATCTTC
At2g01350	QPT	TTGGGAAAGTATCAGGGAATGCAC	TGCAGCATCTGCCATTAACTTGG
At5g55810	NMNAT	TGGCAACTGGGAGTTTCAATCCTC	TCTCTCGCCAGCTCAAACATGC
At1g55090	NADs	CAACAGCTGAGCTTGAGCCCATTC	CCATGTCGACTTCATCGAGCTGAG
At4g36940	NAPRT1	AGAACGAACCACCTCCAAAGGTC	AGCTCTTCCCTAGCTTCATCTGC
At2g23420	NAPRT2	AGTGCCACAACGTGTCGAAGAG	TTCTCTTGCTTCATCTGCACTTCC
At2G22570	NIC1	CGGCAATATGGCTCCAACAAAGC	GCAAGCTTTGCACTTTCCTCCAC
At5G23220	NIC3	ACTCGTCATCGACATGCAGAAC	CCTTTCACTTGCGTCACAGCAC
At4g12720	NUDIX7	AATTCTCTCCAAGGTACACACAGC	CCATAGGTTCCACCATGGTTACAG
At2g31320	PARP1	ATCGTCTACGATACAGCCCAGGTG	TGGTTCAGGCTCATCTCTTGTGC
At4g02390	PARP2	ATGCTACTCTGGCACGGTTCAC	AGGAGGAGCTATTCGCAGACCTTG
At2g37620	Actin	CTTGCACCAAGCAGCATGAA	CCGATCCAGACACTGTACTTCCTT
At5g52310	RD29A	TGGACAAAGCAATGAGCATGAGC	AGGTTTACCTGTTACGCCTGGTG
At5g52300	RD29B	ACTGATCCCACGCATAAAGGTG	CTCGTCGGAAAGTCTTCTTCGC
At4g34000	ABF3	GTT CTC AAC CTG CAA CAC AGT GC	TCC AGG AGA TAC TGC TGC AAC C

Supplementary Table 2: List of primers used in this work to perform qPCR.

Supplementary Table 3 - Analysis of variance (ANOVA) of parameters from plants grown under ambient and elevated CO_2 concentration. Bold values demarcate significantly interactions.

Factor	Interaction *p* value	Factor	Interaction *p* value
Rosette dry weight	0.3279	Rosette area	**0.0094**
Total leaf area	0.866	Specific rosette area	0.7939
Specific leaf area	**0.01**	Root dry weight	**0.0196**
Root/Shoot ratio	0.3314	Leaf number	0.0625
Glucose leaves	0.2784	Fructose leaves	0.5616
Sucrose leaves	0.2005	Starch leaves	0.9147
Amino acids leaves	0.0562	Malate leaves	0.1249
Fumarate leaves	0.4401	Nitrate leaves	0.3742
Protein leaves	0.6916	Chlorophyll *a*	0.5787
Chlorophyll *b*	0.715	Chlorophyll *a* + *b*	0.6428
Chlorophyll *a*/*b*	0.0885	NAD^+	**0.001**
NADH	0.0723	$NADP^+$	**0.0074**
NADPH	0.5408	$NADH/NAD^+$	0.0604
$NADPH/NADP^+$	0.0593	Alpha-alanine	0.1313
Aspartate	0.3996	Beta-alanine	0.0659
Cysteine	0.6807	Glutamate	0.283
Glycine	0.6858	Isoleucine	0.5815
Leucine	0.9143	Phenylalanine	0.4987
Proline	**0.0068**	Serine	**0.0477**
Treonine	0.0842	Tyrosine	0.8701
Valine	0.3072	Isocitrate	**0.0029**
Fumarate (GC-MS)	0.4295	GABA	**0.001**
Gluconate	0.0531	Glycerate	**0.039**
Glycolate	0.1237	Hydroxyglutarate	**0.0012**
Lactate	0.1264	Malate (GC-MS)	0.0784
Maleate	**0.0018**	Pyruvate	0.0965
Fructose	0.7438	Glucose	0.3121
Glycerol	**0.03778**	Maltose	**0.0047**
Mannitol	0.1252	Mannose	0.1358
Quinate	**0.0269**	Raffinose	**0.0186**
Sorbitol	0.2239	Sucrose GC-MS	**0.0332**
Xylose	**0.0284**	Putrescine	**0.0435**
Schikimate	**0.0377**	Root growth suc -	0.1218
Root growth suc +	0.9661	Malate seeds	0.2167
Sucrose seeds	0.3311	Starch seeds	0.0979
Amino acids seeds	**0.001**	Protein seeds	0.4618
Lipid seeds	**0.001**	Silique number	0.3522
Seeds/silique	0.1804	Total seed per plant	0.4875
Silique length	0.001	Silique width	0.001
Total seed weight	0.3323		

Chapter 3: NAD^+ mitochondrial transporter NDT1 is important for cytosolic NADH/NAD^+ dynamics upon environmental cues

Elias Feitosa Araujo[1,2], Philippe Fuchs[2], Markus Schwarzländer[2], Adriano Nunes-Nesi[1]

[1] Departamento de Biologia Vegetal, Universidade Federal de Viçosa, 36570-900 Viçosa, Minas Gerais, Brazil
[2] Institute for Plant Biology and Biotechnology, University of Münster, Schlossplatz 8, D-48143 Münster, Germany

*Correspondence:

Adriano Nunes-Nesi
Departamento de Biologia Vegetal,
Universidade Federal de Viçosa,
36570-900 Viçosa, Minas Gerais, Brazil
Phone: +55-31-3612-5357
Email: nunesnesi@ufv.br

ABSTRACT

Nicotinamide adenine dinucleotide (NAD^+) is used by all living cells as a coenzyme in reduction/oxidation (redox) processes and considered as a pivotal determinant of cellular redox status in plants. The final steps of NAD^+ biosynthesis take place in cytosol and specific carriers transport NAD^+ into the organelles. The distribution of NAD^+ among organelles is fundamental to maintain biological processes and the redox homeostasis in subcellular compartments. Traditionally, NAD(P)(H) measurement are based on enzymatic quantification that do not discriminate in each compartment this molecule is being quantified. To circumvent this issue and understand the NAD(H) dynamics, we transformed plants with reduced expression of *NDT1* gene, which encodes a mitochondrial NAD carrier, with the Peredox-mCherry sensor that allowed us to measure *in vivo* specifically cytosolic NADH/NAD^+ dynamics. Under optimal condition, the cytosol of *ndt1* mutant plants is more reduced compared to the wild-type plants. Furthermore, exogenous feeding of sugars and TCA cycle intermediates led to increased cytosolic NADH/NAD^+ ratio in leaves of *ndt1* mutants. Interestingly, *ndt1* leaf discs treated with light, mETC inhibitors and oxygen deprivation did not show significant differences in cytosolic NADH/NAD^+ ratio compared to WT. Together these results suggest that mitochondrial NAD^+ transport performed by NDT1 protein is essential to maintain the NAD(H) balance in the cytosol of Arabidopsis plants and thus demonstrates the importance of this transporter for the regulation of the cellular redox status.

Key Words: NAD^+ transport, *in vivo* redox sensor, NDT1**,** Peredox

INTRODUCTION

Nicotinamide adenine dinucleotide (NAD^+) and its phosphorylated derivative form ($NADP^+$) are coenzymes required in a wide range of reduction-oxidation reactions (Noctor et al., 2006; Hashida et al., 2009)and are widely known to play a central role in the homeostasis of cellular redox potential in plants (Barron et al., 2000). Pyridine nucleotides are also involved in various signaling processes related to the generation and scavenging of reactive oxygen species (ROS) and in the adaptation of organisms subjected to abiotic stresses such as salinity, ultraviolet (UV) radiation, drought and temperature (Amor et al., 1998; Rizhsky et al., 2004; Chai et al., 2005; Hashida et al., 2009).

NAD^+ biosynthesis occurs through two pathways, *de novo* and salvage pathway (Hashida et al., 2009; Gakière et al., 2018a). The *de novo* pathway starts in plastids being aspartate or tryptophan the precursors, while the salvage pathway begins with nicotinamide (NAM) or nicotinic acid (NA). Both pathways converge to the formation of the mononucleotide nicotinic acid (NaMN), which will posteriorly form NAD^+. The final steps of NAD^+ biosynthesis take place in cytosol and to perform its biological functions inside organelles it must be imported by them (Noctor et al., 2006). Since biological membranes are impermeable to this metabolite, specific membrane proteins are necessary to import and export NAD^+ through this barrier (Millar and Heazlewood, 2003; Palmieri et al., 2011). NAD^+ carrier proteins have been identified and characterized in terms of their biochemical features in different compartments of *A. thaliana*. The genes *At*2g47490 (*NDT1*), *At*1g25380 (*NDT2*) and *At*2g39970 (*PXN*) are responsible to encode NAD^+ transporters from mitochondria and peroxisomes, respectively (Palmieri et al., 2009; Agrimi et al., 2012; de Souza Chaves et al., 2019).

The cellular balance of NAD^+, and its derivative forms, in subcellular compartments is pivotal to maintain the redox status homeostasis (Noctor et al., 2006; Gakière et al., 2018b). Therefore, it is suggested that the NAD^+ transport to organelles, as well as the anabolic and catabolic reactions that use this metabolite as substrate, have a fundamental role in the control of the redox potential in subcellular compartments (Noctor et al., 2006; Cantó et al., 2015; Gakière et al., 2018b).

The quantification and monitoring of redox potential are usually performed in a pool of different cells and tissues following chemical extraction that reduces subcellular resolution of redox related compounds. Thus, the obtained values do not reflect the

redox status in each organelle but, instead, the redox of the whole cells (Queval and Noctor, 2007; Schwarzländer et al., 2008). Several approaches allow the evaluation of the redox potential indirectly through the quantification of specific compounds indicative of potential changes in the redox state. These compounds include glutathione and NAD in their different forms, ROS and the activity of oxidative stress enzymes (Queval and Noctor, 2007; Ray et al., 2012). Although widely used in research, these techniques have several limitations, among them: (i) need for cell tissue homogenization, which does not reflect the conditions occurring *in vivo*; (ii) possible alterations in the redox status of these molecules during their extraction; and (iii) the quantification of these molecules in different compartments requires long steps of subcellular fractionation and do not allow a perfect organelle isolation (Schwarzländer *et al*., 2016). Moreover, the redox machinery found in intact cells, necessary to maintain the pairs NAD^+/NADH, $NADP^+$/NADPH, GSSG/GSH in their ideal oxidized-reduced state, is lost during extraction (Schwarzländer et al., 2016).

To deal with the limitations described above, recently fluorescent protein sensors have been produced and inserted into plants allowing to sensor cofactors, molecules and small ions *in vivo* (Schwarzländer et al., 2016; Grossmann et al., 2018; Hilleary et al., 2018; Walia et al., 2018). These sensors are based in the redox sensibility of yellow (rxYFPs) and green (roGFPs) fluorescent proteins (Østergaard et al., 2001; Hanson et al., 2004; Schwarzländer et al., 2016). This technique is based on the engineering of YFP and GFP proteins that contain two cysteine residues in beta sheets adjacent to the surface of the beta barrel. The cysteine residues are positioned close to the chromophore and are capable of forming disulfide bonds, leading to small structural changes that influence the fluorescence of the protein (Meyer and Dick, 2010; Schwarzländer et al., 2016). This system allows enough sensitivity to measure in real-time changes in redox potential through the disulfide bridge formed by the fluorescent protein. In this way, real-time monitoring of the dynamics of the redox potential in living cells is now possible. In addition, it is possible to precisely target these sensor proteins to different subcellular compartments (Schwarzländer et al., 2016).

The functional characterization of *NDT1*, *NDT2* and *PXN* genes demonstrated that a range of biological processes is affected in plants impaired in NAD^+ uptake into mitochondria and peroxisomes (Bernhardt et al., 2012; de Souza Chaves et al., 2019;

Feitosa-Araujo et al., 2020). The NAD(P)(H) pools were impacted in these plants suggesting unbalanced NAD levels among intracellular compartments and consequently disruption in their redox homeostasis (de Souza Chaves et al., 2019; Feitosa-Araujo et al., 2020). Furthermore, several observed phenotypes in NAD^+ carrier mutants may not be explained without the knowledge of the redox status specifically in individual subcellular compartments (de Souza Chaves et al., 2019; Feitosa-Araujo et al., 2020). Among these phenotypes, altered photosynthetic rates, activation of plastid malate dehydrogenase and starch accumulation were observed in plants with reduced activity of NDT1 transporter (de Souza Chaves et al., 2019). In order to understand these phenotypes and the effects of impaired mitochondrial NAD^+ transport on the redox potential in subcellular compartments, we transformed *NDT1* mutant plants with the Peredox-mCherry sensor (Hung et al., 2011). This biofluorescent sensor allowed us to follow *in vivo* the changes in cytosolic NADH/NAD^+ in *ndt1* mutant plants under different environmental cues.

RESULTS

Excitation and emission spectra of mCherry and T-Sapphire probes in wild-type and *ndt1* mutant lines

To confirm the Peredox-mCherry expression in transformed lines, leaf discs were prepared as described above. The excitation and emission spectra of mCherry and T-Sapphire probes in wild-type and *ndt1* mutant lines were recorded by using the plate reader. For mCherry excitation spectra, emission was measured at 615 ± 18 nm while for its emission spectra excitation was 540 ± 20 nm (Figure 1A). For T-Sapphire excitation spectra, emission was measured at 520 ± 10 nm while for emission spectra excitation was at 400 ± 10 nm Figure 1B. As shown in figure 1A and 1B, the wild-type Peredox (+) and *ndt1*$^-$*:ndt1*$^-$ line 1 and *ndt1*$^-$*:ndt1*$^-$ line 3 presented fluorescence for mCherry and T-Sapphire probes indicating that the gene encoding the protein is stably expressed in the genotypes.

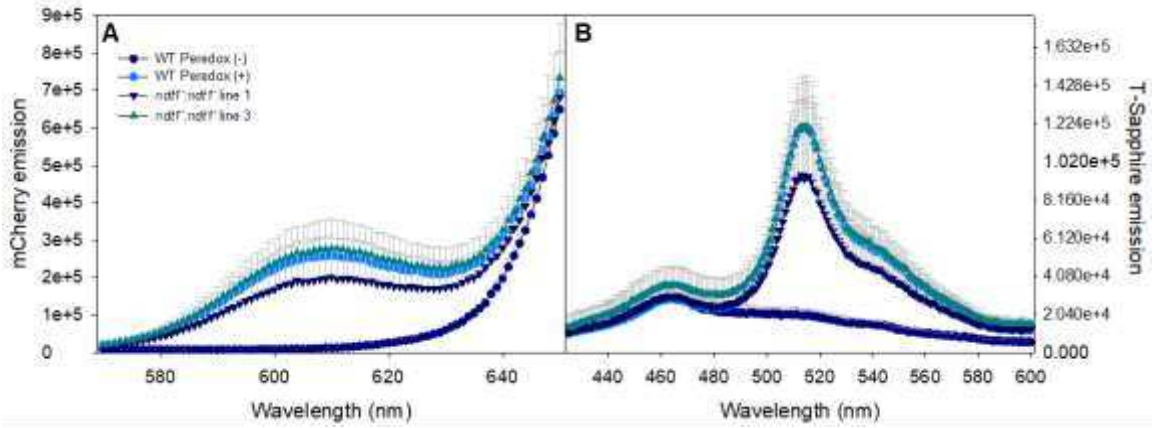

Figure 1: Excitation and emission spectra of mCherry and T-Sapphire proteins in WT and *ndt1* mutant plants.
For mCherry excitation spectra **(A)**, emission was measured at 615 ± 18 nm; for emission spectra, excitation was at 540 ± 20 nm. For T-Sapphire excitation spectra **(B)**, emission was measured at 520 ± 10 nm; for emission spectra, excitation was at 400 ± 10 nm. Values are presented as means ± SD (n=8).

Monitoring the cytosolic NADH/NAD$^+$ dynamics in wild-type and *ndt1* mutant plants

In order to understand the importance of *NDT1* gene in the regulation of cytosolic NADH/NAD$^+$ dynamics, 28-day-old leaf discs of wild-type and *ndt1* mutants transformed with Peredox-mCherry sensor were prepared and placed in 96-well plate filled with assay medium. The plate was transferred to a plate reader and the fluorescence emission was recorded every 3 minutes for 17 hours. Results are plotted as sensor ratio by dividing the single channel fluorescence emission of T-Sapphire per the single channel fluorescence emission of mCherry after correcting this value by subtracting the values recorded for Col-0 leaf discs without sensor. The higher the ratio T-Saphire/mCherry the higher the content of NADH compared to NAD$^+$. Compared to wild-type plants, *ndt1* mutant lines displayed higher NADH/NAD$^+$ ratio over 22 hours (Figure 2A). Time point analysis was also performed by calculating the T-Saphire/mCherry ratio at 0, 2, 4, 8, 12 and 16 hours after the start of the measurement (Figure 2B). In all the time points *ndt1* lines exhibited higher levels of NADH compared to wild-type plants (Figure 2B). The single channel emission intensities are shown in Figure 2C and 2D. The T-Sapphire emission intensity for wild-type, *ndt1 line 1* and *ndt1 line 3* is shown in figure 2C while the mCherry emission intensity is shown in figure 2D. Together, these results suggest that the cytosol of plants with reduced expression

of *NDT1* gene is more reduced than the cytosol of wild-type plants, pointing out the importance of this transporter to regulate the cytosolic level of NAD.

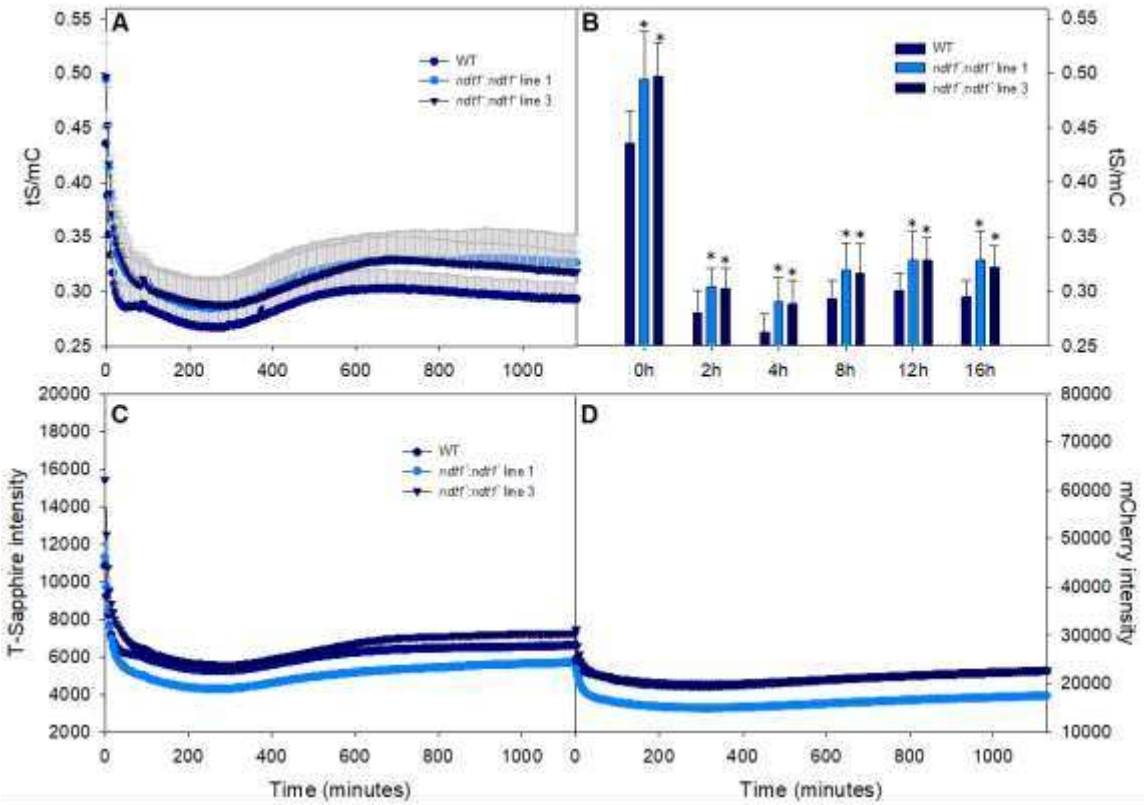

Figure 2: Monitoring the cytosolic NADH/NAD⁺ dynamics in WT and *ndt1* mutant plants.
Peredox-mCherry is a circularly permuted T-Sapphire (tS) chromophore fused to a binding domain that accommodates either NAD⁺ or NADH. mCherry (mC) is a second fluorophore that allows the normalization to sensor abundance and the tS:mC ratio increases when NADH instead of NAD⁺ is bound. In order to monitor NADH/NAD⁺ dynamics in cytosol, leaf discs of 28-day-old plants were placed in 96-well plate filled with assay medium. The plate was transferred into a plate reader and the fluorescence emission was recorded every 3 minutes and the sensor ratio is plotted after fluorescence correction using Col-0 leaves without sensor. **A)** Cytosolic NADH/NAD⁺ dynamics in *ndt1* and WT plants recorded during 22 hours. B) Time point analysis of cytosolic NADH/NAD⁺ dynamics. C) and D) Emission intensities of mCherry and T-Sapphire probes in ndt1 and WT plants. Values are presented as means ± SD (n=8) and asterisks represents values that were judged to be significantly different from the WT (*$p < 0.05$).

Cytosolic NADH/NAD⁺ dynamics in plants with reduced expression of *NDT1* gene under sugar availability

The cytosol of plants with reduced *NDT1* expression and transformed with Peredox-mCherry sensor was more reduced in comparison with wild-type plants growing under optimal environmental conditions (Figure 2). Sugars are substrates for

respiration and thus source of electrons to reduce NAD^+ pool through the glycolysis process. To verify whether the exogenous sugar would lead to altered responses in *ndt1* mutants, leaf discs from 28-day-old plants were placed in 96-well plate prefilled with assay medium supplemented individually with glucose, fructose and sucrose and the emission was recorded for one hour prior to treatment (Figure 3 and Supplemental Figure 1). We observed that after sugar treatment the NADH/NAD^+ ratio was increased in all lines over the time independent of the applied sugar (Figure 3). This result indicates that sugars indeed increase the redox status of the cytosol. Comparing the three sugars, we observed that plants treated with glucose reach the plateau faster than plants treated with sucrose and fructose, respectively (Figure 3A, 3B, 3C). As expected, before the treatment, *ndt1* lines presented again a cytosol more reduced compared to wild-type plants. However, after glucose treatment a remarkable difference between *ndt1* mutant and wild-type plants were not observed (Figure 3A). Concerning the fructose treatment only the *ndt1* line 1 exhibited higher NADH/NAD^+ ratio compared to wild-type during the whole treatment, while *ndt1* line 3 only presented the same result after 300 minutes of treatment (Figure 3B). Interestingly, *ndt1* line 1 and *ndt1* line 3 plants showed faster increase in NADH/NAD^+ ratio right after sucrose feeding compared with wild-type plants (Figure 3C). Additionally, these plants reached the plateau earlier than wild-type plants, showing that the electrons from sucrose breakdown are received by NAD^+ in the cytosol of *ndt1* plants in a faster way (Figure 3C). Time point analysis was performed at 0, 1, 3 and 6 hours after the treatment the NADH/NAD^+ ratio was obtained from each treatment at different time point (Figure 3D, E, F). Therefore, we hypothesized that plants with reduced *NDT1* expression have higher levels of free NAD^+ in cytosol, which could receive electrons from sucrose. On the other hand, the reduced NADH pool cannot be successfully reoxidized due to reduced mitochondrial NAD^+ import, which lead to NADH accumulation in cytosol of *ndt1* plants. This accumulation of NADH in cytosol decreases the free NAD^+ leading the *ndt1* mutant plants to reach the plateau before than WT plants (Figure 3C).

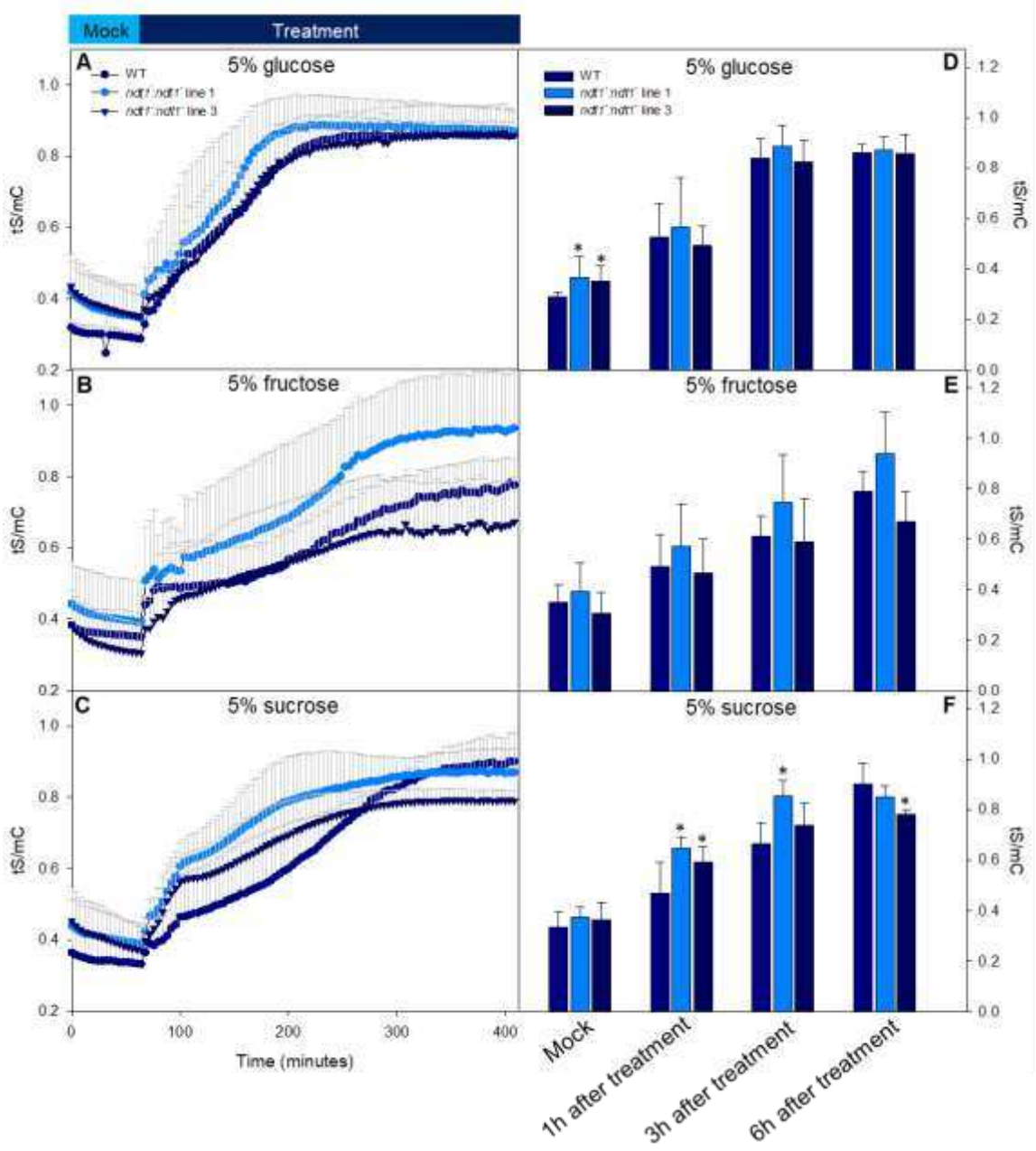

Figure 3: Monitoring the cytosolic NADH/NAD⁺ dynamics in WT and *ndt1* mutant plants after glucose, fructose and sucrose treatment.
Leaf discs of 28-day-old plants were placed in 96-well plate filled with assay medium. Emission was recorded for one hour prior to treatment. Cytosolic NADH/NAD⁺ dynamics in *ndt1* and WT plants after feeding plants with 5% glucose **(A)**, 5% fructose **(b)** and 5% sucrose **(C)** was recorded every 4 minutes. Time point analysis of cytosolic NADH/NAD⁺ dynamics in plants treated with 5% glucose **(D)**, 5% fructose **(E)** and 5% sucrose **(F)**. Values are presented as means ± SD (n=8) and asterisks represents values that were judged to be significantly different from the WT (*$p < 0.05$).

Cytosolic NADH/NAD$^+$ responses of wild-type and *ndt1* mutant plants treated with mitochondrial electron transport chain inhibitors

We next decided to verify whether the inhibition of the mitochondrial electron transport chain would lead to differential responses in *ndt1* mutant plants in terms of their cytosolic NADH/NAD$^+$ levels. With this aim, leaf discs from 28-day-old *ndt1* mutant and wild-type plants were prepared and carefully placed in a 96-well plate prefilled with assay medium treated with antimycin A, SHAM and the combination of antimycin A + SHAM. After treatments, plate was placed back into the plate reader and the fluorescence recorded every 4 minutes. All treatments resulted in increases in cytosolic NADH/NAD$^+$ ratio right after the application of the chemicals (Figure 4A, B, C). Plants treated only with SHAM presented only a slightly increase in NADH/NAD$^+$ ratio while plants treated with antimycin and with the combination of antimycin + SHAM showed higher increased ratios (Figure 4A, 4C and 4B, respectively). Independently from the treatment applied, no apparent differential responses were observed between wild-type and *ndt1* mutant plants. However, in the time point analysis the treatment antimycin A + SHAM resulted in increased cytosolic NADH levels at 2 and 4 hours after treatment in the *ndt1* line 1 compared with the wild-type (Figure 4F). On the other hand, the treatment with antimycin A and SHAM did not lead to significant changes in the cytosolic NADH content when *ndt1* lines and wild-type were compared (Figure 4D, E). These results suggest that when the mitochondrial electron transport chain is inhibited the levels of NADH in the cytosol of *ndt1* mutants and wild-type plants are quite similar.

Cytosolic NADH/NAD$^+$ responses in *NDT1* mutants submitted to low oxygen stress

Oxygen is the final electron acceptor in the mitochondrial electron transport chain during aerobic respiration. In the absence of oxygen, the NADH/$FADH_2$ reduced in the TCA cycle cannot be reoxidized and the mitochondrial respiration is negatively affected. Because the mitochondrial respiration rate is decreased in hypoxic conditions, the NADH/NAD$^+$ ratio in cytosol is kept higher. To verify the behavior of plants with reduced *NDT1* expression in low oxygen condition, we used the Atmospheric Control Unit (ACU) which allows the regulation of O_2 levels within the microplate reader chamber. plants.

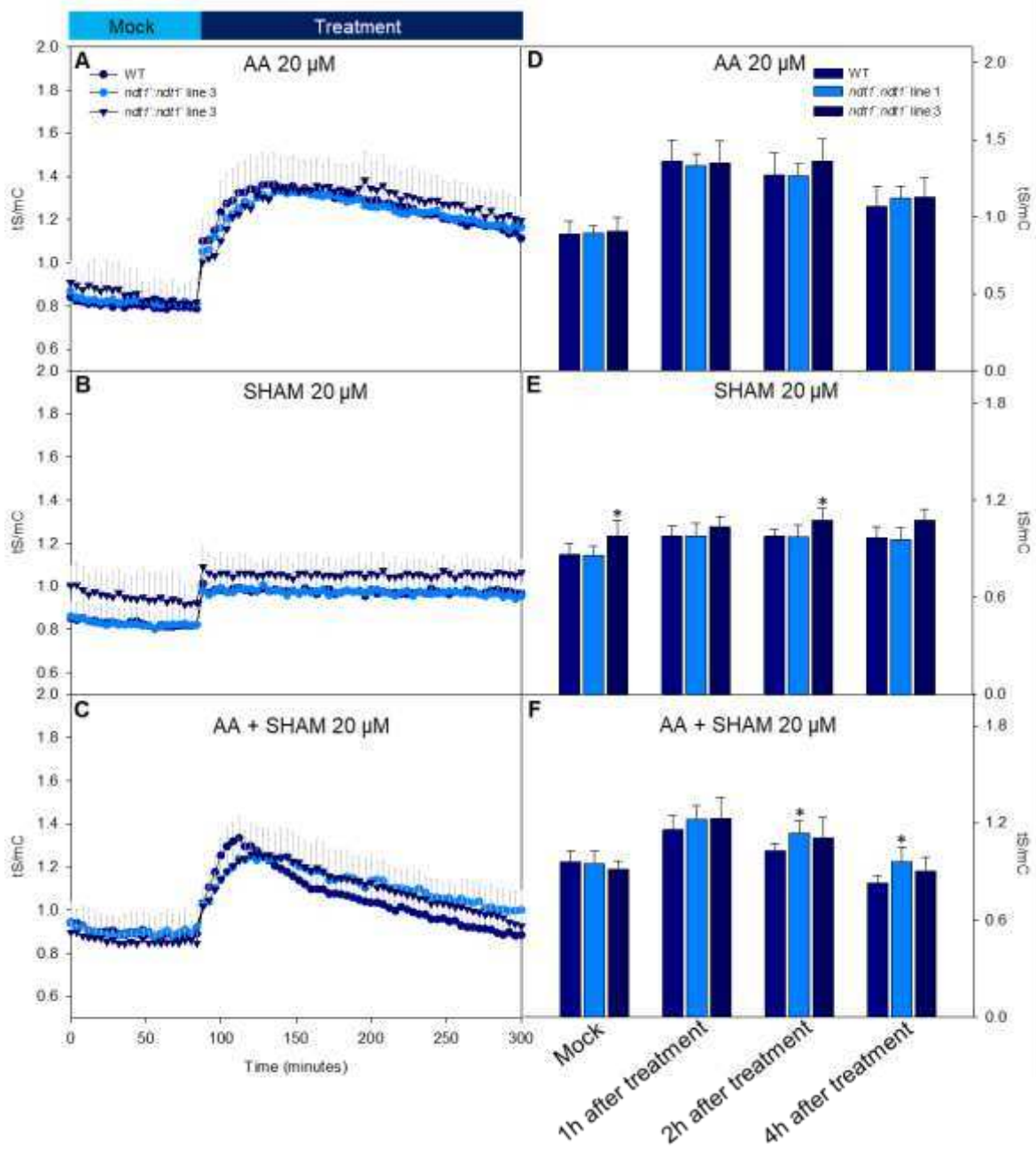

Figure 4: Cytosolic NADH/NAD⁺ responses in WT and *ndt1* mutant plants after treatment with mitochondrial electron transport chain inhibitors.
Leaf discs of 28-day-old plants were placed in 96-well plate filled with assay medium. Emission was recorded during 90 minutes prior to treatment. Cytosolic NADH/NAD⁺ dynamics in *ndt1* and WT plants after feeding plants with antimycin 20 µM **(A)**, SHAM 20 µM **(b)** and antimycin + SHAM 20 µM **(C)** was recorded every 4 minutes. Time point analysis of cytosolic NADH/NAD⁺ dynamics in plants treated with antimycin 20 µM **(D)**, SHAM 20 µM **(E)** and antimycin + SHAM 20 µM **(F)**. Values are presented as means ± SD (n=8) and asterisks represents values that were judged to be significantly different from the WT (*$p < 0.05$).

Leaf discs of 28-day-old plants from *ndt1* lines and WT were placed in 96-well plate filled with assay medium and the fluorescence was recorded for one hour before the hypoxia treatment. After one hour, nitrogen gas was inserted into the system controlled by the ACU until the system reached 0% O_2 concentration. Plants were submitted to hypoxia treatment during 5 hours and subsequently the system was oxygenated again. The kinetics of NADH/NAD^+ ratio of each line is shown in Figure 5A. No apparent cytosolic NADH/NAD^+ differences were observed between wild-type and *ndt1* mutant plants in response to low oxygen stress (Figure 5A). Furthermore, time point analysis confirmed that both *ndt1* mutant and wild-type plants exhibited the same behavior during hypoxia treatment (Figure 5B). In agreement with the previous results, the inhibition of mitochondrial electron transport chain promoted by the lower O_2 availability does not lead to differences in cytosolic NADH/NAD^+ ratio of wild-type and *ndt1* mutant plants.

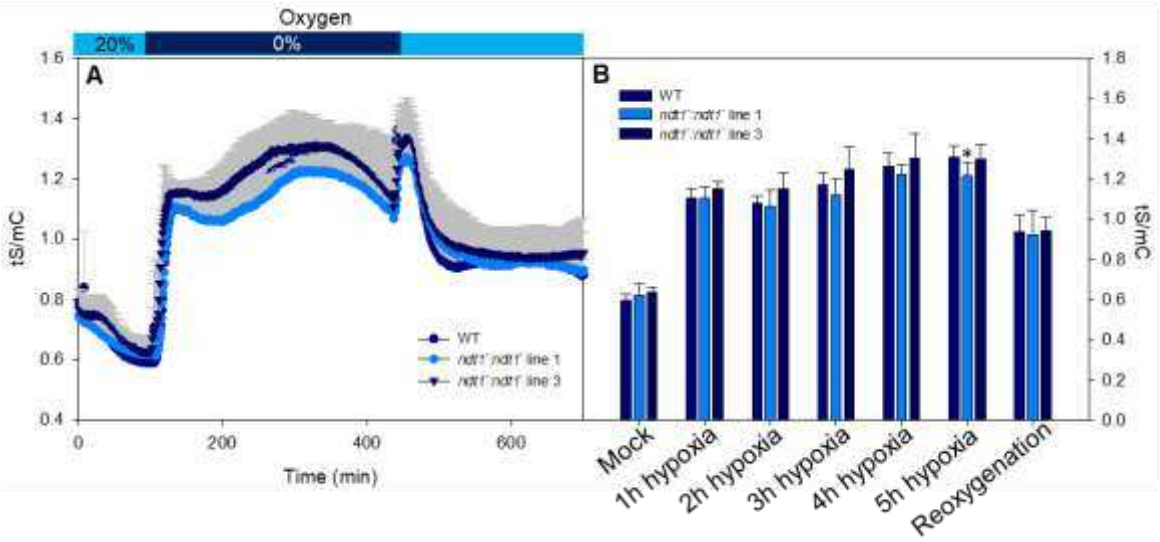

Figure 5: Monitoring the cytosolic NADH/NAD^+ dynamics in WT and *ndt1* mutant plants in response to low oxygen stress.
Leaf discs of 28-day-old plants were placed in 96-well plate filled with assay medium. In order to decrease the O_2 concentration the Atmospheric Control Unit (ACU) was used. The ACU allows the regulation of both O_2 and CO_2 gas levels within the microplate reader chamber. **A)** Emission was recorded for one hour prior to hypoxia treatment. Plants were submitted to hypoxia for 5 hours and them the reoxygenation was implemented in the system. **B)** Time point analysis of cytosolic NADH/NAD^+ dynamics in plants submitted to hypoxia. Values are presented as means ± SD (n=8) and asterisks represents values that were judged to be significantly different from the WT (*$p < 0.05$).

Light treatment and the cytosolic NADH/NAD$^+$ changes in plants with reduced *NDT1* expression

Given that light may contribute to NADH levels in cytosol trough photosynthesis and pentose phosphate pathway we decided to study the possible effects that light could trigger in cytosolic NADH/NAD$^+$ dynamics of *ndt1* mutants and wild-type plants. Fluorescence emission was recorded in the dark and the plates containing leaf discs of *ndt1* and wild-type plants were transferred to light. Plants were submitted to light treatment the fluorescence was recorded (Figure 6A, B, C). As shown in figure 6A and 6B, light treatment leads to strong cytosolic NADH increase. 3-(3,4-dichlorophenyl)-1,1-dimethylurea (DCMU), an inhibitor of the electron transport in PSII complex, was used as light control, showing that the effects presented in figure 6A and 6B are caused by light. No significant differences in cytosolic NADH/NAD$^+$ ratio were observed between *ndt1* mutants and wild-type plants submitted to light treatment. Interestingly, these results suggest that electrons from photosynthetic organelles impact the cytosolic redox state of *ndt1* mutant in a similar manner exhibited by the wild-type.

Changes in cytosolic NADH/NAD$^+$ dynamics in *NDT1* mutant plants treated with TCA cycle intermediates

The TCA cycle enzymes isocitrate dehydrogenase, 2-oxoglutarate dehydrogenase and malate dehydrogenase use NAD$^+$ as coenzyme. Furthermore, glutamate dehydrogenase generates NADH when glutamate is used as substrate and delivers 2-oxoglutarate to the TCA cycle (Jacoby et al., 2015). Since it is expected that the reduced expression of *NDT1* gene leads to a reduction in NAD$^+$ uptake from cytosol to mitochondria, we applied the substrates for isocitrate dehydrogenase (citrate), malate dehydrogenase (malate) and glutamate dehydrogenase (glutamate) to verify the impact of these chemicals in cytosolic NADH/NAD$^+$ dynamics in wild-type and *ndt1* mutant plants. All treatments resulted in increases in NADH/NAD$^+$ ratio in cytosol of wild-type and *ndt1* mutant lines (Figure 7A, B and C). After malate treatment, *ndt1* mutant lines exhibited a faster and higher increase in cytosolic NADH content compared to wild-type (Figure 7A). Furthermore, the kinetic of the *ndt1 line* 3 was shown to be higher than the control line, demonstrating that malate leads to a higher NADH concentration in the cytosol of these plants (Figure 7A). Additionally, time point analysis indicated that upon malate treatment the cytosol of *ndt1* mutant plants are

kept in a more reduced manner because the levels of NADH are higher compared to control at each time point measured (Figure 7D).

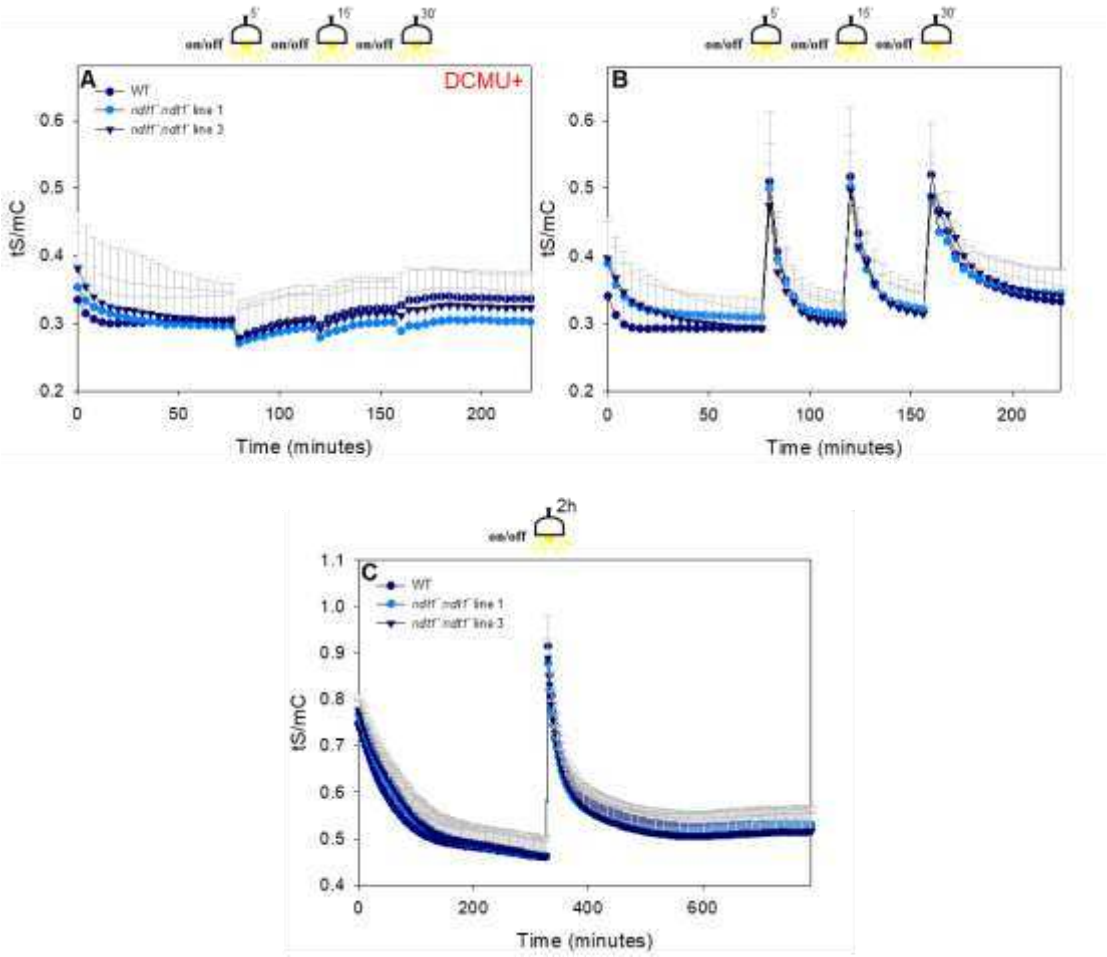

Figure 6: Changes in cytosolic NADH/NAD⁺ dynamics in WT and *ndt1* mutant plants in response to light treatment.
Leaf discs of 28-day-old plants were placed in 96-well plate filled with assay medium and the emission was recorded for approximately 5 hours in the dark. Posteriorly the plate was transferred to light (400 µmol·m^{-2}·s^{-1}). **A)** Cytosolic NADH/NAD⁺ dynamics after Light + DCMU treatment. **B)** Cytosolic NADH/NAD⁺ dynamics after light treatment for 5, 15 and 30 minutes. **C)** cytosolic NADH/NAD⁺ dynamics after light treatment for 1 hour. Values are presented as means ± SD (n=8) and asterisks represents values that were judged to be significantly different from the WT (*$p < 0.05$).

After citrate administration, the three lines exhibited increases in cytosolic NADH content (Figure 7B). However, the NADH content returned to initial levels few minutes after citrate feeding (Figure 7B). The control line presented reduced levels of NADH after citrate treatment compared to *ndt1* mutant lines (Figure 7B). Furthermore, after 1, 3 and 9 hours of treatment the *ndt1* line 3 showed significant increases of NADH content compared to wild-type (Figure 7E). A similar response was observed after glutamate administration (Figure 7C).

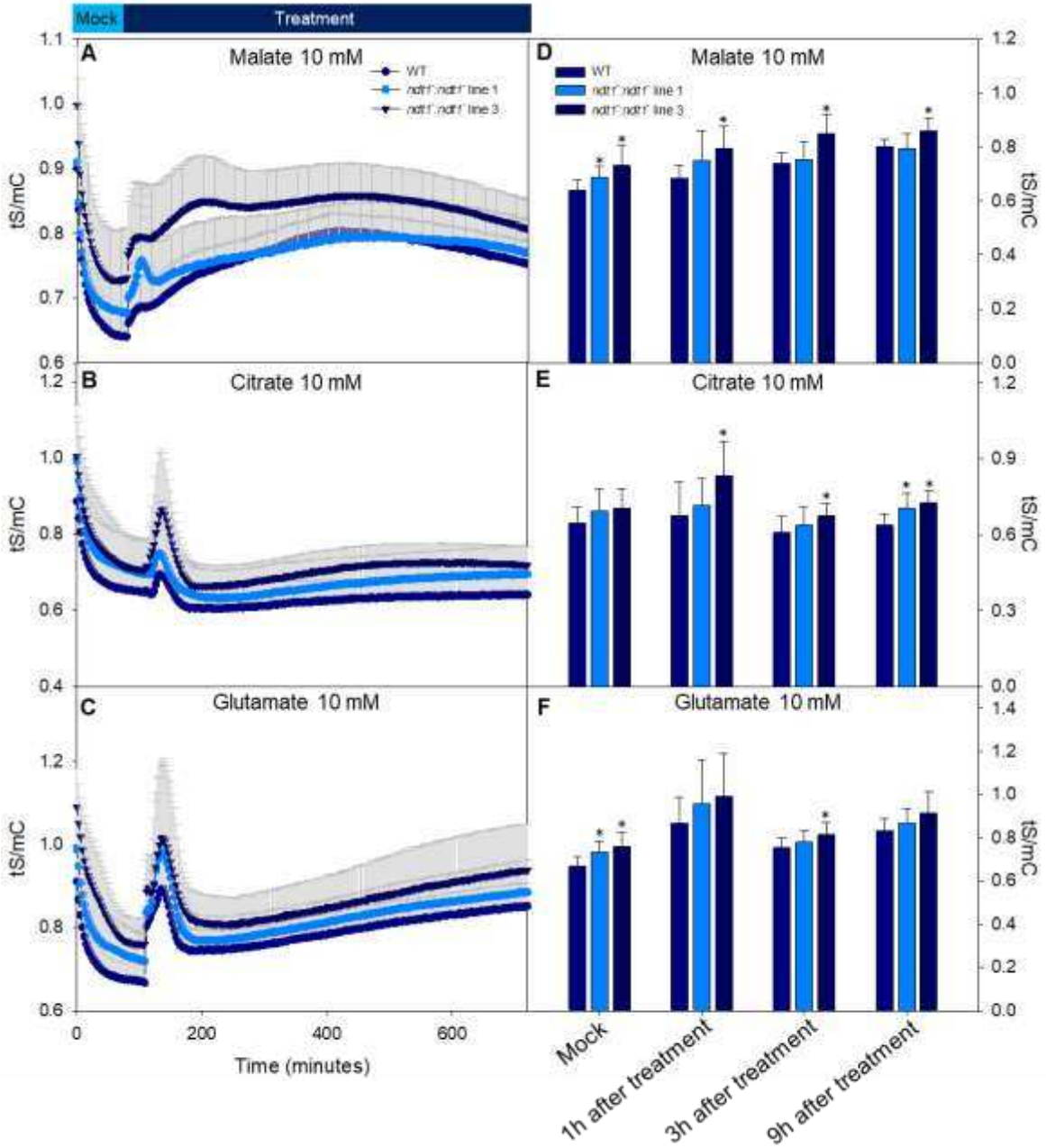

Figure 7: Changes in cytosolic NADH/NAD⁺ dynamics in WT and *ndt1* mutant plants treated with malate, citrate and glutamate.
Leaf discs of 28-day-old plants were placed in 96-well plate filled with assay medium and the emission was recorded for approximately 90 minutes prior to treatment. **A)** Cytosolic NADH/NAD⁺ dynamics after malate 20 mM treatment. **B)** Cytosolic NADH/NAD⁺ dynamics after citrate 20 mM feeding. **C)** Cytosolic NADH/NAD⁺ dynamics after glutamate 20 mM treatment. Time point analysis of cytosolic NADH/NAD⁺ dynamics in plants treated with malate 20 mM **(D)**, citrate 20 mM **(E)** and glutamate 20 mM **(F)**. Values are presented as means ± SD (n=8) and asterisks represents values that were judged to be significantly different from the WT (*$p < 0.05$).

Glutamate treatment led to rapid increases in NADH content in all lines and returned to its initial levels few minutes after the treatment. However, NADH levels start

to be increased again over time (Figure 7C). Prior and after glutamate treatment *ndt1* line 1 and *ndt1* line 3 presented higher levels of cytosolic NADH compared to wild-type plants (Figure 7C, F). Interestingly, these results suggest that chemicals that impact TCA cycle strongly impact the redox status in cytosol and this response is more pronounced in plants impaired in NAD^+ uptake into mitochondria.

Cytosolic NADH/NAD^+ response in *ndt1* mutant plants treated with exogenous NAD^+

To verify the responses of exogenous NAD^+ on wild-type and *ndt1* plants two different treatments were administrated: (i) seedlings were grown for 8 days in a medium containing or not NAD^+ while in the another one (ii) leaf discs were fed with NAD^+ as the experiments described above. After 8 days, higher cytosolic NADH/NAD^+ ratio was observed in seedlings treated with NAD^+ during the whole experiment (Figure 8A, B). This result shows that the exogenous application of NAD^+ leads the cytosol to a more reduced state most probably because NAD^+ accepts free electrons. Next, NAD^+ was applied in leaf disc of wild-type and *ndt1* mutant plants. Significant differences were observed between treated and non-treated plants but no differences were found between lines (Figure 8B, D). This finding suggest that NAD^+ application impact internal NAD(H) levels but *ndt1* mutants do not behave in a different way when compared to wild-type plants.

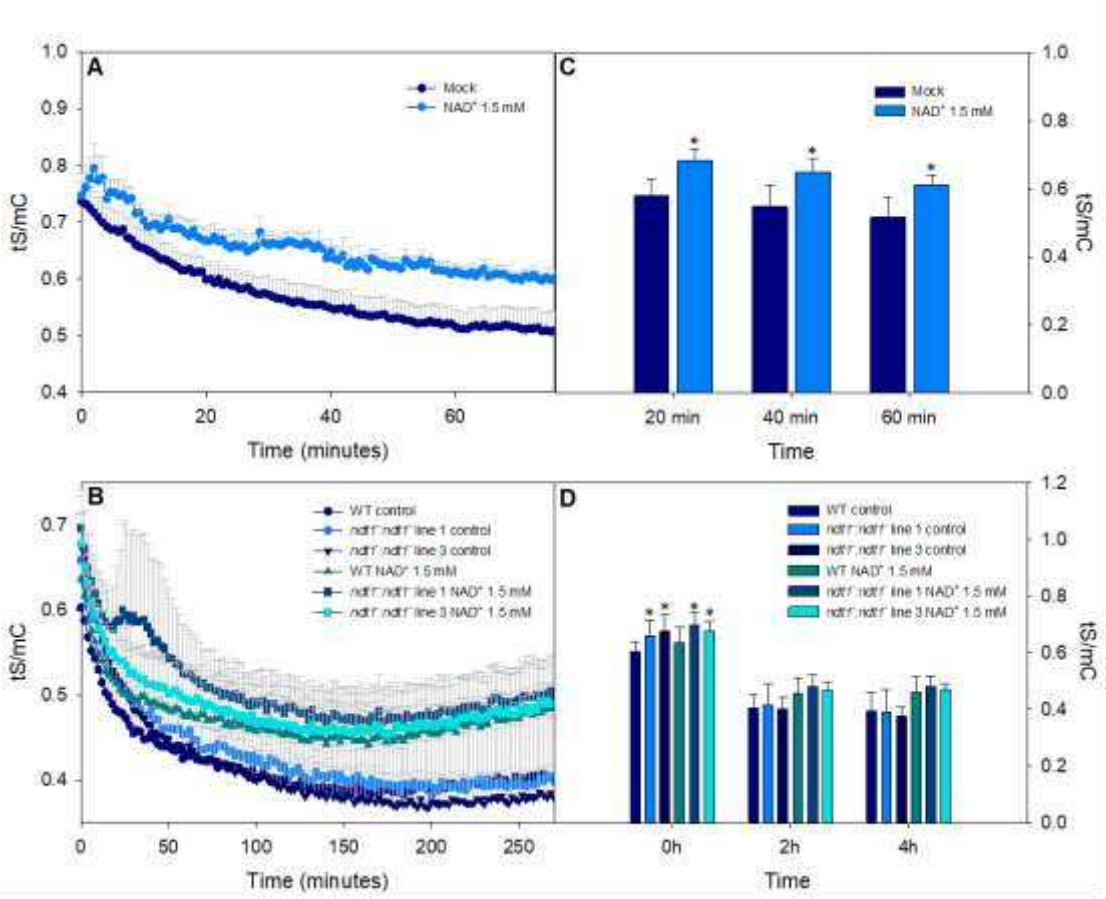

Figure 8: Cytosolic NADH/NAD⁺ response after NAD⁺ treatment.
A) Seeds of WT plants transformed with Peredox-mCherry sensor were spread in medium containing 1.5 mM of NAD⁺ and were grown for 8 days. Subsequently the Cytosolic NADH/NAD⁺ dynamics from seedlings was recorded during one hour. **B)** Leaf discs of 28-day-old plants were placed in 96-well plate filled with assay medium containing or not NAD⁺ 1.5 mM and the emission was recorded. **C)** and **D)** Time point analysis of cytosolic NADH/NAD⁺ dynamics in seedlings and plants treated with NAD⁺ 1.5 mM, respectively. Values are presented as means ± SD (n=8) and asterisks represents values that were judged to be significantly different from the WT (*$p < 0.05$).

DISCUSSION

The functional characterization of NDT1 deficient plants exhibited phenotypes clearly related with changes in plastid redox potential (de Souza Chaves et al., 2019), including higher photosynthetic rates, accumulation of starch and increased activation state of NADP-dependent malate dehydrogenase (NADP-MDH) (de Souza Chaves et al., 2019). These phenotypes led us to investigate *in vivo* specific redox changes in the present work. *NDT1* mutant plants transformed with Peredox-mCherry sensor (Hung et al., 2011) exhibited higher cytosolic NADH/NAD$^+$ ratio compared with the control, suggesting that the cytosolic redox status in mutants are impacted and kept more reduced by reduced mitochondrial import of NAD via NDT1 transporter (Figure 2). We, thus, hypothesized that increased NADH/NAD$^+$ ratio in *ndt1* mutants may be a consequence of higher activity of cytosolic NAD-dependent malate dehydrogenase (NAD-MDH) as consequence of impairment of NAD uptake into mitochondria (Figure 9).

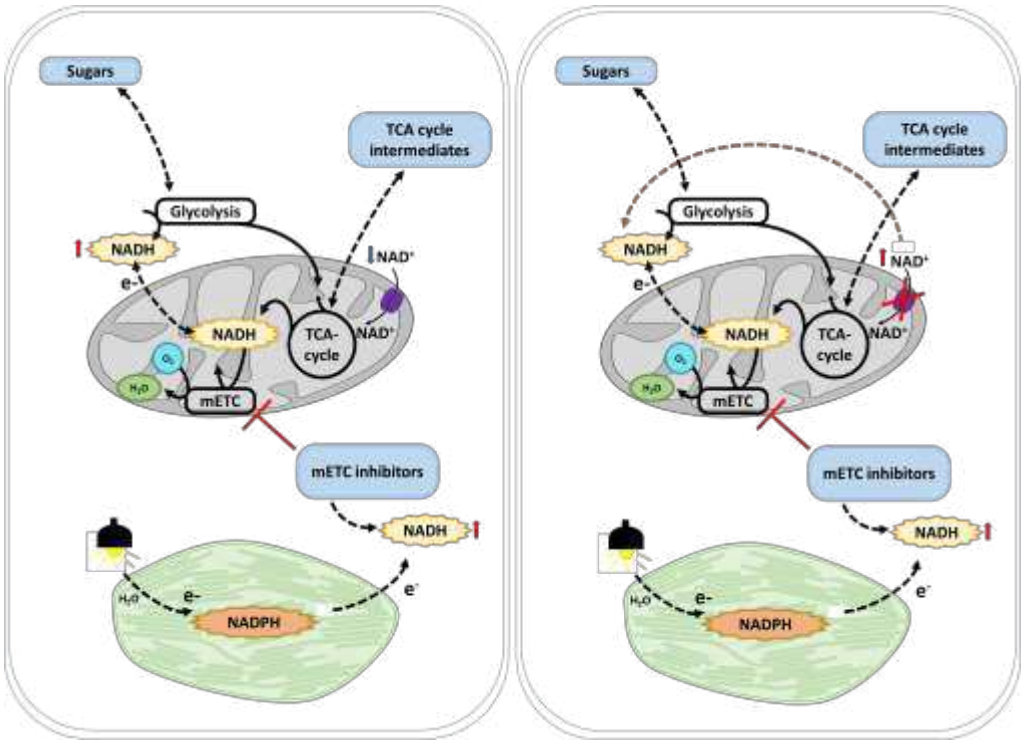

Figure 9: Hypothetical model connecting the cytosolic NADH accumulation in WT and *ndt1* mutant plants upon environmental cues.
The reduced NAD$^+$ import into mitochondria in *ndt1* mutant may contribute to increases in NAD$^+$ and NADH levels in cytosol. Upon sugar treatment, the cytosolic NADH content increase in WT and *ndt1* plants but much more prominent in the mutants most likely to higher free cytosolic NAD to accept electrons. Due to impaired NAD$^+$ import, the TCA cycle of *ndt1* mutants must be deregulated leading to reduced oxidation of TCA cycles intermediates applied thus increasing cytosolic NADH content in *ndt1*

plants. The mitochondrial electron transport inhibition does not lead to significant changes between lines as well as reductants from illuminated chloroplasts.

Consequently, the oxaloacetate, a product of the cytosolic NAD-MDH activity, may enter into the chloroplasts leading to higher NADP-MDH activity, which was observed in leaves from *ndt1* mutants (Chaves et al., 2019). Moreover, upon illumination several Calvin-Benson cycle (CBC) and ADP-glucose pyrophosphorylase (AGPase), a key enzyme of starch biosynthesis, are activated via the Fd-Trx system which are activated by NADP(H) levels (Ballicora et al., 2000; Lemaire et al., 2007; Schürmann and Buchanan, 2008). Given that, most probably, chloroplast´s stroma of *ndt1* plants is more reduced, we would expect higher activity of CBC enzymes as well as AGPase activity and consequently higher photosynthetic rates and starch accumulation (de Souza Chaves et al., 2019). Therefore, these hypotheses were only possible to be postulated after using *in vivo* measurement of NADH/NAD^+ dynamics in specific compartments, in the present work cytosol (Figure 2).

Recent study demonstrates that cytosolic NADH/NAD^+ dynamics are responsive to environmental cues such as hypoxia stress and sugar availability (Wagner et al., 2019). Therefore, in the present work we verified the importance of NAD^+ import into mitochondria performed by NDT1 protein to regulate the cytosolic redox potential (Figure 9). It has been demonstrated that cytosolic NADH pool can be increased by oxidation of carbohydrates during glycolysis (Stein and Granot, 2019; Wagner et al., 2019), increased cytosolic NAD-MDH after malate export from illuminated chloroplasts (Selinski and Scheibe, 2019), hypoxia stress (Wagner et al., 2019) and inhibition of mitochondrial electron transport chain (Wagner et al, 2019). Our results indicate that the correct level of NAD^+ transport into mitochondria mediated by NDT1 protein is fundamental to maintain the redox homeostasis in cytosol upon different environmental cues (Figure 9). Upon sugar feeding, *ndt1* mutants displayed increased cytosolic NADH/NAD^+ ratio must probably reflecting the higher free NAD^+ content in these plants that are prompt to receive electrons from carbohydrate oxidation. Recent evidences indicate that mutants for *NDT2* gene, a second mitochondrial NAD^+ carrier, have lower NAD^+ content inside mitochondria (Luo et al., 2019) which probably impact the activity of NAD-dependent TCA cycle enzymes (Araújo et al., 2012) In this context, we hypothesized that NDT1 deficient plants have less NAD^+ in mitochondria as observed for *NDT2* mutants. In agreement, we observed

that plants with reduced *NDT1* expression presented lower cytosolic NADH/NAD^+ ratio compared to the control following feeding with TCA cycle intermediates, that are catalyzed by NAD-dependent enzymes (Figure 7). These results indicated that changes in the cytosolic redox potential might be displayed by lower TCA cycle activity promoted by reduced NAD mitochondrial import.

Interestingly, wild-type and NDT1 deficient plants displayed similar cytosolic NADH/NAD ratio upon altered electron transport flow via inhibition of mETC or light treatment (Figure 4 and 6). These results suggest that the cytosolic redox potential controlled by NDT1 protein may be specific depending on the internal condition. Furthermore, Arabidopsis genome encodes another mitochondrial NAD^+ transporter named *NDT2* (Palmieri et al., 2009) and a peroxisomal NAD^+ carrier called PXN (Bernhardt et al., 2012) that may contribute to regulate cytosolic redox potential in the conditions previously described. In agreement, Feitosa-Araujo et al., (2020) demonstrated that NDT2 deficient plants impact the expression of *NDT1* and *PXN* genes, thus suggesting that reduced activity of one transporter may alter the activity of others. Despite having the same functions as mitochondrial NAD^+ transporters, NDT1 and NDT2 proteins display different features that could lead to differential activity (Palmieri et al., 2009) . The Vmax of NDT2 is 3.4-fold greater than that of NDT1 and the Km of NDT2 for external NAD^+ is half that of NDT1 thus suggesting that a compensation in NDT2 activity in *ndt1* mutant depending on the treatment may explain some of the results found in this study.

Collectively the results demonstrate the importance of NAD^+ transport performed by NDT1 protein to regulate the potential redox in different compartments under optimal and different environmental challenges. Further studies are still required to unravel the function of NDT2 and PXN proteins to regulate the redox potential in subcellular compartments as demonstrated for NDT1. Furthermore, the targeting of fluorescent biosensor proteins to mitochondria, chloroplasts and peroxisomes would hence the comprehension of the importance of these transporters to regulate redox homeostasis.

EXPERIMENTAL PROCEDURES

Plant material and transformation

The *Arabidopsis thaliana* (Col-0) lines expressing the Peredox-mCherry (Hung et al., 2011) were obtained by inserting the Peredox-mCherry sequence into the binary vector pSS02 (Moseler et al., 2015) and transforming into *Agrobacterium tumefaciens* strain C58C1. *NDT1* mutant plants previously characterized (de Souza Chaves et al., 2019) were transformed through floral dip (Clough and Bent, 1998)to generate *UBQ10*:cyt-Peredox-mCherry. The selection of transformed plants was based on hygromycin resistance and fluorescence as previously described (Hung et al., 2011). Two *ndt1*$^{-}$*:ndt1*$^{-}$ lines were selected and named as *ndt1*$^{-}$*:ndt1*$^{-}$ line 1 and *ndt1*$^{-}$*:ndt1*$^{-}$ line 3. Homozygous plants for cytosolic-Peredox-mCherry were surface sterilized with ethanol 70% and plated in MS medium containing 1% sucrose. Plates were kept in a growth chamber under long day conditions (16 h at 19°C and 60-80 µmol photons $m^{-2}s^{-1}$, 8 h at 17° C and darkness) after stratification for 2 days in the dark. After 6 days, seedlings were transferred to plastic pots containing soil and kept in the same conditions for more 22 days.

Plate reader experiments

Transparent 96-well plates (#82.1581; Sarstedt, Nümbrecht, Germany) with a volume of 400 µl per well were filled with 200 µl assay medium (10 mM 2-(N-morpholino)ethanesulfonic acid (MES), pH 5.8 (potassium hydroxide), 10 mM magnesium chloride, 10 mM calcium chloride, 5 mM potassium chloride). Leaf discs from rosette leaves of 4-week-old WT and *ndt1* mutant plants carrying the Peredox-mCherry sensor were carefully prepared and placed in individual wells prefilled with assay medium using soft tweezers. After plate preparation, it was inserted into a CLARIOstar plate reader (BMG Labtech, Ortenberg, Germany) pre-equilibrated to 25°C. In order to avoid photosynthetic effects, plates were kept in the dark for one hour before fluorescence was recorded. The excitation (Ex) and emission (Em) wavelength for the Peredox-mCherry sensor was: Ex: 400 ± 10 nm and 540 ± 20 nm; Em: 520 ± 10 nm and 615 ± 18 nm.

Chemical treatments

Leaf discs of wild-type and *ndt1* mutant plants carrying the Peredox-mCherry sensor were prepared as described above and gently placed in plates prefilled with the assay medium. The fluorescence was recorded for at least one hour prior to any treatment applied. In order to study the changes in NADH/NAD^+ dynamics in cytosol of plants under different environmental cues, some treatments were performed. Leaf discs were administrated with the following chemicals in independent treatments: 5% sucrose, 5% glucose, 5% fructose, 10 mM malate, 10 mM citrate, 10 mM glutamate, 1.5 mM NAD^+, 20 µM antimycin A (inhibitor of complex III) and 20 µM salicylhydroxamic acid (SHAM, a classical inhibitor of alternative oxidase). To apply the indicated treatments, light was kept off and the plate was removed from the plate reader. A minimal volume of each chemical was administrated to each well and the plate was moved back into the plate reader and fluorescence emission readings was restarted.

Hypoxia treatment

The Atmospheric Control Unit (ACU) is coupled to the CLAROstar plate reader and allows the regulation of O_2 levels within the microplate reader chamber. Thus, leaf discs of 28-day-old *ndt1* lines and WT plants were placed in 96-well plate filled with assay medium and the fluorescence was recorded for one hour before the hypoxia treatment. After one hour, nitrogen gas was applied into the device controlled by the ACU until the whole system reached 0% O_2 concentration. Plants were submitted to hypoxia treatment during 5 hours and subsequently the system was oxygenated again.

Light treatment

It is known that light provide the energy needed to oxidize water and release electrons during the photochemical phase of photosynthesis. Furthermore, the electrons received by $NADP^+$ at this phase can be transferred to oxaloacetate forming malate and posteriorly to NAD^+ in cytosol through the well described malate valve (Scheibe, 2004). In order to study the effects of light in cytosolic NADH/NAD^+ dynamics in wild-type and *ndt1* mutant plants, the experiment was prepared as previously described. 3-(3,4-dichlorophenyl)-1,1-dimethylurea (DCMU) in a concentration of 20 µM was used as control. After recording the fluorescence in the dark for at least 1 hour, the plate was removed from the reader and kept in light (400 µmol photons m^{-2} s^{-1}) for

5, 15, 30 or 120 minutes. After each light treatment period, the plate was moved back into the reader and fluorescence emission readings was restarted.

Statistical analysis

All data was obtained from experiments using a completely randomized design with eight biological replicates of each genotype. Student´s t-test was performed using the algorithm embedded into Microsoft Excel (Microsoft, Seattle, USA) with an alpha of 0.5.

ACKNOWLEDGMENTS

Financial support was provided by Conselho Nacional de Desenvolvimento Científico e Tecnológico (CNPq), Fundação de Amparo à Pesquisa do Estado de Minas Gerais (FAPEMIG). Research fellowships granted by CNPq to EFA, ANN and WLA, Coordenação de Aperfeiçoamento de Pessoal de Nível Superior (CAPES PrInt program) to EFA are also gratefully acknowledged.

REFERENCES

Agrimi, G., Russo, A., Pierri, C. L., and Palmieri, F. (2012). The peroxisomal NAD+carrier of Arabidopsis thaliana transports coenzyme A and its derivatives. *J. Bioenerg. Biomembr.* **44**:333–340.

Amor, Y., Babiychuk, E., Inzé, D., and Levine, A. (1998). The involvement of poly(ADP-ribose) polymerase in the oxidative stress responses in plants. *FEBS Lett.* **440**:1–7.

Araújo, W. L., Nunes-Nesi, A., Nikoloski, Z., Sweetlove, L. J., and Fernie, A. R. (2012). Metabolic control and regulation of the tricarboxylic acid cycle in photosynthetic and heterotrophic plant tissues. *Plant. Cell Environ.* **35**:1–21.

Ballicora, M. A., Frueauf, J. B., Fu, Y., Schürmann, P., and Preiss, J. (2000). Activation of the potato tuber ADP-glucose pyrophosphorylase by thioredoxin. *J. Biol. Chem.* **275**:1315–1320.

Barron, J. T., Gu, L., and Parrillo, J. E. (2000). NADH/NAD redox state of cytoplasmic glycolytic compartments in vascular smooth muscle. *Am. J. Physiol. - Hear. Circ. Physiol.* **279**:2872–2878.

Cantó, C., Menzies, K. J., and Auwerx, J. (2015). NAD+ Metabolism and the Control of Energy Homeostasis: A Balancing Act between Mitochondria and the Nucleus. *Cell Metab.* **22**:31–53.

Chai, M. F., Chen, Q. J., An, R., Chen, Y. M., Chen, J., and Wang, X. C. (2005). NADK2, an Arabidopsis chloroplastic NAD kinase, plays a vital role in both chlorophyll synthesis and chloroplast protection. *Plant Mol. Biol.* **59**:553–564.

Clough, S. J., and Bent, A. F. (1998). Floral dip: A simplified method for Agrobacterium-mediated transformation of Arabidopsis thaliana. *Plant J.* **16**:735–743.

de Souza Chaves, I., Feitosa-Araújo, E., Florian, A., Medeiros, D. B., da Fonseca-Pereira, P., Charton, L., Heyneke, E., Apfata, J. A. C., Pires, M. V., Mettler-Altmann, T., et al. (2019). *The mitochondrial NAD+ transporter (NDT1) plays important roles in cellular NAD+ homeostasis in Arabidopsis thaliana*.

Feitosa-Araujo, E., de Souza Chaves, I., Florian, A., Fonseca-Pereira, P., Apfata, JAC., Heyneke, E., Medeiros, D. B., Pires, M.V., Mettler-Altmann, T., Neuhaus, H.E., Palmieri, F., Araújo, W.L., Obata, T., Weber, A.P.M., Linka, N., Fernie, A.R., Nunes-Nesi, A. (2020). Down-regulation of a mitochondrial NAD+

transporter (NDT2) alters seed production and germination in Arabidopsis. Plant Cell Physiol.

Gakière, B., Hao, J., Bont, L. De, Pétriacq, P., Fernie, A. R., Gakière, B., Hao, J., Bont, L. De, Pétriacq, P., Gakiére, B., et al. (2018a). NAD biosynthesis and signaling in plants. *CRC. Crit. Rev. Plant Sci.* **37**:259–307.

Gakière, B., Fernie, A. R., and Pétriacq, P. (2018b). More to NAD + than meets the eye: A regulator of metabolic pools and gene expression in Arabidopsis. *Free Radic. Biol. Med.* **122**:86–95.

Grossmann, G., Krebs, M., Maizel, A., Stahl, Y., Vermeer, J. E. M., and Ott, T. (2018). Green light for quantitative live-cell imaging in plants. *J. Cell Sci.* **131**.

Hanson, G. T., Aggeler, R., Oglesbee, D., Cannon, M., Capaldi, R. A., Tsien, R. Y., and Remington, S. J. (2004). Investigating Mitochondrial Redox Potential with Redox-sensitive Green Fluorescent Protein Indicators. *J. Biol. Chem.* **279**:13044–13053.

Hashida, S. N., Takahashi, H., and Uchimiya, H. (2009). The role of NAD biosynthesis in plant development and stress responses. *Ann. Bot.* **103**:819–824.

Hilleary, R., Choi, W. G., Kim, S. H., Lim, S. D., and Gilroy, S. (2018). Sense and sensibility: the use of fluorescent protein-based genetically encoded biosensors in plants. *Curr. Opin. Plant Biol.* **46**:32–38.

Hung, Y. P., Albeck, J. G., Tantama, M., and Yellen, G. (2011). Imaging cytosolic NADH-NAD+ redox state with a genetically encoded fluorescent biosensor. *Cell Metab.* **14**:545–554.

Jacoby, R. P., Millar, H., and Taylor, N. L. (2015). Assessment of respiration in isolated plant mitochondria using Clark-type electrodes. In *Plant Mitochondria: Methods and Protocols*, pp. 1–303.

Lemaire, S. D., Michelet, L., Zaffagnini, M., Massot, V., and Issakidis-Bourguet, E. (2007). Thioredoxins in chloroplasts. *Curr. Genet.* **51**:343–365.

Luo, L., He, Y., Zhao, Y., Xu, Q., Wu, J., Ma, H., Guo, H., Bai, L., Zuo, J., Zhou, J. M., et al. (2019). Regulation of mitochondrial NAD pool via NAD+ transporter 2 is essential for matrix NADH homeostasis and ROS production in Arabidopsis. *Sci China Life Sci* **62**:991–1002.

Meyer, A. J., and Dick, T. P. (2010). Fluorescent protein-based redox probes. *Antioxidants Redox Signal.* **13**:621–650.

Millar, A. H., and Heazlewood, J. L. (2003). Genomic and proteomic analysis of mitochondrial carrier proteins in Arabidopsis. *Plant Physiol.* **131**:443–453.

Moseler, A., Aller, I., Wagner, S., Nietzel, T., Przybyla-Toscano, J., Mühlenhoff, U., Lill, R., Berndt, C., Rouhier, N., Schwarzländer, M., et al. (2015). The mitochondrial monothiol glutaredoxin S15 is essential for iron-sulfur protein maturation in Arabidopsis thaliana. *Proc. Natl. Acad. Sci. U. S. A.* **112**:13735–13740.

Noctor, G., Queval, G., Gakière, B., and Gakie, B. (2006). NAD(P) synthesis and pyridine nucleotide cycling in plants and their potential importance in stress conditions. *J. Exp. Bot.* **57**:1603–1620.

Østergaard, H., Henriksen, A., Hansen, F. G., and Winther, J. R. (2001). Shedding light on disulfide bond formation: Engineering a redox switch in green fluorescent protein. *EMBO J.* **20**:5853–5862.

Palmieri, F., Rieder, B., Ventrella, A., Blanco, E., Do, P. T., Nunes-Nesi, A., Trauth, A. U., Fiermonte, G., Tjaden, J., Agrimi, G., et al. (2009). Molecular identification and functional characterization of Arabidopsis thaliana mitochondrial and chloroplastic NAD+ carrier proteins. *J. Biol. Chem.* **284**:31249–31259.

Palmieri, F., Pierri, C. L., Grassi, A. De, Nunes-Nesi, A., Fernie, A. R., Group, M. P., Vic, U. F. De, Mu, A., De Grassi, A., Nunes-Nesi, A., et al. (2011). Evolution, structure and function of mitochondrial carriers: A review with new insights. *Plant J.* **66**:161–181.

Queval, G., and Noctor, G. (2007). A plate reader method for the measurement of NAD, NADP, glutathione, and ascorbate in tissue extracts: application to redox profiling during Arabidopsis rosette development. *Anal. Biochem.* **363**:58–69.

Ray, P. D., Huang, B. W., & Tsuji, Y. (2012). Reactive oxygen species (ROS) homeostasis and redox regulation in cellular signaling. Cellular signalling, **24**(5), 981-990.

Rizhsky, L., Liang, H., Shuman, J., Shulaev, V., Davletova, S., Mittler, R., Rizhsky L., Liang H., Shuman J., Shulaev V., et al. (2004). When defense pathways collide. The response of Arabidopsis to a combination of drought and heat stress. *Plant Physiol* **134**:1683–1696.

Scheibe, R. (2004). Malate valves to balance cellular energy supply. *Physiol Plant* **120**:21–26.

Schürmann, P., and Buchanan, B. B. (2008). The ferredoxin/thioredoxin system of oxygenic photosynthesis. *Antioxidants Redox Signal.* **10**:1235–1273.

Schwarzländer, M., Fricker, M. D., Müller, C., Marty, L., Brach, T., Novak, J., Sweetlove, L. J., Hell, R., and Meyer, A. J. (2008). Confocal imaging of glutathione redox potential in living plant cells. *J. Microsc.* **231**:299–316.

Schwarzländer, M., Dick, T. P., Meyer, A. J., and Morgan, B. (2016). Dissecting redox biology using fluorescent protein sensors. *Antioxidants Redox Signal.* **24**:680–712.

Selinski, J., and Scheibe, R. (2019). Malate valves: old shuttles with new perspectives. *Plant Biol.* **21**:21–30.

Stein, O., and Granot, D. (2019). An overview of sucrose synthases in plants. *Front. Plant Sci.* **10**:1–14.

Wagner, S., Steinbeck, J., Fuchs, P., Lichtenauer, S., Elsässer, M., Schippers, J. H. M., Nietzel, T., Ruberti, C., Van Aken, O., Meyer, A. J., et al. (2019). Multiparametric real-time sensing of cytosolic physiology links hypoxia responses to mitochondrial electron transport. *New Phytol.* **224**:1668–1684.

Walia, A., Waadt, R., and Jones, A. M. (2018). Genetically Encoded Biosensors in Plants: Pathways to Discovery. *Annu. Rev. Plant Biol.* **69**:497–524.

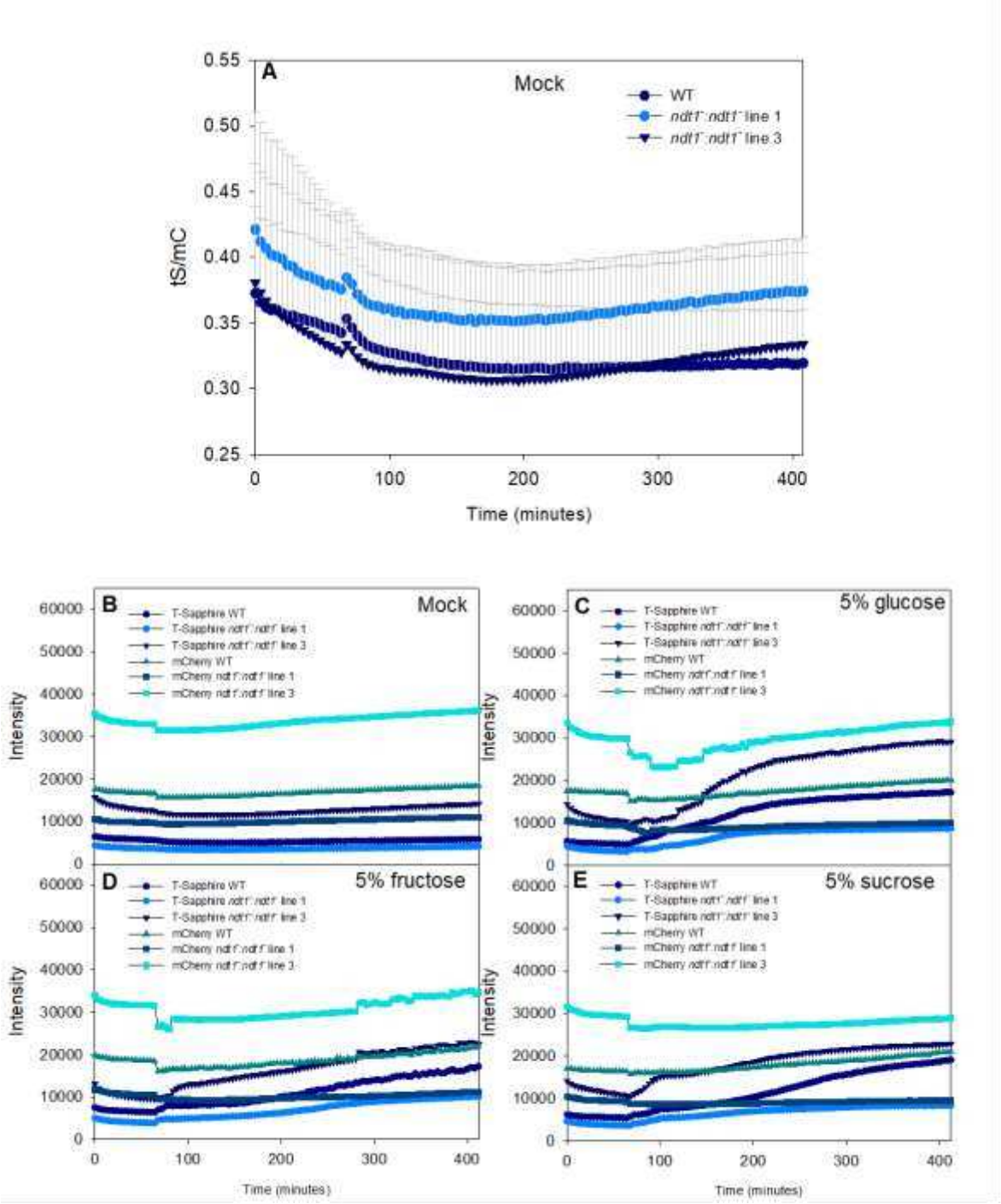

Supplementary Figure 1: Excitation and emission spectra of mCherry and T-Sapphire probes in WT and *ndt1* mutant plants treated with glucose, fructose and sucrose.

A) Cytosolic NADH/NAD$^+$ dynamics in untreated plants. **B)**, **C)**, **D)**, **E)** Excitation and emission spectra of mCherry and T-Sapphire probes in control, 5% glucose, 5% fructose and 5% sucrose treated plants, respectively. For mCherry excitation spectra, emission was measured at 615 ± 18 nm; for emission spectra, excitation was at 540 ± 20 nm. For T-Sapphire excitation spectra, emission was measured at 520 ± 10 nm; for emission spectra, excitation was at 400 ± 10 nm. Values are presented as means ± SD (n=8).

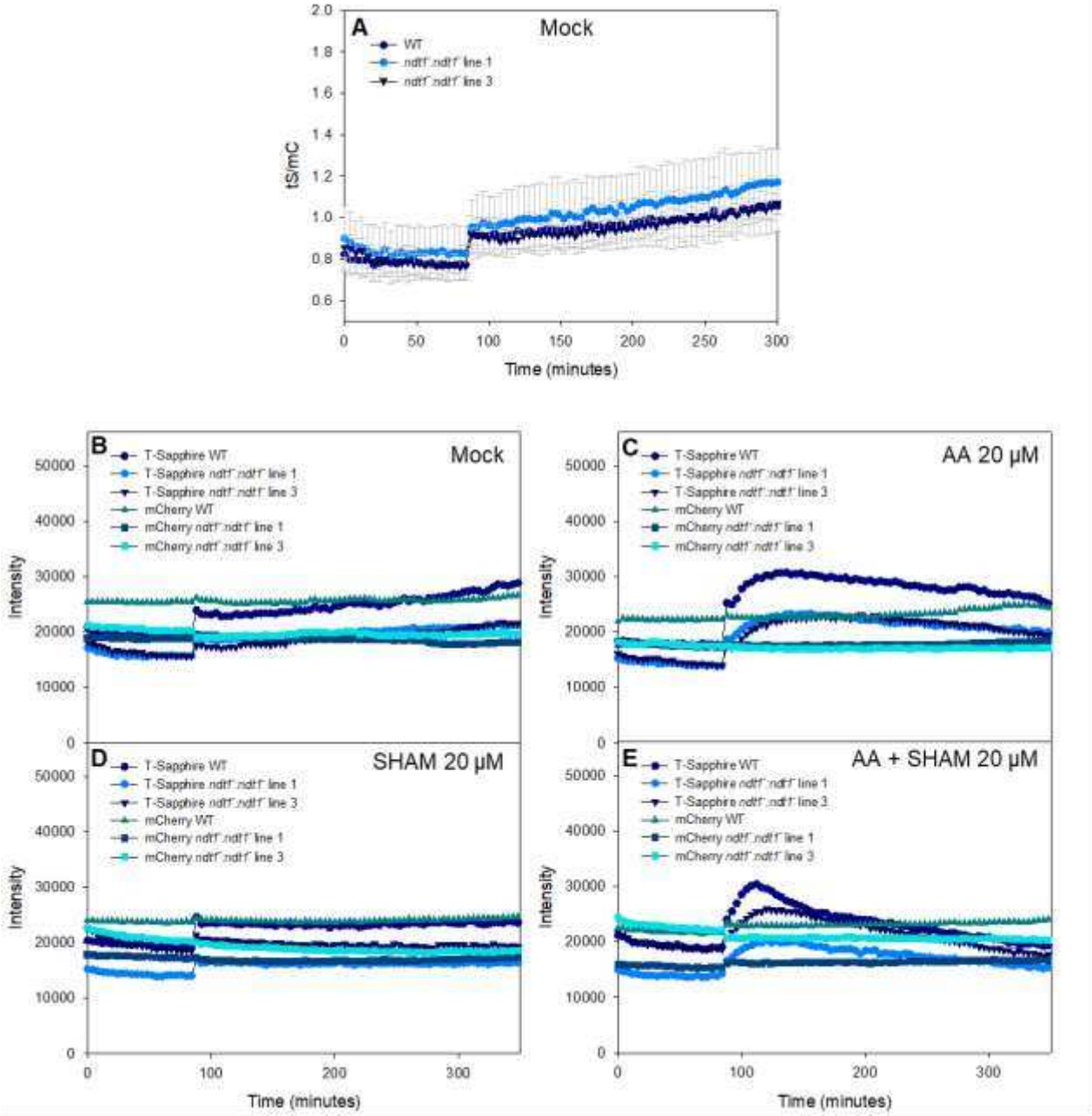

Supplementary Figure 2: Excitation and emission spectra of mCherry and T-Sapphire probes in WT and *ndt1* mutant plants treated with antimycin A and SHAM.

A) Cytosolic NADH/NAD$^+$ dynamics in untreated plants. **B)**, **C)**, **D)**, **E)** Excitation and emission spectra of mCherry and T-Sapphire probes in control, antimycin 20 µM, SHAM 20 µM and antimycin + SHAM 20 µM treated plants, respectively. For mCherry excitation spectra, emission was measured at 615 ± 18 nm; for emission spectra, excitation was at 540 ± 20 nm. For T-Sapphire excitation spectra, emission was measured at 520 ± 10 nm; for emission spectra, excitation was at 400 ± 10 nm. Values are presented as means ± SD (n=8).

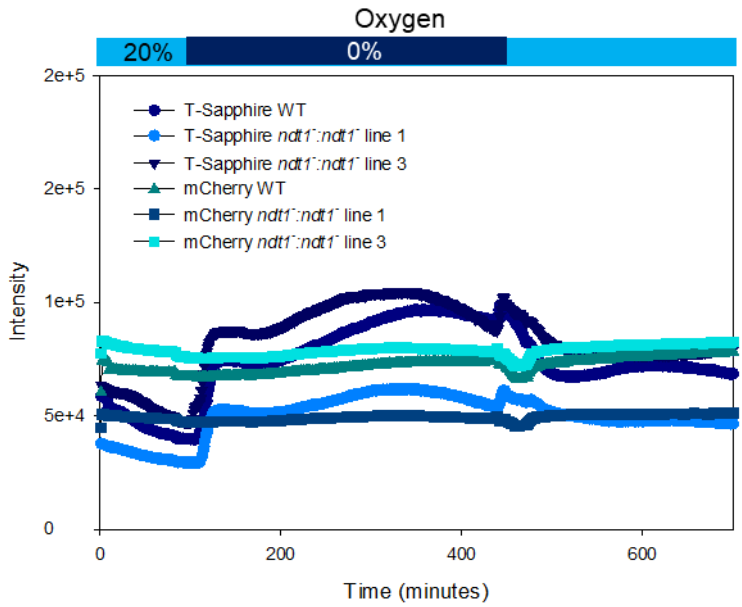

Supplementary Figure 3: Excitation and emission spectra of mCherry and T-Sapphire probes in WT and *ndt1* mutant plants submitted to hypoxia stress. Excitation and emission spectra of mCherry and T-Sapphire probes plants submitted to low oxygen stress were recorded. For mCherry excitation spectra, emission was measured at 615 ± 18 nm; for emission spectra, excitation was at 540 ± 20 nm. For T-Sapphire excitation spectra, emission was measured at 520 ± 10 nm; for emission spectra, excitation was at 400 ± 10 nm. Values are presented as means ± SD (n=8).

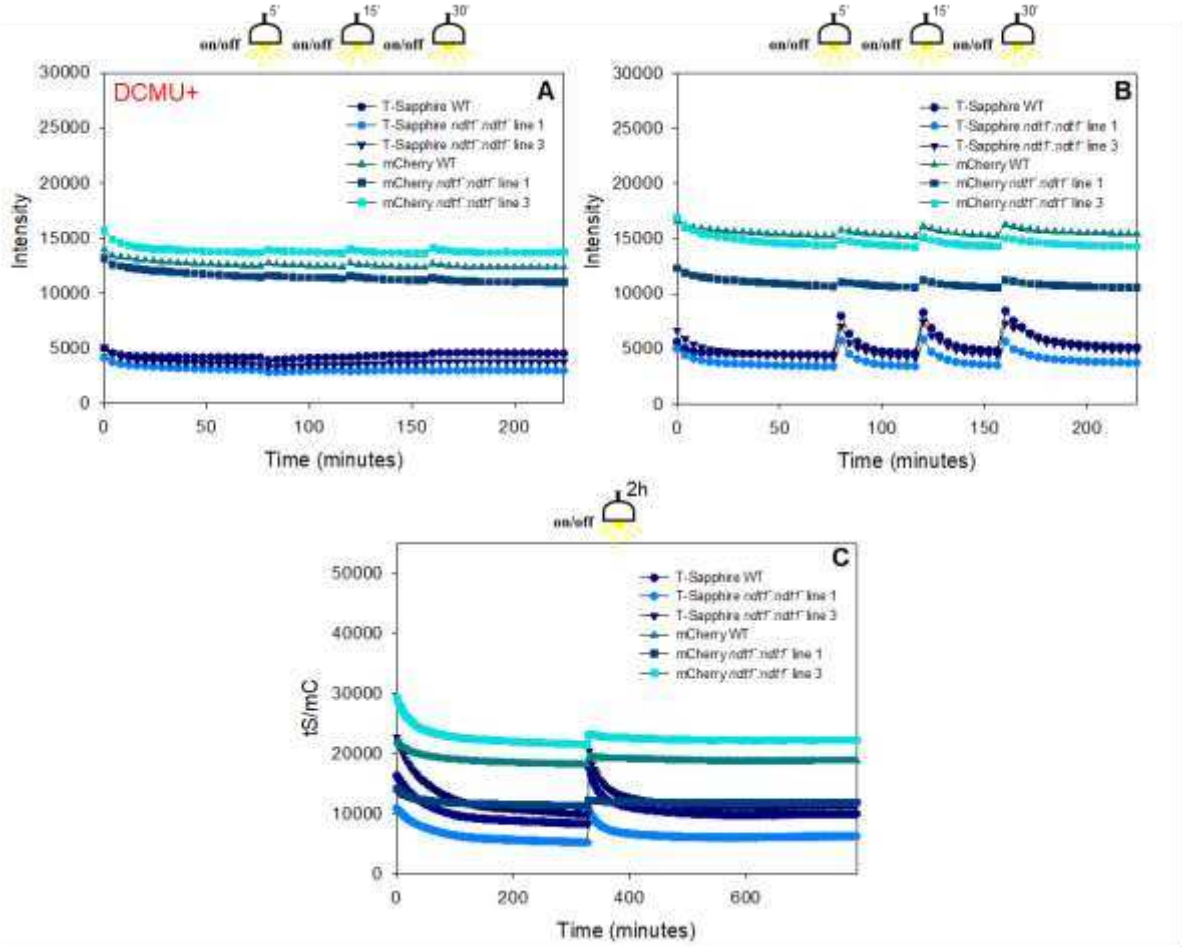

Supplementary Figure 4: Excitation and emission spectra of mCherry and T-Sapphire probes in WT and *ndt1* mutant plants treated with light.
A), **B)**, **C)** Excitation and emission spectra of mCherry and T-Sapphire probes in light + DCMU and only light treated plants, respectively. For mCherry excitation spectra, emission was measured at 615 ± 18 nm; for emission spectra, excitation was at 540 ± 20 nm. For T-Sapphire excitation spectra, emission was measured at 520 ± 10 nm; for emission spectra, excitation was at 400 ± 10 nm. Values are presented as means ± SD (n=8).

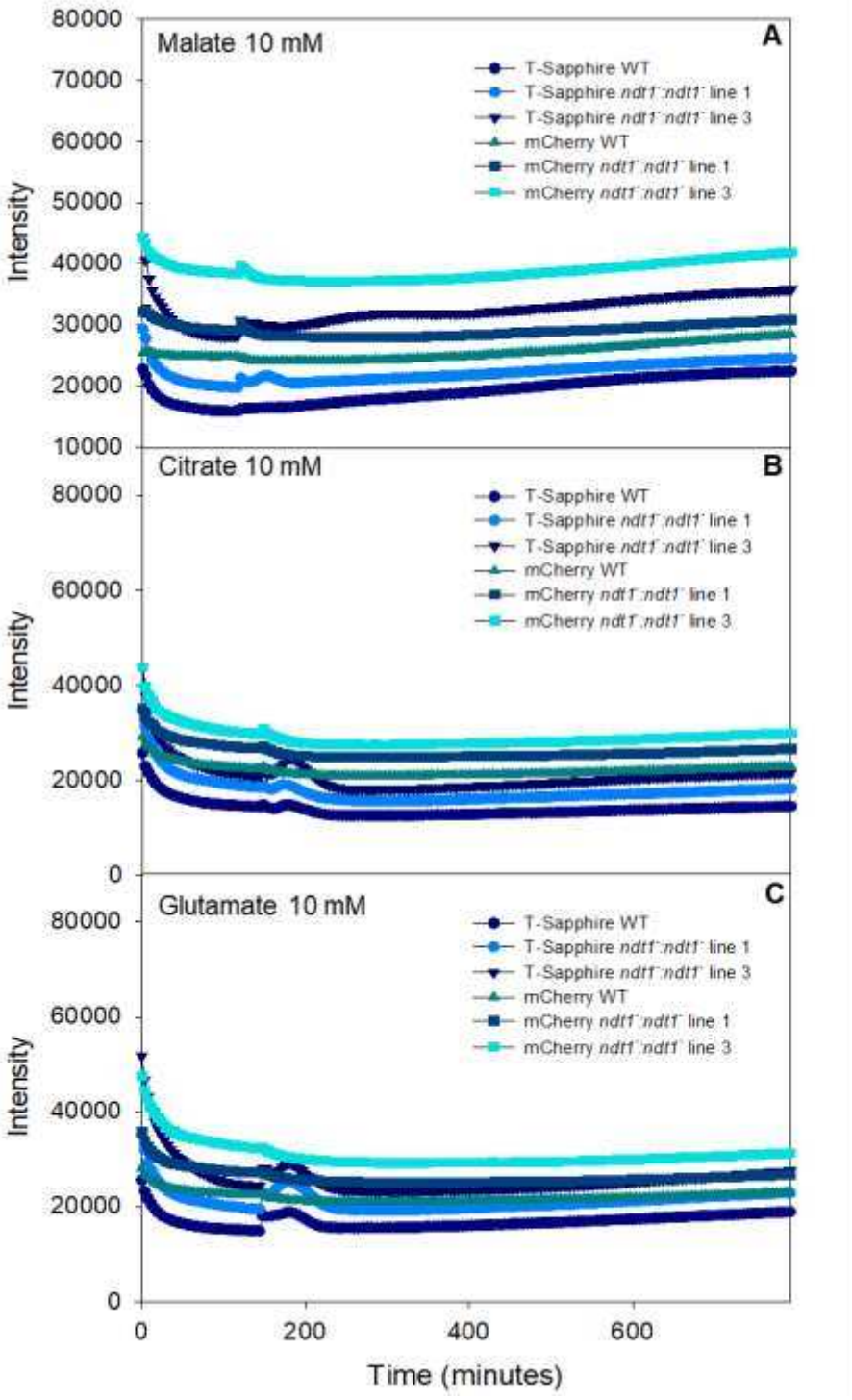

Supplementary Figure 5: Excitation and emission spectra of mCherry and T-Sapphire probes in WT and *ndt1* mutant plants treated with TCA cycle intermediates.

A), **B)**, **C)** Excitation and emission spectra of mCherry and T-Sapphire probes in malate 10 mM, citrate 10 mM and glutamate 10 mM treated plants, respectively. For mCherry excitation spectra, emission was measured at 615 ± 18 nm; for emission spectra, excitation was at 540 ± 20 nm. For T-Sapphire excitation spectra, emission was

measured at 520 ± 10 nm; for emission spectra, excitation was at 400 ± 10 nm. Values are presented as means ± SD (n=8).

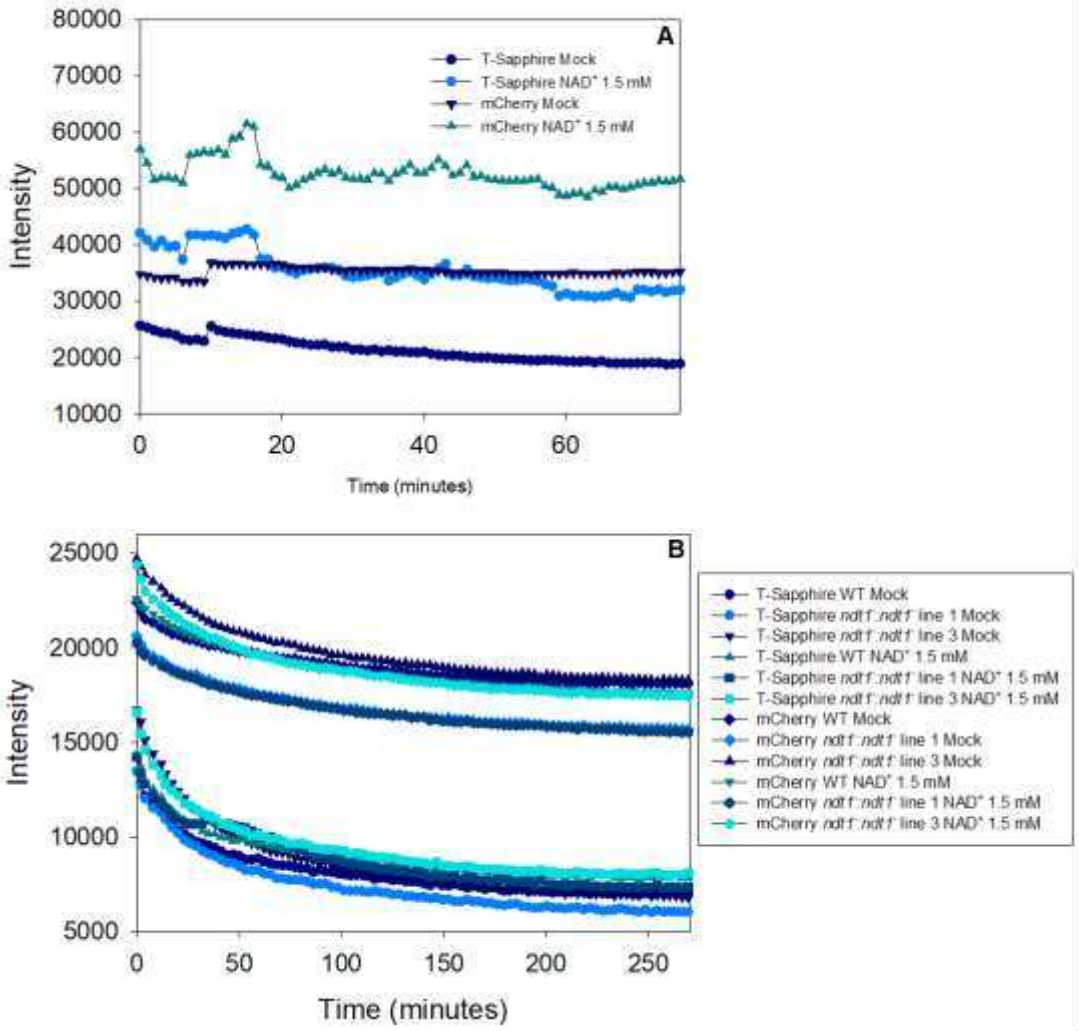

Supplementary Figure 6: Excitation and emission spectra of mCherry and T-Sapphire probes in WT and *ndt1* mutant plants treated with NAD⁺.

A) Excitation and emission spectra of mCherry and T-Sapphire probes in seedlings grown in medium containing 1.5 mM of NAD⁺ for 8 days. **B)** Excitation and emission spectra of mCherry and T-Sapphire probes in leaf discs treated with 1.5 mM of NAD⁺. For mCherry excitation spectra, emission was measured at 615 ± 18 nm; for emission spectra, excitation was at 540 ± 20 nm. For T-Sapphire excitation spectra, emission was measured at 520 ± 10 nm; for emission spectra, excitation was at 400 ± 10 nm. Values are presented as means ± SD (n=8).

GENERAL CONCLUSION

The functional characterization of genes encoding mitochondrial and peroxisomal NAD^+ transporters revealed that not only NAD^+ content but also NAD^+ distribution in subcellular compartments is crucial to modulate several biological processes. We demonstrated in the present study that unbalanced internal NAD^+ content displayed by reduced NAD^+ import into mitochondria and peroxisomes, impaired NAD^+ breakdown along with exogenous NAD^+ feeding perturb the cellular redox balance. As a consequence, ABA metabolism and signaling are enhanced thus leading to the inhibition of stomatal development in Arabidopsis cotyledons. Additionally, we presented a link between NAD^+ transport and high CO_2 concentrations. Overall, the correct NAD^+ distribution is required under both ambient and elevated CO_2 to regulate processes related to biomass gain, stomatal development, stomatal conductance and seed production. We observed that the benefits provided by CO_2 fertilization to plants are abolished or at least not pronounced in plants deficient in NAD^+ compartmentalization. Furthermore, by using the Peredox-mCherry sensor we were able to measure *in vivo* dynamics of cytosolic NADH/NAD^+ ratio under optimal and upon environmental challenges. In general, plants with reduced mitochondrial NAD^+ import exhibited a cytosol in a more reduced manner, both in optimal and in stress conditions. Although this thesis revealed remarkable new roles for NAD^+ regarding early developmental process such as stomatal development and its importance in elevated CO_2 condition, further studies are required to address the following questions: How does NAD^+ transport control stomatal movements? What would be the consequences of reduced expression of *NDT1* and *NDT2* genes in the same mutant? Why do plants have two mitochondrial NAD^+ transporters? Do plants have two mitochondrial carriers to face environmental stresses? Altogether, the results obtained reinforced the crucial importance of NAD+ dynamics to drive essential biological processes in plants.